Research Article

A novel hybrid methodology for multi-objective optimisation of dual-axis solar tracking systems with artificial intelligence

Federico Gabriel Camargo^{a,b,c*} , Francisco Guido Rossomando^{a,b} , Daniel Ceferino Gandolfo^{a,b} , Esteban Antonio Sarroca^c , Omar Roberto Faure^d , Gonzalo Sosa^c

^aUniversidad Nacional de San Juan, Facultad de Ingeniería, Instituto de Automática, Capital, San Juan, Argentina ^bConsejo Nacional de Investigaciones Científicas y Técnicas, Capital, San Juan, Argentina

^cUniversidad Tecnológica Nacional, Facultad Regional La Rioja, Grupo de Actividades Tecnológicas y Energías Renovables, La Rioja, Argentina

^dUniversidad Tecnológica Nacional, Facultad Regional Concepción del Uruguay, Grupo de Mecánica Computacional y Estructuras, Concepción del Uruguay, Entre Ríos, Argentina

*federicogcamargo@gmail.com

Abstract

Paper aims: This article introduces a novel hybrid methodology in order to optimise dual-axis photovoltaic tracking systems in three Argentinian provinces by combining artificial intelligence, swarm intelligence and the productive chain. It identifies the most suitable strategy by balancing fixed-panel worst-case scenarios with continuous-tracking best-case scenarios and incorporating the decision makers' preferences.

Originality: Firstly, the novel research methods listed below combine mathematical modelling and graphical analysis, and highlighting their complementarity and distinct contributions. Secondly, theoretical, methodological and practical gaps are identified and addressed in Argentina and other under-explored regions. This offers decision-makers a viable interim solution.

Research method: Firstly, it involves the novel mathematical modelling, simulation, optimisation, comparison of dual-axis solar tracking in fixed and mobile cases using multi-criteria techniques, while also validating across provinces and extreme scenarios. Secondly, it consists of a novel hybrid multi-criteria optimisation model combining particle swarm optimisation with constriction factor and a fuzzy-guided feedback metaheuristic system. It is for dynamic boundary-reflected constraints, the Analytic Hierarchy Process, and radial basis function neural networks. Thirdly, this survey is based on data obtained through the present line of research, including government and meteorological station data, manufacturer data and independent research.

Main findings: This methodology improves energy efficiency by 10–27% and economic performance by 40–110% compared to fixed panels, depending on regional and technical conditions.

Implications for theory and practice: This novel, scalable hybrid methodology combines the aforementioned research methods (theory) with support for decision-making in the planning of renewable energy projects in constrained economies (practice).

Keywords

Multi-objective hybrid methodology. Artificial Intelligence. Swarm-based optimisation techniques. Tracking solar system and Argentinean production chain. Satisfactory decision making.

How to cite this article: Camargo, F. G., Rossomando, F. G., Gandolfo, D. C., Sarroca, E. A., Faure, O. R., & Sosa, G. (2025). A novel hybrid methodology for multi-objective optimisation of dual-axis solar tracking systems with artificial intelligence. *Production*, *35*, e20240139. https://doi.org/10.1590/0103-6513.20240139.

Received: Dec. 6, 2024; Accepted: Sept. 15, 2025.

Financial Support

The authors have no financial support to declare.

Conflict of Interest

The authors have no conflicts of interest to declare.

Ethical Statement

The authors have no Ethical statement to declare.

Editor(s) Adriana Leiras



1. Introduction

Artificial Intelligence (AI) is a set of computational tools that can outperform human reasoning in terms of speed and accuracy. By simulating operational scenarios, AI identifies the most efficient solutions for complex systems. Industry 4.0 refers to the fourth industrial revolution, driven by the integration of advanced technologies, including AI, into industrial processes. This transformation increases productivity and competitiveness, while promoting energy efficiency and sustainable energy use - key factors in reducing environmental impact and optimising resource consumption, especially in renewable solar energy systems (Alizamir et al., 2023; Azam et al., 2024; Saraji et al., 2024).

In this context, the following aspects are important for the production and efficient use of energy:

- (1) Energy and costs invested in the operation of the energy source and the production chain during its life cycle. A production chain is the set of interconnected processes and activities that transform resources into products or services (renewable power sources), from their origin to their final consumption. By adopting smart technologies, industry can better manage and optimise energy consumption, ensuring long-term sustainability while addressing future energy challenges. Life Cycle Assessment (LCA) of renewable energy sources helps to assess operational costs and provides significant economic, social and environmental benefits (Alizamir et al., 2023; Koshkarbay et al., 2024; Güler et al., 2025).
- (2) Energy and benefits generated: The focus is on the energy and economic benefits gained over the lifetime of a solar system. Optimising energy input, output and economic returns in renewable energy generation particularly solar energy has become increasingly important. Biaxial solar tracking systems adjust the position of solar panels throughout the day to maximise solar energy capture. These systems modify both tilt and elevation angles, although challenges such as variations in solar radiation, local climatic conditions and mechanical limitations can complicate the process (Kuttybay et al., 2024; Sobirov et al., 2023; Praveen & Menaka, 2024; Hadroug et al., 2023).

Tables 1 to Table 4 summarise the existing literature as of March 2025 and provide a structured gap analysis. They highlight the limitations of current solar tracking optimisation methodologies and support the theoretical, methodological and practical contributions of this study. Table 1 shows the search results from the Scopus database (conducted in march 2025) with the authors, country, key techniques used: Analytical Hierarchy Process (AHP), Life Cycle Analysis (LCA), Artificial Neural Network (ANN), Fuzzy Decision Making (FDM), Particle Swarm Optimisation (PSO).

Table 2 shows the techniques used in search results in the Scopus database (conducted in march 2025) and countries (Ctry) according to the United Nations Statistical Division.

Table 3 shows a qualitative evaluation of the methodologies used to search the Scopus database in March 2025, as well as an evaluation of countries according to the United Nations Statistical Division.

General Challenges: However, there are several general challenges that need to be overcome in order to optimise solar energy systems (see Table 1 to Table 4):

- (1) Optimisation of Solar Tracking Systems: Optimising solar tracking systems involves many variables (e.g. panel position, time of day and local conditions) interacting in a complex, non-linear way. It is a multi-objective problem that requires balancing conflicting objectives such as maximising energy output, minimising costs and reducing environmental impact. The more accurately a solar panel tracks the sun, the more efficient it becomes, but this increases energy, economic and manufacturing costs. As a result, traditional mathematical methods often struggle to find the global optimum, and advanced techniques such as Al and optimisation techniques based on swarm intelligence, such as Particle Swarm Optimisation (PSO), are increasingly being used to find more robust solutions (Azam et al., 2024; Sun et al., 2024; Kizielewicz et al., 2024).
- (2) Inefficiencies in determining optimal panel angles: Determining the optimum angle for solar panels is challenging due to variables such as variations in solar radiation, cloud cover and local climate conditions. These factors are difficult to predict and can have a significant impact on solar system performance. The optimisation process becomes even more complex when non-monetary metrics such as environmental impact, sustainability or long-term energy efficiency are included. These objectives often conflict with traditional financial metrics, making it necessary to balance immediate economic returns with broader sustainability goals. To meet these challenges, more flexible models using Al and fuzzy decision systems are needed to account for both measurable and intangible factors (Sarroca et al., 2024; Sameera et al., 2024; Kuttybay et al., 2024).

- (3) Complexity of mathematical modelling: The modelling of the energy produced by a photovoltaic system is still under discussion. This is because there are several different methods of determining the panel's energy irradiance. The influence of angles requires complex astronomical calculations based on the site's geographical location. In addition, climatic factors such as cloud cover can affect the results by reducing the panel's energy production. Therefore, optimising solar energy systems requires balancing factors such as energy output, economic cost, environmental impact and system efficiency. However, as these factors are often measured in different units, direct comparisons are difficult. Linear programming uses linear weighting systems to standardise these metrics, but selecting the right weights and understanding how they interact is complicated. Even small changes in weighting can significantly impact optimisation results, so careful attention is essential to balance these factors effectively (Kizielewicz et al., 2024; Wen & Ajay, 2024; Sameera et al., 2024; Koshkarbay et al., 2024).
- (4) Dynamic solar tracking optimisation: Current methods of optimising solar tracking systems dynamically (i.e. on an hourly or daily basis) often fail to accurately model economic and environmental uncertainties. Furthermore, these methods are not cost-effective in real-world applications. This presents an opportunity to refine Al tools to find optimal solutions for solar energy systems. Al techniques, such as neural networks and optimisation algorithms, can analyse large data sets and identify patterns that traditional methods might overlook. However, Al models must also account for uncertainties such as variations in solar radiation, local climate changes, and mechanical limitations. These models must balance multiple objectives maximising energy output, minimising costs and considering environmental impacts while maintaining system efficiency (Azam et al., 2024; Sun et al., 2024; Kazem et al., 2024). Integrating these four aspects makes it more difficult to develop metrics that enable decision-makers to make dynamic decisions in the face of multiple constraints. This presents a challenge in developing metrics that facilitate real-time decision-making in solar energy systems. While annual and monthly optimisation of panel angles is achievable with current technology (see Table 1), more frequent dynamic adjustments (hourly and daily) are limited by modelling and computational challenges. This restricts the design of investment plans and production systems that could optimally supply the energy chain in response to changing environmental and economic scenarios.

Table 1. Search results in the Scopus database (conducted in march 2025) and countries (Ctry) according to the United Nations Statistical Division.

Authors	Ctry	Key techniques	AHP	LCA	ANN	FDM	PSO	Statistic
Hammi et al. (2024)	Global (GL)	Renewable comparative analysis on energy and cost using Statistical and Life Cycle Analysis (LCA).	Χ	Χ				Х
Azam et al. (2024)	Global (GL)	Semi-continuous tracking performance evaluation using Statistical analysis for efficiency comparison.	Χ					Χ
Zou et al. (2024)	CHN	Concentrating solar systems and tracking with temperature effects with Statistical analysis.		Χ				Χ
Sameera et al. (2024)	Global (GL)	Partial shade movement analysis to maximize power using PSO and Al-based optimisation.				Χ	Χ	
Kuttybay et al. (2024)	Global (GL)	Performance comparison of solar trackers using Fuzzy inference and Neural Networks.			Χ	Χ		
Hadroug et al. (2023)	DZ	Dual-axis performance optimisation (tilt/orientation) using Fuzzy inference and Neural Networks.			Χ	Χ		
Güler et al. (2025)	KG	Single-axis tracking performance improvement via Fuzzy inference and Swarm Optimization.				Χ	Χ	
Lu & Qin (2024)	CHN	Single-axis performance improvement via Statistical analysis and Swarm Optimization.					Χ	Χ
Saraji et al. (2024)	LT	Single and dual-axis tilt/orientation optimisation using Fuzzy Decision methods and Linear Programming.	Χ			Χ		
Praveen & Menaka (2024)	AUS	Dual-axis optimisation using Neural Networks and Swarm Optimization.			Χ		Χ	
Yadav et al. (2024)	1N	Solar radiation prediction for fixed panels using Neural Networks.			Χ			
Alizamir et al. (2023)	IRQ	Daily solar radiation forecasting using Neural Networks and Statistical analysis with meteorological inputs.			Χ			Χ
Sun et al. (2024)	Global (GL)	Real-time tracking of horizontal single-axis systems using Neural Networks and Statistical analysis.			Χ			Χ
Koshkarbay et al. (2024)	KAZ	Dual-axis tracker performance under weather variability using Neural Network and Statistical analysis.			Χ			Х

The acronym in the table are: Analytical Hierarchy Process (AHP), Life Cycle Analysis (LCA), Artificial Neural Network (ANN), Fuzzy Decision Making (FDM), Particle Swarm Optimisation (PSO). Source: The Authors.

Table 2. Techniques used in search results in the Scopus database (conducted in march 2025) and countries (Ctry) according to

the United Nations Statistical Division.								
Authors	Ctry	Theoretical Gap	Methodological Gap	Practical Gap				
Hammi et al. (2024)	Global (GL)	Low integrated framework between mathematical models and Al-based optimisation.	Low integration between Al-based dynamic optimisation and LCA indicators.	There is limited ability to assess the trade-offs between energy gains and costs.				
Azam et al. (2024)	Global (GL)	Lacks a theoretical basis for adaptive systems under changing conditions.	It does not explore hybrid intelligent systems for real-time optimisation in varying conditions.	It restricts the dynamic adaptation to weather variability, responsiveness and efficiency.				
Zou et al. (2024)	CHN	Lacks a systems-based approach for multi-criteria energy decision-making.	Lacks a multi-criteria dynamic optimisation approach with environmental and economic indicators.	Hinders balanced decision-making, potentially leading to suboptimal performance in real-world deployment.				
Sameera et al. (2024)	Global (GL)	Does not provide a theoretical link between sustainability and Al algorithms.	Lacks a multi-criteria dynamic optimisation approach with environmental and economic indicators.	Reduces the potential to balance energy output with sustainability and cost-effectiveness.				
Kuttybay et al. (2024)	Global (GL)	No unified theoretical framework combining Al techniques.	It does not propose a unified AI framework that combines multiple techniques.	Limits practical applicability and scalability of the proposed solutions.				
Hadroug et al. (2023)	DZ	Does not consider region-specific adaptation within the optimisation theory.	Does not address uncertainty or regional adaptation in dual-axis optimization.	These models may be less accurate or efficient in different geographical or climatic contexts.				
Güler et al. (2025)	KG	Fails to consider increasing complexity in variable environments.	Restricted to single-axis tracking and lacks multi-objective analysis or regional validation.	Narrows the scalability and ignores performance optimization in more complex environments.				
Lu & Qin (2024)	CHN	Lacks a theoretical foundation for adaptive feedback control.	Does not integrate fuzzy logic or learning-based feedback for dynamic adjustment.	Reduces system adaptability to real-time changes, such as shifting weather patterns.				
Saraji et al. (2024)	LT	It does not explore dynamic optimisation in variable conditions.	Lacks real-time adaptability and robustness under variable conditions.	Undermines the system's ability to maintain optimal performance in dynamic environments.				
Praveen & Menaka (2024)	AUS	No theoretical basis linking fuzzy decision-making and Theoretical model.	No consideration of model indicators or fuzzy decision-making in system model.	Weakens decision-making in uncertain or multi-criteria scenarios, common in real-world applications.				
Yadav et al. (2024)	IN	Does not extend predictive models into dynamic system control theory.	Lacks applicability to dynamic systems or integration with optimization algorithms.	Inadequate for improving performance in tracking systems, where dynamic adjustment is critical.				
Alizamir et al. (2023)	IRQ	Lacks conceptual connection between prediction and control in solar systems.	Predictive model not linked to optimisation of control or tracking systems.	Prevents prediction outputs from being used to actively improve energy capture.				
Sun et al. (2024)	Global (GL)	No decision-making model based on Al-powered prediction.	Lacks optimisation layer or decision-making logic.	Limits the usefulness of the predictions in guiding system behaviour for better efficiency.				
Koshkarbay et al. (2024)	KAZ	Lacks a theoretical framework for adaptive hybrid control.	Does not address hybrid optimisation under weather variability.	The system underperforms in unpredictable environmental conditions.				

Table 3. A qualitative evaluation of the methodologies used to search the Scopus database (conducted in March 2025) and of countries (Ctry), according to the United Nations Statistical Division.

	countries (C	Ctry), according to	the United Nation	s Statistical Division.		
Authors	Methodology Complexity	Solution Quality / Efficiency	Mathematical model Constraints Complexity	Economic / Technical Cost	Long-term scalability	Future applicability to prototypes
Hammi et al. (2024)	Low: Simple Statistical analysis	Low: suboptimal solutions	Low: Includes weather without a model	Low: computational and setup cost	Low: Limited Long-term scalability	Low: Usable as baseline or reference
Azam et al. (2024)	Low: Simple Statistical analysis	Low: suboptimal solutions	Low: Includes weather without a model	Low: computational cost	Low: Limited Long-term scalability	Low: Static prototypes
Zou et al. (2024)	Low: Simple Statistical analysis	Low: suboptimal solutions	Low: Includes weather without a model	Low: computational cost	Low: Limited Long-term scalability	Low: Usable as baseline or reference
Sameera et al. (2024)	Medium: PSO based with multiple variables	Medium: good performance in energy output	Low: Lacks dynamic indices and constraints	Low: computational and setup cost	Medium: Replicable across similar industrial cases	Medium: Suitable for prototyping
Kuttybay et al. (2024)	Medium: Hybrid Al with fuzzy model	Medium: good performance in energy output	Low: estimated mathematical model and constraints	High: Technically demanding	Medium: Replicable across similar industrial cases	Low: Limited for practical deployment
Hadroug et al. (2023)	High: fuzzy optimization	Medium: good performance in static energy output	Low: Lacks dynamic indices and constraints	High: Technically demanding	Medium: Replicable across similar industrial cases	Medium: Suitable for simulated prototyping
Güler et al. (2025)	Medium: Hybrid Al with fuzzy model	Low: suboptimal solutions	Medium: Soft constraint incorporation	Medium: computational and setup cost	Medium: Replicable across similar industrial cases	Medium: Suitable for basic prototyping
Lu & Qin (2024)	Medium: Hybrid PSO and statistical model	Medium: Reliable within data range	Low: Lacks dynamic indices and constraints	Medium: computational and setup cost	Medium: Replicable across similar industrial cases	Low: Usable as baseline or reference
Saraji et al. (2024)	Medium: Hybrid Fuzzy and Linear Programming	Low: suboptimal solutions	Low: Linearised non-dynamic indices and constraints	Low: resource use	Low: Limited Long-term scalability	Low: Usable as baseline or reference
Praveen & Menaka (2024)	Medium: Hybrid PSO plus a neural network	Low: suboptimal solutions	Low: Lacks dynamic indices and constraints	Medium: computational and setup cost	Medium: Replicable across similar industrial cases	Medium: Suitable for basic prototyping
Yadav et al. (2024)	Low: Prediction-oriented	Medium: Good for trend forecasting	Low: Ignores dynamic and real-time constraints	Low: Simple implementation	High: Generalizable predicted model	Medium: for basic prototyping
Alizamir et al. (2023)	Medium: Al-based methodology	Medium: Seasonal patterns	Low: Lacks dynamic indices and constraints	Medium: Resource-efficient	Medium: Moderately adaptable	Low: Basic Al systems
Sun et al. (2024)	Low: single axis system	Low: suboptimal solutions	Low: No decision-making prediction model based on Al	Low: cost but underperfomedsystem	Low: long-term scalability potential	High: limited useful prototyping
Koshkarbay et al. (2024)	Low: Lacks a theoretical dual axis model	Low: suboptimal solutions	Low: It does not optimise under weather variability	Low: cost but underperfomed system	Low: long-term scalability potential	Low: Basic simulated prototyping

Table 4. Comparative assessment of Analytic Hierarchy Process (AHP), Fuzzy Decision-Making, Radial Basis Function (RBF) and Particle Swarm Optimization (PSO) and a Combination of all tools.

Criterion	AHP	FDM	RBF	PSO PSO	Fixed Panels	Combination of all tools
Theoretical Gap	Requires predefined criteria weights; lacks learning ability	Requires expert knowledge, fixed rules, limited adaptability	Accuracy affected by climatic noise; requires extensive training	Risk of getting trapped in local optima; sensitive to parameter tuning	Without multiple criteria (economic, environmental, operational)	Overcomes gaps via hybridization and multi- criteria decision logic
Methodological Gap	Static structure; lacks feedback or adaptation	Not scalable for complex dynamic environments	Requires clean data and tuning of structure	Needs careful parameter selection and validation	Lacks intelligent learning/ adaptation	Fuses multiple Al models for robust dynamic control
Practical Gap	High dependence on expert input; limited for real-time use	Hard to generalize to new regions or contexts	Limited interpretability and high computation in training	Risk of poor performance under unseen conditions	Cannot adjust in real-time	Designed for adaptive, region-aware, low-cost deployment
Contribution	Structured decision support in criteria weighting	Solar tracking and fuzzy fitness function with dynamic restrictions	This will be used to model solar tracking and climatic conditions.	Hybridized with FDM, AHP, RBF and Fixed Panels cases	Modeling of the maximum and minimum dynamic constraints	Hybrid Intelligent, multi-objective optimal solution
Considers Multiple Criteria	Yes	Yes	No	No	No	Yes (hybrid optimization)
Weather variability	No	No	Yes	Yes	No	Yes (fully integrated)
Solution Quality vs Effort or Cost	Low (Weighting subjectivity)	Medium-Low (Calibration dependent)	Medium–Low (Data dependent)	Medium (Suboptimal convergence)	Low (Dynamic inefficiency)	Medium-High (Expected)
Applicability to Prototypes and Scalability	Low	Medium-Low	Medium-Low	Medium	Low	Medium-High (Expected)
Published in the state of the art	Yes	Yes	Yes	Yes	Yes	No

Main tools: These articles address the challenges posed by some of the tools that make up the current methodology (Table 1 to Table 4):

(1) Fuzzy Decision-Making Theory provides valuable tools for solving complex optimisation problems in uncertain situations. For instance, it can be employed to determine the optimal tilt angle of a photovoltaic system, achieving a balance between energy production, cost and sustainability. Fuzzy inference systems (FIS) can process vague or imprecise information by assigning degrees of membership to different conditions (Cao et al., 2024; Kuttybay et al., 2024). This allows for more nuanced and realistic decision-making in environments where precise data is unavailable or unreliable. Conversely, fuzzy optimisation models use FIS to identify optimal solutions in uncertain environments by considering multiple factors, such as minimising costs or maximising efficiency. This flexibility makes them particularly well-suited to real-world energy systems that operate under variable climatic and operational conditions (Kizielewicz et al., 2024; Hadroug et al., 2023; Güler et al., 2025).

However, these models also have significant limitations. Their performance depends heavily on the design of the membership functions and rule base, which often requires subjective decisions and expert input. Furthermore, applying fuzzy optimisation to complex systems or large datasets can be computationally intensive and costly. They may also struggle to provide clearly defined outputs when deterministic or binary decisions are required. Additionally, the lack of standardised validation procedures can affect their generalisability and reliability when applied to different case studies. The optimal use of preference functions, t-norms and weighting schemes, particularly in the context of multi-objective photovoltaic tracking problems where balancing competing criteria is delicate and highly context-dependent, remains a topic of ongoing discussion. To address these challenges, fuzzy models can be effectively combined with data-driven, population-based techniques, neural networks, and swarm intelligence. This enables automatic rule tuning, improved generalisation, and dynamic adaptation to environmental variability. This increases the robustness and interpretability of the optimisation process. In the long term, this would make industrial systems more flexible, scalable, cost-effective, sustainable and adaptable to the needs of the production chain.

(2) Artificial neural networks, inspired by the human brain, consist of layers of artificial neurons that process information hierarchically. Radial Basis Function (RBF) networks are powerful modelling and prediction tools for complex systems involving nonlinear relationships. They can analyse data to identify intricate patterns involving variables such as solar irradiance, time, temperature and panel orientation. This allows them to predict energy output with a high degree of accuracy. Their ability to quickly learn and adapt to changing input conditions makes them particularly useful in dynamic environments such as solar tracking systems, where real-time responsiveness is important. Despite their strengths, RBFs also have several limitations. Effective training usually requires large, diverse, and high-quality datasets. In the presence of noise or insufficient data, their performance can degrade significantly. Designing the architecture, particularly selecting basis functions, determining the number of hidden nodes, and tuning parameters, can be computationally demanding and often relies on heuristic choices or expert knowledge (Praveen & Menaka, 2024; Yadav et al., 2024; Sun et al., 2024; Cuevas et al., 2024).

Furthermore, neural networks are often considered 'black boxes' due to their low interpretability. This can hinder trust and adoption in applications that require transparency. Overfitting is another concern, particularly when the training data is limited or does not represent future operating conditions accurately. Although RBF can adapt to new data, they often require retraining or fine-tuning as system dynamics evolve, which can be resource-intensive. For these reasons, RBF networks are often more effective when combined with other techniques that can compensate for their weaknesses. For example, integrating fuzzy logic can incorporate expert knowledge and improve interpretability, while metaheuristic algorithms such as particle swarm optimisation (PSO) can automatically adjust network parameters to improve accuracy and generalisation. In hybrid systems, RBFs provide powerful predictive capabilities, while fuzzy systems and swarm intelligence add robustness, transparency, and optimisation capacity. This makes the overall system more reliable and adaptive in real-world solar energy applications.

(3) Swarm intelligence, and particle swarm optimisation (PSO) in particular, is a powerful technique inspired by the collective behaviour of biological populations. In PSO, each 'particle' represents a potential solution and explores the search space, guided by its own experience and that of its neighbours. This makes PSO highly effective at solving complex optimisation problems. PSO is particularly well-suited to multi-objective scenarios, such as solar energy systems, where balancing conflicting criteria — such as maximising energy output, minimising cost, and reducing environmental impact — is essential. One of PSO's key strengths is its ability to efficiently explore large search spaces and converge on globally optimal solutions without requiring gradient information. However, PSO has its limitations. It can exhibit premature convergence, particularly in high-dimensional or rough search spaces where particles can become trapped in local optima. Its performance is also sensitive to parameter settings such as inertia weight, cognitive and social learning factors, and swarm size. These settings may require careful tuning for each specific problem. Furthermore, scalability can become challenging as problem size increases, requiring more computational time and memory. In dynamic environments such as real-time solar tracking, adaptive strategies may be necessary to maintain exploration and solution quality (Lu & Qin, 2024; Praveen & Menaka, 2024; Güler et al., 2025).

Comparative GAP: Table 4 provides a comparative assessment of key techniques explored in the literature, such as fuzzy decision-making, RBF and PSO, and summarises how these compare to traditional solar tracking approaches. It also highlights the theoretical, methodological and practical limitations of these techniques and the final column introduces its combination. This comparative framework justifies the methodological choices made and outlines the broader vision of the research. Specifically, it demonstrates how integrating intelligent decision systems, predictive models and adaptive optimisation can make solar tracking solutions more scalable, efficient and cost-effective. These tables therefore act as a roadmap, positioning this work within the existing state of the art and indicating its anticipated short- and medium-term contributions.

The identified challenges have sparked a growing interest in dynamic industrial hybrid approaches that combine PSO with other intelligent techniques to improve performance. Similarly, when applied to FIS, PSO can refine membership functions and rule sets, thereby making decision-making processes more flexible and interpretable. These approaches are particularly beneficial in solar energy applications, where simultaneous consideration of challenges such as data-driven prediction, uncertainty management, and multi-criteria decision-making is required. Despite significant research into solar tracking optimisation using Al techniques, most existing studies are limited to isolated models or simulations. Often, these studies lack integration with real production data or the inclusion of multi-criteria constraints tailored to specific regional contexts. Furthermore, there is a notable absence of comprehensive frameworks that integrate fuzzy modelling and optimisation, neural networks, and swarm intelligence into a coherent methodology reflecting realistic operational and economic conditions. Notably, no integrated optimisation approach has been proposed for Argentina and other Latin American regions that considers technical performance, economic feasibility, system-level constraints and decision-maker preferences simultaneously.

This innovative work introduces an intelligent, multi-objective optimisation framework specifically designed for the solar energy sector. It addresses the methodological and regional limitations of solar energy system optimisation. The framework combines advanced mathematical modelling, artificial intelligence, and swarm-based optimisation techniques. This approach considers real-world constraints, decision-maker preferences, and multi-criteria evaluations. Consequently, it fills the theoretical, methodological and practical gaps in the field. In theory, the methodology can model the dynamic relationship between solar panel movement and environmental variables such as climate, location and time of day, while also taking technical and economic limitations into account. In practice, this study employs a hybrid approach combining fuzzy decision theory, radial basis functions (RBFs) and a fuzzy-guided feedback system within a particle swarm optimisation approach incorporating a constriction factor (HFRCPSO-CF) to solve multi-criteria optimisation problems. This system is designed to identify intermediate solutions offering favourable cost-benefit trade-offs in an uncertain environment.

Finally, this methodology is employed to design intelligent, region-specific prototypes suited to the conditions in Argentina's San Juan (SJ), La Rioja (LR) and Entre Ríos (ER) provinces. Unlike conventional fixed- or mobile-angle systems (see Section 2.3.1), the proposed model uses Gaussian fuzzy inference and RBFs to simulate optimal tracking strategies in changing conditions. Both hard and soft constraints are embedded in the mathematical formulation and fitness function to ensure physically feasible motion and reduce unnecessary vibrations. The effectiveness of the methodology is validated through mathematical and graphical comparisons of fixed systems, fuzzy rule-based tracking, RBF-based control and swarm intelligence optimisation. In this context, optimality is defined as a compromise that balances multiple criteria within the bounds of real-world feasibility and decision-maker preferences in complex, uncertain environments, rather than as a single best solution. The proposed model is a scalable, adaptable decision-support tool designed for sustainable energy planning in Argentina and other emerging regions.

This work is structured as follows: Section 2 develops the contributions and results of the proposed novel methodology. This section covers the proposed methodology (Section 2.1), its programs (Section 2.2) and its practical contributions (Section 2.3). Finally, Section 3 presents the conclusions of this work. Mathematical models (Appendix A Section A.1) and radial basis neural networks and Gaussian fuzzy inference system parameters (Appendix A Section A.2).

2. Contributions and results of the novel proposed novel methodology

2.1. Proposed novel methodology

Main methodology (see Section 2.2.2): Figure 1 illustrates the overall structure of the proposed intelligent, multi-criteria optimisation methodology for dual-axis solar tracking. The process begins with the loading of climatic and solar radiation data from national stations in Argentina, focusing on three representative provinces: San Juan (SJ), La Rioja (LR) and Entre Rios (ER). Using this input, the solar position is computed via astronomical modelling to determine sunrise and sunset times for each day and latitude. In this context, the Radial Basis Function (RBF) neural network plays two distinct roles in the study (see Section 2.2.2 and Section 2.2.4). Firstly, it simulates meteorological conditions such as temperature, dew point, rainfall and precipitation, using historical data from national weather stations. This provides realistic inputs for the solar energy model. Secondly, it is employed as a tracking strategy (Case 8), learning from optimal movements observed in various scenarios to generate tilt and orientation angles for the panel. This dual application improves both the accuracy of the modelling and the practical relevance of the methodology. Additionally, life cycle analysis (LCA) of the Argentine production process provides economic data on the costs of energy, material extraction, manufacturing, transportation and waste management.

The following scenarios are analysed for the purposes of analysis, comparison, validation and obtaining the hybrid restrictions, which will be detailed in Figure 2.

Case 1 to Case 4 (fixed panels): North-facing horizontal panel (Case 1), 15° panel facing north (Case 2), 30° panel facing north (Case 3), 45° panel facing north (Case 4).

Case 5: Mixed case with manually adjustable inclination and variable orientation according to the solar zenith angle A_7 .

Case 6 (see Appendix A Section A.1): a variable tilt angle and orientation according to the angle of incidence θ_z and solar zenith angle A_z .

Case 7 (see Section 2.2.3.): a variable tilt angle and orientation according to a fuzzy inference system.

Case 8 (see Section 2.2.4.): a variable tilt angle and orientation according to a Radial Basis Function (RBF) Neural Network.

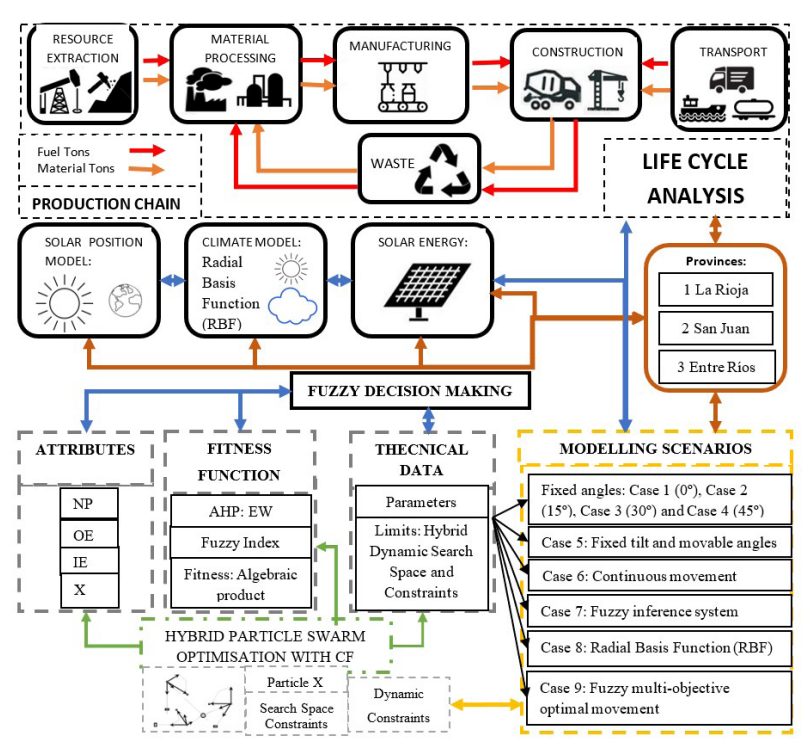


Figure 1. Proposed methodology: Multi-Objective (Fuzzy Decision Making and analytic hierarchy process), hybrid particle swarm optimisation with constriction factor and radial basis function of a tracking solar system in an Argentinean production chain with scenarios.

Source: The authors.

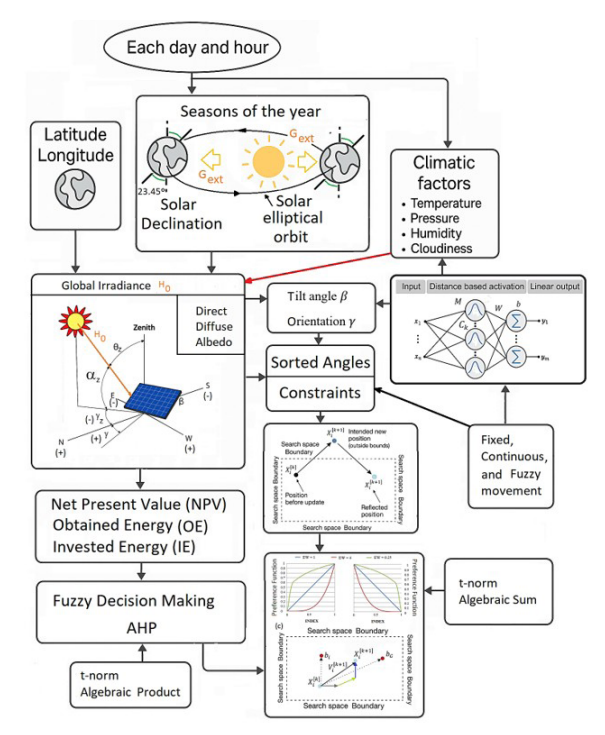


Figure 2. Novel fuzzy fitness function for calculating the system attributes with climatic factors, fuzzy decision theory, t-norm combination and Hybrid Fuzzy-Rigid Constraint Particle Swarm Optimisation with constriction factor (HFRCPSO-CF).

Source: The authors.

Case 9 (see Section 2.2.11.): The multi-objective fuzzy-guided feedback system within Hybrid Fuzzy-Rigid Constraint Particle Swarm Optimisation with constriction factor (HFRCPSO-CF) solves for a variable tilt angle and orientation. This novel fuzzy model, along with physical and economic indicators, feeds into the fuzzy decision-making system, which uses an Analytic Hierarchy Process (AHP) to assign exponentially weighted (EW) preferences to each index. A novel fitness function is then constructed using t-norm aggregation (product and sum), and is optimised using the HFRCPSO-CF, which handles constraints and searches for optimal tilt (β) and orientation (γ) angles.

This overall architecture enables the integration of climatic modelling, energy analysis, and intelligent optimisation into a unified, flexible methodology tailored to regional and operational contexts in Argentina (see Section 2.3.1). This framework forms the basis of the developments shown in Figures 2 to Figure 6, each of which focuses on a specific layer of the methodology. To avoid repetition, any aspects not explained in a given figure are covered in subsequent ones.

Fitness function and hybrid constraints: Figure 2 shows how the fuzzy fitness function is developed for use in the HFRCPSO-CF optimisation process. This function combines three energy indicators — Net Present Value (NPV), Obtained Energy (OE) and Invested Energy (IE) — with user-defined preferences derived through the AHP. These preferences are represented as EW in fuzzy functions that translate normalised performance values into prioritised decision criteria.

The methodology incorporates two types of constraints:

- Hard constraints, which define strict physical or technical limits (e.g. limits on panel tilt/orientation), are enforced by modifying particle positions using the sort strategy explained in Section 2.2.9 and applying a boundary reflection strategy (see Section 2.2.11 and Appendix A Section A.1.1). This approach yields technically feasible solutions, albeit potentially at the expense of losing promising candidate solutions.
- Soft constraints, in contrast, are introduced by fuzzifying the search space using empirical motion limits derived from historical performance in cases 1–8. This means that these empirical bounds are derived from the system's behaviour in these cases, enabling more flexible exploration of the search space. This allows for more flexible navigation of the optimisation landscape without ruling out promising solutions. The fuzzy T-norm operator applies the algebraic product to optimise performance indices and the algebraic sum to handle soft constraints (see Sections 2.2.3 and Appendix A Section A.1.1).

This dual aggregation strategy enhances the model's ability to explore feasible, high-quality solutions under uncertainty and dynamic trade-offs. Any aspects not explained in this figure are covered in subsequent ones to avoid repetition.

Neural Network training, optimisation, simulation and hybrid constraints:

Figure 3 shows how an RBF is integrated with the HFRCPSO-CF. First, the RBF is trained using weather data (e.g. temperature, dew point, rainfall and precipitation), followed by calendar variables (day and hour).

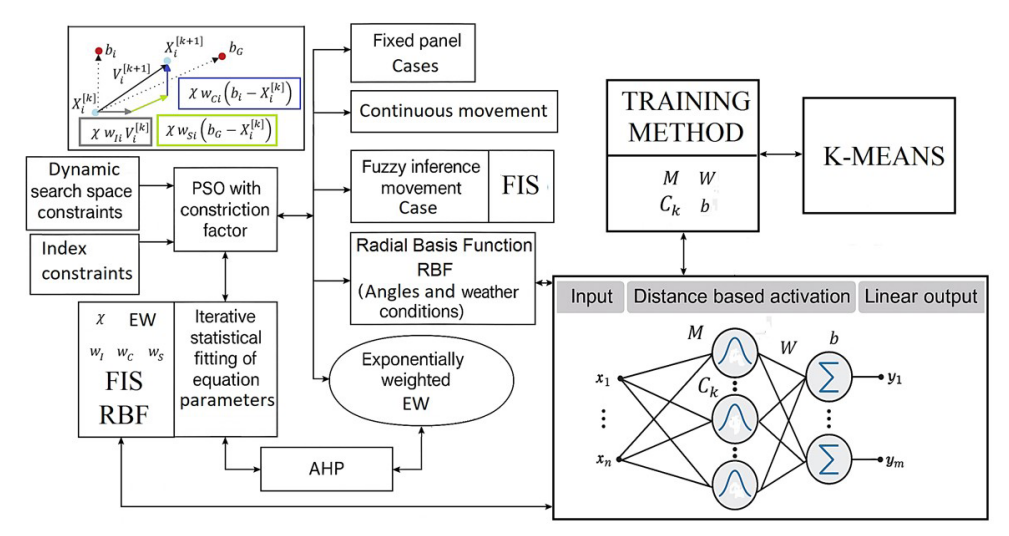


Figure 3. Hybrid Fuzzy-Rigid Constraint Particle Swarm Optimisation with Constriction Factor (HFRCPSO-CF) and a radial basis function.

Source: The authors.

This allows the climatological data and the optimal β and γ angles for each location to be estimated (Case 8). These weather predictions provide a data-driven estimate of how the system will behave under different environmental conditions. During RBF training, the K-means method is used to adjust the number and positions of neurons in the hidden layer (see Section 2.2.2 and Section 2.2.4). The performance of the RBF model is evaluated using the mean squared error (MSE) metric to compare the predicted and actual values during training. Training of the RBF model continued until the MSE fell below a predefined threshold. This strikes a balance between model accuracy and complexity.

The HFRCPSO-CF uses this information to inform the optimisation process, improving convergence and enabling adaptive responses to regional variability. As previously demonstrated, the metaheuristic incorporates hybrid dynamic boundary constraints and decision weights derived from fuzzy logic and AHP (see Section 2.2.3). The novelty lies in combining these Al tools. Together, they enable the system to anticipate and refine optimal configurations through evolutionary search, thereby enhancing robustness and accuracy in real-world scenarios. Any aspects not explained in this figure are covered in subsequent ones, to avoid repetition.

Novel optimisation, hybrid constraints and boundary reflection: Figure 4 shows how the fuzzy-guided feedback system works in HFRCPSO-CF, in terms of position updates and boundary handling with hybrid constraints.

Panel (a) illustrates the velocity and position update rule. Here, each particle adjusts its trajectory based on three components: inertia, personal best, and global best. These components are scaled by a constraint factor (γ), which regulates the magnitude of the updates and improves convergence stability. Panel (b) illustrates the strategy for addressing hard constraints. When a particle moves beyond the boundaries of the feasible search space (i.e. the maximum or minimum of β and γ), it is reflected symmetrically back into the domain. This reflection mechanism enforces physical feasibility without abruptly discarding the solution, thus preserving swarm dynamics. Together, these elements ensure the optimisation process remains technically viable and robust while maintaining search efficiency when navigating complex environments with multiple constraints, such as those encountered in real-world solar tracking systems.

Figure 5 illustrates the impact of exponentially weighted (EW) preferences on the fuzzy decision-making process and the optimisation behaviour of the HFRCPSO-CF. Panels (a) and (b) illustrate how the shape of the preference function changes with different EW values. Higher EW values result in sharper, more selective functions, whereas lower EW values soften the preference response, allowing greater tolerance in attribute evaluation. Panel (c) illustrates the incorporation of preference-modified index values, such as NPV, OE and IE, into the HFRCPSO-CF's position update mechanism. Rather than applying a strict, threshold-based evaluation, the fuzzy system uses these dynamic preferences to guide the swarm within a 'soft-constrained' search space. Using EW preferences in both fuzzy inference and PSO enables the optimisation process to be fine-tuned according to the priorities of human decision-makers. This improves adaptability and the quality of solutions in multi-objective, constraint-laden solar tracking scenarios.

Analytic Hierarchy Process (AHP): Figure 6 shows how the AHP (Kizielewicz et al., 2024; Kuttybay et al., 2024; Hadroug et al., 2023; Güler et al., 2025; Saraji et al., 2024; Chrifi-Alaoui et al., 2025; Camargo, 2022; Camargo et al., 2024) is used to derive exponentially weighted (EW) priorities for the attributes involved in the optimisation process ($a_{ij} = \frac{EW_i}{EW_i}$).

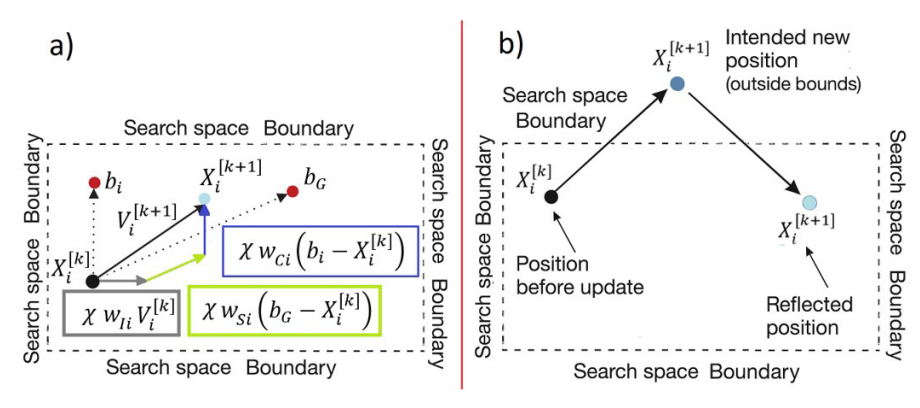


Figure 4. Hybrid Fuzzy-Rigid Constraint Particle Swarm Optimisation with Constriction Factor (HFRCPSO-CF): (a) Boundary reflection and (b) Rigid constraints.

Source: The authors.

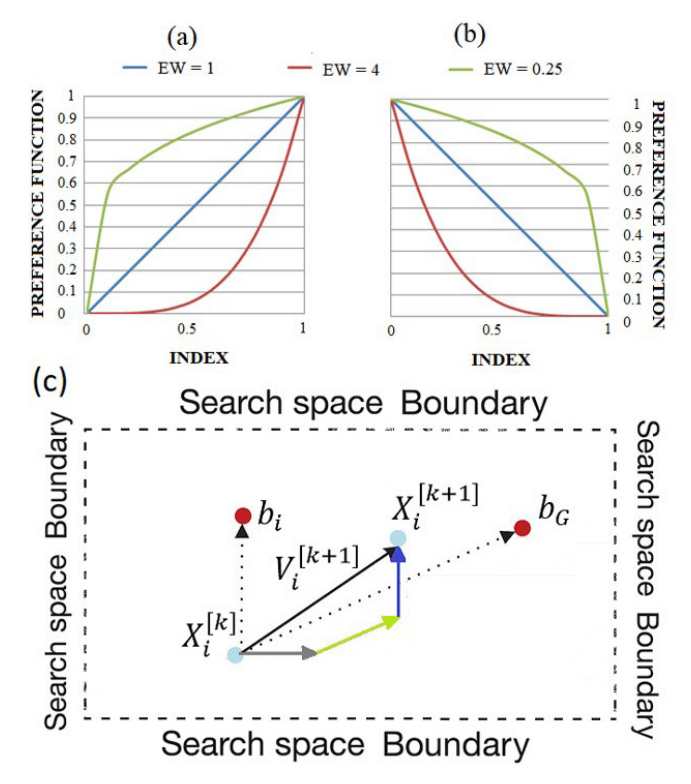


Figure 5. (a) Decreased function, (b) Growth function and (c) Search space boundary with fuzzy constraints.

Source: The authors.

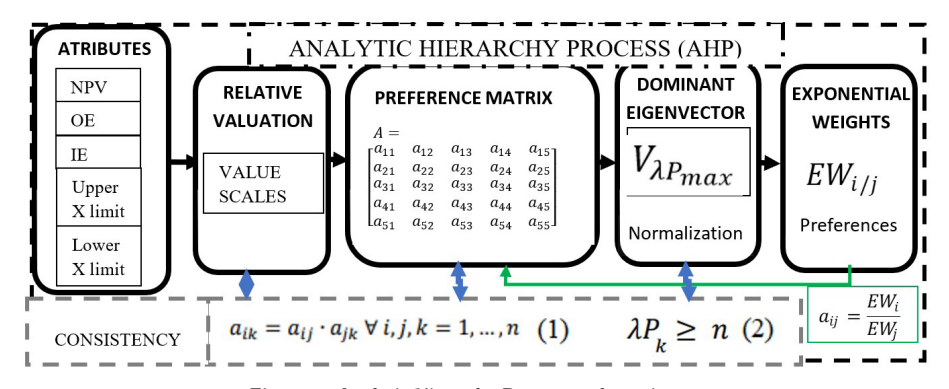


Figure 6. Analytic Hierarchy Process and consistency.

Source: The author.

The relative importance of each attribute $a_{ij} = \frac{1}{a_{ji}}$ – namely, NPV, OE, IE, and the search space constraint –

is encoded in a pairwise comparison matrix that satisfies the consistency condition, thereby ensuring logical coherence in the preference structure. The Perron theorem is then applied to extract the dominant eigenvector from the matrix. This is normalised to produce the exponential weights (EWs). The EWs are then used to shape the fuzzy preference functions shown in Figure 1 to Figure 5. They are also incorporated into the HFRCPSO-CF fitness evaluation. This approach enables decision-makers to express their preferences flexibly while ensuring mathematical consistency. It also directly influences the direction of the search and the evaluation of solutions in the HFRCPSO-CF, thereby ensuring that the optimisation process aligns with technical criteria and stakeholder priorities. The next section provides insights into the implementation of the algorithms of this methodology.

2.2. Programs of the proposed novel methodology

This section outlines the key programmes developed to implement the methodology detailed in the previous section. Due to space limitations, the detailed derivations of many equations have been omitted. These equations have been refined and condensed using established models from the literature to reduce space, computational load while capturing the influence of key climatic factors more accurately (see Tables 1 to Table 4 and Section 2.2.1). The fundamental mathematical developments supporting this implementation can be found in the Appendix A.

2.2.1. Main parameters used in programs of this section

The parameters used in the beginning of the program in this methodology are obtained from four clearly defined sources:

- (1) Government (Argentina, 2025a, b; Compañía Administradora del Mercado Mayorista Eléctrico, 2025) and data from governmental and private meteorological stations (Entre Ríos, 2025; La Rioja, 2025; San Juan, 2025; Meteored, 2025; Meteoblue, 2025; WeatherSpark, 2025; Straffelini et al., 2023; Ovando et al., 2021; Palmero et al., 2022).
- (2) Technical specifications from regional manufacturers, industry and software (lchi, 2025; National Renewable Energy Laboratory, 2025; Hoseinpoor et al., 2020, National Instruments, 2025; Photovoltaic Geographical Information System, 2025; Ré et al., 2021; Ceballos et al., 2023; Ortega et al., 2024. In addition, the available works, models and software of the tools are used to build and validate the proposed models.
- (3) Results from our own experimental and methodologic work (Camargo, 2022; Camargo et al., 2024; Sarroca et al., 2024).
- (4) Reviewed literature, as clarified in the provided tables (see Table 1 to Table 4).

Table 5 shows a summary of the data (latitude $\varphi[\circ]$, longitude $L[\circ]$, time zone $t_{zone}[h]$, Altitude[masl] and the constants $C_1\left[\frac{10^{-4}\ u}{masl}\right]$ and $C_2[u]$ to obtain the total solar irradiance, average summer temperature,

Average winter temperature, average precipitation and average relative humidity $SRH \lfloor \% \rfloor$ for all provinces. $\varphi \lceil \circ \rceil$ and $L \lceil \circ \rceil$ have a direct effect on the climate of each city: LR (further north and at a lower altitude) has a warmer climate, with summer temperatures of $30^{\circ}C$ and rainfall of 640 mm. SJ, further south and at a higher altitude (800 m), has more extreme temperatures, especially in winter ($5^{\circ}C$), and less rainfall (200 mm). ER, further south and at a lower altitude (127 m), has a temperate climate with more frequent rainfall (1284 mm) and moderate temperatures. $\varphi \lceil \circ \rceil$ influences solar radiation and the general climate, while altitude and geographical position also play an important role in temperatures and rainfall.

 C_2 is a constant, independent of the location, while C_1 has been calibrated with the mean air mass $AM \left[u \right]$ data from the meteorological stations in order to minimise the mean square error with respect to the calculated value (see Equation 57). The neural network (see Section 2.2.4. and Appendix A Section A.2) was trained with two inputs (day and time) and two outputs (ambient temperature, cloud cover and precipitation) using data available from the weather record. The margin of error of this was 3% and is therefore considered acceptable. For reasons of space, this is not developed in this article.

Table 5. Parameters used in the mathematical model for all provinces.

Provinces	$\varphiigl[\circigr]$	L[°]	$t_{zone}[h]$	Altitude [<i>masl</i>]	$\begin{bmatrix} C_1 \\ 10^{-4} & u \\ masl \end{bmatrix}$	$C_2[u]$	Average Summer T[°C]	Average Winter $T[^{\circ}C]$	Average precipitation [mm]	Average SRH [%]
La Rioja	-29.41	-66.85	-4	515	4.9	1.2	30 ± 7	10±5	332	50±10
San Juan	-31.53	-68.53	-4	800	4	1.2	33±7	5±5	102	40 ± 12
Entre Ríos	-32.48	-58.23	-3	127	10	1.2	25 ± 7	12 ± 7	1184	64 ± 5

Source: The Authors.

The maximum, minimum and average restrictions for tilt angles, orientation and beta are obtained from an analysis of radiation maps produced by this model. These maps showed that for inclinations between 45° and 60°, a higher level of energetic irradiance is not achieved; rather, it decreases. Therefore, an inclination of up to 60° was considered. The minimum restriction of 15° was determined by calculating the minimum viable inclination to prevent water accumulation on the panels, which could affect their performance. A safety factor was applied to this calculation. The solar panel is designed to have a maximum difference of 90° with respect to the sun's orientation, and these limits are defined accordingly (Appendix A Sections A.1. and A.2).

Table 6 presents the Lower U^{Low} and upper U^{Up} limits of objective and constraint, Exponential Weights EW_m and their maximisation ($\xi=1$) or minimisation ($\xi=0$) for all provinces. Appendix A Sections A.1 and A.2. outlines the parameters employed in the radial basis neural network and the Gaussian fuzzy inference system.

2.2.2. Main program

As shown in Figure 1, the Main Program is a complex process involving the simulation and optimisation of a solar power generation system. This system uses a Radial Basis Function (RBF) to predict weather data and determine the best parameters for the system. The programme begins by collecting technical and power data from various energy sources using input particles (X), which are associated with different tilt and orientation scenarios. An RBF is then trained to predict climatological data, such as temperature and precipitation. This RBF is subsequently applied to specific fixed-angle, tilt and motion scenarios in order to evaluate the total solar radiation, voltage, current and power generated.

An algorithm of objective functions and constraints is used to optimise the fitness function associated with the different scenarios, and the results for tilt (β) and orientation (γ) are returned. Life cycle analysis of a solar panel with a productive chain programme (Camargo, 2022; Camargo et al., 2024; Hammi et al., 2024) calculates the cost of producing the solar panel, taking into account material and fuel flows at each stage of the production chain (see Figure 1).

BEGIN /* Main Program */

Data: climatological, technical and life cycle data of solar system (see Section 2.2.1.).

Output: scenarios of the tilt β and orientation γ of solar system in X.

BEGIN /* Life Cycle Analysis of solar panel with productive chain */

Data: material composition of solar panel (see Section 2.1. and Section 2.2.1.).

Step 1: Calculate material and fuel flows by stage in the production chain: resource extraction, material processing, manufacturing, construction, transport and waste. Calculate the production costs of solar system associated (investment cost $C_I \left[USD \right] = 1000$, economic investment cost overhead $ECO \left[u \right]$ and energy price $p_g \left[\frac{USD}{kWh} \right] = 0.25$).

Step 2: Define X in relation to the relevant cases or scenarios. The options are: A) fixed angles: 0° (Case 1), 15° (Case 2), 30° (Case 3) and 45° (Case 4); B) fixed tilt and motion angles (Case 5); C) continuous motion (Case 6); and D) fuzzy inference system motion (Case 7).

FOR Case = 1:9 DO

BEGIN /* Training a Radial Basis Function (RBF) Neural Network (see Section 2.2.4.) */

Table 6. Lower U^{Low} and upper U^{Up} limits of objective and constraint, Exponential Weights EW_m and their maximisation ($\xi = 1$) or minimisation ($\xi = 0$) for all provinces.

Attributes	Upper Limits $\emph{U}^{\emph{Up}}$	Lower Limits $oldsymbol{U^{Low}}$	EW	ξ
Obtained Energy [kWh]	Best case or combination best case	Worst-case or combined worst-case	1.25	1
Invested Energy kWh	Best case or combination best case	Worst-case or combined worst-case	1.00	0
Net Present Value [USD]	Best case or combination best case	Worst-case or combined worst-case	1.00	1
Upper constraint of $oldsymbol{eta}$	$\min\left(\theta_z + 15, 60\right)$	$ heta_z$	0.50	1
Lower constraint of $oldsymbol{eta}$	$ heta_z$	15	0.50	1
Upper constraint of γ	$\min\left(A_z + 90,90\right)$	A_z	0.50	0
Lower constraint of γ	A_Z	$\max\left(A_z - 90, -90\right)$	0.50	1

Source: The Authors.

Step 3: If Case = 1, then start Training a RBF for input hour and day and outputs climatological data: temperature T_e , dew point temperature T_d , rainfall and precipitation F_{clim} .

Step 4: If Case = 8, then start training a RBF for input hour and day and outputs (inclination β and orientation γ) of the obtained cases. Save the inclination β and orientation γ in the particle X (Case 8).

BEGIN /* Fuzzy fitness function */

Step 5: start Fuzzy fitness function program (see Section 2.2.10.).

BEGIN /* Hybrid Fuzzy-Rigid Constraint Particle Swarm Optimisation with Constriction Factor */

BEGIN /* Algorithm of Objective Functions and Constraints */

Step 6: If Case = 9 then start the Objective Functions and Constraints program with the boundary cases (Section 2.2.8. and Section 2.3.2.) and start HFRCPSO-CF (see Section 2.2.11.).

2.2.3. Fuzzy fitness function

The Fuzzy fitness function program optimise a solar power generation system, using parameters such as the tilt (β) and orientation (γ) of the generation sources. It starts with the analysis of technical and power data of each power source, and then an algorithm is applied to calculate the main parameters of the system. Several factors are evaluated, such as total solar radiation and generated voltage, current and power variables. Fuzzy decision-making functions are also incorporated to optimise system decisions, which is evaluated using an objective function and constraint (see Section 2.2.5. to Section 2.2.10.).

BEGIN /* Fuzzy fitness function */

Data: Power and technical data (see Section 2.2.1.).

Input: Particle X corresponding to swarm (tilt β and orientation γ), for each generation source studied.

Output: Fuzzy fitness function f(X), attributes U.

BEGIN /* Algorithm of main parameters */

Step 1: Start Algorithm of main parameters program (see Section 2.2.5.).

BEGIN /* Fuzzy decision making with this new methodology */

Step 2: Start The total solar radiation program (see Section 2.2.6.).

Step 3: Start Solar Voltage, Current and Power program (see Section 2.2.7.).

Step 4: Start Algorithm of Objective Functions and Constraints program (see Section 2.2.8.).

Step 5: Obtain the EW using the AHP (see Section 2.1.) and start HFRCPSO-CF (see Section 2.10.).

2.2.4. Radial Basis Function (RBF) program

A radial basis function (RBF) training algorithm uses the K-means method to produce desired outputs from training data. An RBF consists of two layers: a hidden layer applying a radial activation function and a linear output layer combining the hidden layer's outputs (Praveen & Menaka, 2024; Koshkarbay et al., 2024; Molu et al., 2024).

BEGIN /* Training a Radial Basis Function (RBF) Neural Network */

Data: Initially, the centres of the hidden neurons are equal to the input set $(C_k = x)$. The influence of each neuron in the input space d_{max} is obtained by trial and error and statistical data (see Section 2.2.1., Appendix A Section A.2, Table 5 and Table A1).

Input: Input data set x with N inputs and S samples and a desired output set Y with Q outputs and S samples.

Output: predicted output set Y_{new} with Q outputs and S samples.

WHILE $((MSE \ge 3\%Y_d))$ DO

Step 1: through the K-means method, the number of hidden layers (M) and centres (C_k) are adjusted to minimise the mean squared error (MSE). At each stage of the process, the Gaussian domains and the distance $x-C_k$ are calculated by allocating x to C_k . Then x will then belong to the centre C_k whose calculated distance is smallest.

Step 2: The new centres, C_k , are calculated as the average of the x-values belonging to C_k . Convergence has been achieved and learning is complete if C_k does not differ from the previous iteration.

Step 3: Equation 1 calculates the Gaussian activation function ε_k of the distance $x-C_k$.

$$\varepsilon_k = \exp\left(-\frac{\left(x - C_k\right)^2}{2\sigma^2}\right) \quad \forall \left(\sigma^2 = \frac{\left(d_{max}\right)^2}{2M}\right)$$
 (1)

Step 4: Equation 2 create the hidden layer output matrix with activations [Nx(M+1)]. A column of ones is added to include the bias b in the linear combination of the hidden neuron.

$$O = \begin{bmatrix} \varepsilon_1 & \varepsilon_2 \dots \varepsilon_k & Ones_M \end{bmatrix}$$
 (2)

Step 5: Equation 3 calculates the output weights W and biases b by solving this system of linear equations (with a linear regression method). In this equation $\left(O^TO\right)^{-1}O^T$ is the pseudoinverse of O.

$$[W \ b] = pseudoinverse(O) \ Y = \left(\left(O^T O \right)^{-1} O^T \right) Y$$
(3)

Step 6: Equation 4 calculate the output value Y_{new} as a linear combination of the radial layer neurons outputs O, the output weights W and the bias b (see Equation 3). The MSE is used to evaluate the performance of the RBF. This equation is used to predict outputs for new input data once it has been trained.

$$(Y_{new} = W O + b) \bigcap \left(MSE = \sqrt{\sum \frac{(Y_{new} - Y)^2}{size(Y)}} \right)$$
(4)

2.2.5. Algorithm of main parameters program

The Algorithm of main parameters program describes the calculation of key parameters for determining the position of the sun and the lighting conditions in a solar power system. Where $\varphi[\circ]$ is the latitude of the location, $\delta[\circ]$ is the solar declination (which varies throughout the year) and ω is the hour angle, $\beta[\circ]$ is the tilt angle $(0 < \beta < 90^\circ)$, γ is the orientation angle $(-90^\circ < \gamma < 90^\circ)$ and $sign(\varphi)$ take into account the sign of the latitude (northern or southern hemisphere). $\omega[\circ]$ measures the angular displacement of the Sun from the solar meridian or solar noon. The tilt angle $\beta[\circ]$ is 0 at horizontal and 90° at maximum tilt. The orientation angle gamma is -90° when facing east, 0 when facing north and 90° when facing east. Equation 11 is obtained by analysing the different vectors resulting from the angles involved and making the corresponding projections by means of scalar products (Wu, et al., 2022; Ichi, 2025; Sobirov et al., 2023; Kuttybay et al., 2024; Azam et al., 2024). Many bibliographies (see Table 1) have studied the northern hemisphere, which causes problems in the results when trying to apply them to the southern hemisphere, so a factor has been taken into account that changes the sign of some of the components.

BEGIN /* Algorithm of main parameters */

Data: latitude, longitude and time zone (see Section 2.2.1.).

Output: it returns the time of sunrise, sunset, the length of the day (H_{sun}) and the associated constraints. Step 1: Firstly, Equation 5 calculates the fractional year $x[\circ]$. Other constants available are Const = -3 or Const = -10. Secondly, Equation 6 calculates the angle of solar declination $\delta[\circ]$ which is the projection of the Sun on the celestial sphere relative to the Earth's equator. Thirdly, Equation 7 calculates the equation of time EoT[min] (Sobirov et al., 2023).

$$x^{[\circ]} = \frac{365}{180} (m - \text{Const}) = \frac{2\pi}{365} \left(m - 1 - \frac{h - 12}{24} \right) \quad \forall \left((1 < m < 365) \cap (1 < h < 24) \right)$$
 (5)

$$\delta[^{\circ}] = \frac{180}{\pi} 10^{-3} \begin{pmatrix} 7 - 399 \cos(x) + 702 \sin(x) - 7 \cos(2x) + \\ 0.9 \sin(2x) - 3 \cos(3x) + 1.48 \sin(3x) \end{pmatrix} = \begin{cases} -23.45 \cos(x), & \text{(Upper Limit)} \\ (+), & \text{($\varphi < 0$)} \cap (80 < m < 264) \\ 23.45, & \text{($\varphi < 0$)} \cap (m = 355) \\ (-), & \text{($\varphi < 0$)} \cap ((264 < m) \cap (m < 80)) \\ -23.45, & \text{($\varphi < 0$)} \cap (m = 172) \end{cases}$$
(6)

$$EoT\lceil min \rceil = 229.1810^{-3} \left(0.075 + 1.8\cos(x) - 32\sin(x) - 14\cos(2x) - 40\sin(2x) \right) \tag{7}$$

Step 2: Equation 8 calculates the sunrise angle $W_{\mathcal{S}}$ and Equation 9 calculates the hour angle ω [°]. They are for a given location with a longitude L[°] time zone t_{zone} [h] according to its time difference from UTC. For the special case of sunrise or sunset, the $\theta_{\varepsilon}=90.83$ with an approximate correction for atmospheric refraction (Sobirov et al., 2023).

$$W_{s}[\circ] = a\cos\left(\frac{\cos(90.83)}{\cos(\varphi)\cos(\delta)} - \tan(\varphi)\tan(\delta)\right) \ge a\cos\left(-\tan(\varphi)\tan(\delta)\right)$$
(8)

$$\omega[^{\circ}] = \left(\frac{\left(60 \ h + 4\left(L - 15t_{zone}\right) + EoT\right)}{4} - 180\right) \quad \forall \left((1 < m < 365) \cap \left(H_{Sem} \le h \le H_{Stm}\right)\right) \tag{9}$$

Step 5: the present work uses Equation 10 to calculate the Solar noon time $H_{soon}[h]$, sunshine time $H_{soon}[h]$ and the sunset time $H_{soon}[h]$. Where EoT is in minutes and the latitude $\varphi[\circ]$ is positive to the east of the Prime Meridian.

$$\begin{pmatrix}
H_{Sn} \\
H_{Se} \\
H_{St}
\end{pmatrix} = \text{round} \left(12 - \frac{L - 15t_{zone}}{15} \right) \begin{pmatrix} 1 \\ 1 \\ 1 \end{pmatrix} + \frac{EoT}{60} \begin{pmatrix} 0 \\ -1 \\ 1 \end{pmatrix} \right) \tag{10}$$

Step 6: In the present work, Equation 11 calculates the solar incidence angle θ_z [°] and the azimuth angle A_z [°]. Finally, the present work uses Equation 12 to calculate the constraints with upper and lower limits.

$$\begin{pmatrix} \theta_z \\ A_z \end{pmatrix} = \begin{pmatrix} a\cos\left(\sin(\varphi)\sin(\delta) + \cos(\varphi)\cos(\delta)\cos(\omega)\right) \\ - a\tan\left(\frac{\cos(\varphi)\cos(\delta)\sin(\omega)}{\sin(\delta) - \sin(\varphi)\cos(\theta_z)}\right) \end{pmatrix}$$
 (11)

$$Constraint = \left(\min\left(\theta_z + 15, 60\right) \ge \beta \ge 15\right) \cap \left(\min\left(\left(A_z + 90\right), -90\right) \ge \gamma \ge \max\left(\left(A_z - 90\right), -90\right)\right) \tag{12}$$

2.2.6. Total solar radiation program

The total solar radiation program calculates the total solar irradiance $G_{\beta,\gamma}$ reaching an inclined and oriented panel, taking into account the atmospheric conditions (Sobirov et al., 2023; Praveen & Menaka, 2024; Azam et al., 2024). The programme returns $G_{\beta,\gamma}$, which is used in the performance analysis of the solar energy system. BEGIN /* The total solar radiation */

Data: latitude angle φ , declination δ , tilt β , orientation γ , hour angle ω , altitude and temperature T_e (see Section 2.2.1.).

Input: tilt or inclination β and orientation γ .

Output: total solar irradiance $G_{\beta,\gamma}\left\lceil \frac{kW}{m^2}\right\rceil$.

Step 1: In the present work, Equation $1\vec{3}$ is improved to calculate the factor $\cos\theta$ with any panel tilt angle β and orientation γ . When the beta angle is zero (i.e. there is no tilt) and the gamma angle is also zero (i.e. it is oriented north), the azimuthal angle $\theta[\circ]$ is equal to the $\theta_z[\circ]$ angle (Ahamed et al., 2021; Kuttybay et al., 2024).

$$\cos\theta[u] = \sin(\varphi) \sin(\delta) \cos(\beta) - \operatorname{sign}(\varphi) \cos(\varphi) \sin(\delta) \sin(\beta) \cos(\gamma) + \cos(\varphi) \cos(\delta) \cos(\beta) \cos(\varphi) + \operatorname{sign}(\varphi) \sin(\varphi) \cos(\delta) \sin(\beta) \cos(\gamma) \cos(\varphi) + \cos(\varphi) \cos(\delta) \sin(\beta) \sin(\gamma) \sin(\varphi) \ge 0.1 \quad \forall (15 \le \beta \le 60) \cap (-90 < \gamma < 90)$$

Step 2: Equation 14 calculates the extra-terrestrial daily and hourly mean horizontal radiation. On the other hand, Equation 15 gives the extra-terrestrial daily and hourly horizontal irradiance $H_{0\beta,\ \gamma}$ for any tilt β and orientation γ (Sobirov et al., 2023; Praveen and Menaka, 2024; Azam et al., 2024).

$$G_{ext}\left[\frac{kW}{m^2}\right] = G_{sc}\left(\frac{r}{r_0}\right)^2 = 1.367\left(1 + 0.033\cos\left(180\frac{m-1}{365}\right)\right) \ \forall \ \left(1 < m < 365\right)$$
 (14)

$$H_{0\beta, \gamma} \left[\frac{kW}{m^2} \right] = \begin{cases} G_{ext} \cos(\theta), \ \forall (15 \le \beta \le 60) \cap (-90 < \gamma < 90) \\ G_{ext} \cos(\theta_z), \ \forall (\beta = 0) \cap (\gamma = 0) \end{cases}$$
(15)

Step 3: In the present work, Equation 16 is improved to calculate the air mass AM (Wu, et al., 2022; lchi, 2025) as a function of the angle of solar incidence θ_z , the ambient temperature T_e and atmospheric pressure (which varies with altitude).

$$AM = \begin{cases} \frac{1}{\cos(\theta_z) + 0.15(93.88 - \theta_z)^{-1.25}} \left(\frac{273}{273 + T_e} \right) \left(\frac{288.15}{288.15 - 0.0065 \text{ Altitude}} \right) \\ & \downarrow \qquad \qquad \downarrow \qquad \qquad \downarrow \\ Air Mass & Temperature & Pressure \\ correction & correction & correction \end{cases}$$
(16)

Step 4: In the present work, Equation 17 is improved to calculate the atmospheric transmission coefficient K_T and the factor f. Next, Equation 18 calculates the diffuse factor $\frac{H_d}{H}$ as a function of K_T (Sobirov et al., 2023; Kuttybay et al., 2024; Zou et al., 2024).

$$\left(K_T \left[u\right] = \frac{H}{H_0} = \left(1 - e^{-\left(C_1 \ Altitude + C_2\right)}\right)^{AM^{0.678}} F_{clim}\right) \cap \left(f\left[u\right] = \sqrt{1 - \frac{H_d}{H}}\right) \quad (17)$$

$$\frac{H_d}{H} \left[u \right] = \begin{cases}
1 - 0.09 \, KT, \ K_T <= 0.22 \\
0.95 - 0.16 \, K_T + 4.38 \left(K_T \right)^2 - 16.63 \left(K_T \right)^3 + 12.33 \left(K_T \right)^4, \ 0.22 \le K_T \le 0.80 \\
0.165, \ 0.8 \le K_T
\end{cases} \tag{18}$$

Step 5: In the present work, Equation 19 calculates the direct $R_{DIR\beta,\gamma}[u]$, diffuse $R_{DIF\beta,\gamma}[u]$, and albedo $R_{ALB\beta,\gamma}[u]$ irradiance for each day m and hour h. Finally, Equation 20 calculates the global solar irradiance $G_{\beta,\gamma}\left[\frac{kW}{m^2}\right]$ (Kuttybay et al., 2024; Zou et al., 2024; Kuttybay et al., 2024; Sobirov et al., 2023).

$$\begin{pmatrix}
R_{DIR\beta,\gamma} \\
R_{DIF\beta,\gamma} \\
R_{ALB\beta,\gamma}
\end{pmatrix} = \begin{pmatrix}
\left(\frac{\cos(\theta)}{\cos(\theta_z)}\right) K_T f^2 \left(1 + \frac{H_d}{H} K_T\right) \\
K_T \left(\frac{H_d}{H}\right) \left(1 - K_T f^2\right) \left(\frac{1 + \cos(\beta)}{2}\right) \left(1 + f\left(\sin\left(\frac{\beta}{2}\right)\right)^3\right) \\
0.15 \left(\frac{1 - \cos(\beta)}{2}\right)
\end{pmatrix} \tag{19}$$

$$G_{\beta,\gamma}\left[\frac{kW}{m^2}\right] = H_{0\beta,\gamma}\left(R_{DIR\beta,\gamma} + R_{DIF\beta,\gamma} + R_{ALB\beta,\gamma}\right) \qquad \forall \left(1 \le m \le 365\right) \cap \left(H_{Sem} \le h \le H_{Stm}\right) \quad (20)$$

The constant $G_{sc}\left[\frac{kW}{m^2}\right] = 1.367$ is the solar irradiance at the top of the atmosphere. The variable $\left(\frac{r}{r_0}\right)^2$ is

the eccentricity for the instantaneous distance and mean distance from the Sun to the Earth \mathbf{r} and r_0 , respectively.

The variable $H_{0\beta,\ \gamma}$ is the solar energy that reaches the Earth's surface directly from the Sun, without scattering or reflection. It occurs when the Sun is largely unobstructed by clouds, with the irradiance being more intense when the Sun is higher in the sky. It is proportional to the $\cos(\theta)$, so the energy production of the system depends mainly on this value. $\cos(\theta_z)$ adjusts the air mass AM according to θ_z , while the additional factor corrects this value by taking into account the non-linear behaviour of the atmosphere at different heights from the Sun. As the Sun moves away from the zenith (i.e. as θ_z increases), the irradiance has to pass through more of the atmosphere. This adjustment is particularly important when the sun is close to the horizon, as the irradiance passes through more atmosphere, increasing the AM. The factor 93.88 is an empirical constant that helps to adjust the model and formula for atmospheric conditions. The exponent -1.25 is a non-linear correction factor for the relationship with the angle θ_z , reflecting the behaviour of the atmosphere. The change in temperature and atmospheric pressure with ambient temperature correction is also included in this equation (Sobirov et al., 2023; Praveen and Menaka, 2024; Azam et al., 2024).

The atmospheric transmission coefficient K_T and the $\frac{H_d}{H}$ ratio play a crucial role in determining the amount of diffuse and direct irradiance reaching the Earth's surface. A lower K_T indicates a more cloudy atmosphere, resulting in a higher proportion of diffuse H_d irradiance compared to global H irradiance, while a higher K_T indicates a clearer sky and a higher proportion of direct irradiance. The $\frac{H_d}{H}$ ratio adjusts this behaviour, being higher when K_T is low and vice versa. The γ and β directly affect the amount of direct irradiance received by the system. Correct orientation maximises direct irradiance and minimises diffuse irradiance, particularly in partly cloudy conditions or when there is high atmospheric diffusion (Wu, et al., 2022; lchi, 2025).

The factor $\left(1-e^{-\left(C_1 \ Altitude + C_2\right)}\right)$ models the effect of altitude on irradiance transmission; as altitude

increases, the density of the atmosphere decreases, allowing more irradiance to pass through. It is an altitude-corrected, instantaneous clearness index that is linked to the absorption and dispersion coefficients of the Lambert-Beer-Bouguer law, and is integrated over a wide range of wavelengths (Sobirov et al., 2023; Kuttybay et al., 2024). Under clear sky conditions, the index characterises the attenuation of solar irradiance from a wavelength-integrated perspective due to atmospheric absorption and dispersion. The factor $AM^{0.678}$ adjusts for the influence of the air mass (AM), which depends on the position of the Sun, since when the Sun is lower in the sky (near the horizon) the irradiance has to pass through a larger portion of the atmosphere, increasing its scattering and absorption. This relationship is useful to obtain the total or average annual or monthly energy obtained by the solar panel, but difficult to apply when it is considered instantaneously in each hour and day of the year. Then, in this work the weather factor $F_{c\, lim}$ corrects the KT factor for cloudiness (Kuttybay et al., 2024; Zou et al., 2024).

2.2.7. Solar Voltage, Current and Power program

The Solar Voltage, Current and Power program calculates the power, voltage and current produced by a photovoltaic system, taking into account temperature variations and their effect on the performance of the solar panels.

BEGIN /* Solar Voltage, Current and Power */

Data: technical and economic data of solar system and temperature (see Section 2.2.1.).

Input: total solar irradiance $G_{\beta,\gamma}\left[\frac{kW}{m^2}\right]$ (see Section 2.6.).

Output: It returns the values of voltage (V_p) , current (I_p) and power (P_p) generated by the solar system.

Step 1: In the present work, Equation 21 is improved to calculate the variation of the coefficients with relative humidity SRH[%] (Hoseinpoor et al., 2020), where T_d is the dew point temperature. In this work,

Equation 22 gives the coefficients of variation of power $\mu_P \left[\frac{W}{^{\circ}C} \right]$, voltage $\mu_V \left[\frac{V}{^{\circ}C} \right]$ and current $\mu_I \left[\frac{A}{^{\circ}C} \right]$

using the dot product operator to multiply element by element. The correction coefficients are provided by the manufacturer and $(T_e < 25)$ is a Boolean value (0 or 1).

$$SRH\left[\%\right] = \begin{cases} 0, T_d \ll T_e \\ 100e^{\left(17.62\left(\frac{234.04\left(T_d - T_e\right)}{\left(234.04 + T_d\right)\left(234.04 + T_e\right)}\right)\right)}, T_d < T_e \\ 100, T_d = T_e \end{cases}$$
 (21)

$$\begin{pmatrix} \mu_P \\ \mu_V \\ \mu_I \end{pmatrix} = -\frac{1}{100} \begin{pmatrix} 0.43 \\ 0.33 \\ 0.06 \end{pmatrix} - \begin{pmatrix} T_e < 25 \end{pmatrix} \begin{pmatrix} 0.03 \\ 0.03 \\ 0.02 \end{pmatrix} \cdot \begin{pmatrix} 1 \\ 1 \\ 1 \end{pmatrix} + \frac{SRH}{100} \begin{pmatrix} 0.2 \\ 0.1 \\ 0.15 \end{pmatrix} \quad \forall \begin{pmatrix} G_{\beta,\gamma} \ge 0.1 \end{pmatrix}$$
 (22)

Step 3: Equation 23 actualise the temperature for panel T_P . Next, in the present work, Equation 24 is improved to calculate the maximum power point $P_{max_n}[W]$, voltage V_n) and current $Isc_{Ref_n}[A]$ for the effect of temperature variation with respect to 25°C. In this equation, the dot product operator is used to multiply element by element. They are based on the references (Zou, Y., Qin et al., 2024; Hraich & Haddi, 2025).

$$T_{P} \left[{}^{\circ}C \right] = T_{e} + \left(\frac{TONC - T_{ref}}{G_{ref}} \right) G_{\beta,\gamma} = T_{e} + \left(\frac{45 - 25}{1} \right) G_{\beta,\gamma} = T_{e} + 20 G_{\beta,\gamma}$$
 (23)

$$\begin{pmatrix} P_{max_n} \\ V_n \\ Isc_{Ref_n} \end{pmatrix} = \begin{pmatrix} P_{max} \\ V_{end} \\ Isc_{Ref} \end{pmatrix} \cdot \begin{pmatrix} P_{max} \\ V_{end} \\ Isc_{Ref} \end{pmatrix} + (T_e - 25) \begin{pmatrix} \mu_P \\ \mu_V \\ \mu_I \end{pmatrix}$$
(24)

Step 4: In the present work, Equation 25 calculates the thermal voltage $V_T[V]$ and the current of solar system I[A] iteratively. They are based on the references (Hraich & Haddi, 2025).

$$\begin{pmatrix} V_{T} \\ I \end{pmatrix} = \begin{pmatrix} k_{B} \left(\frac{T_{p} + 273.15}{q} \right) \\ max \left(\frac{\min\left(G_{m,h}, G_{ref}\right)}{G_{ref}} \right) Isc_{Ref_{n}} - \left(\frac{Isc_{Ref_{n}}}{\left(\frac{V_{n}}{N_{s} \ a \ V_{T}}\right)} - 1 \right) \left(e^{\left(\frac{V + I \ R_{s}}{N_{s} \ a \ V_{T}}\right)} - 1 \right) - \left(\frac{V + I \ R_{s}}{R_{sh}} \right), 0 \end{pmatrix} \right) \tag{25}$$

Step 5: Finally, in the present work, Equation 26 is improved to calculate the voltage $V_p[V]$, current $I_p[A]$ and the power $P_p[W]$ for each hour h and day m. The maximum power point of the voltage-current curve is sought, with which the power obtained by the solar system is calculated.

$$\begin{pmatrix} V_p \\ I_p \\ P_p \end{pmatrix} = \begin{pmatrix} V_{I \ V = \max(I \ V)} \\ I_{I \ V = \max(I \ V)} \\ \min \left(V_p \ I_p \eta \ , P_{\max} \right) \end{pmatrix}$$
(26)

2.2.8. Algorithm of Objective Functions and Constraints program

The Algorithm of Objective Functions and Constraints program optimises a power generation system by calculating objective functions and constraints.

BEGIN /* Algorithm of Objective Functions and Constraints */

Data: Power and technical data, the t_d discount rate and UL represents the life of the project (see Section 2.2.1.). Input: the initial investment cost $C_I \begin{bmatrix} USD \end{bmatrix}$, the production cost per unit of energy produced P_g (see Section 2.7.).

Output: Objective and Restriction Functions U.

Step 1: Equation 27 calculates the Capital Recovery Factor (Camargo, 2022; Camargo et al., 2024) and the generation cost $C_G \left[USD \right]$ are calculated in at a useful life UL of 30 years and a given discount rate (t_d) .

$$CRF\left[u\right] = \frac{t_d \left(1 + t_d\right)^{UL}}{\left(1 + t_d\right)^{UL} - 1} = \frac{0.1 \left(1 + 0.08\right)^{30}}{\left(1 + 0.08\right)^{30} - 1} = 0.11 \Rightarrow C_G\left[USD\right] = CRF C_I = 234 \left[USD\right]$$
(27)

BEGIN /* Sort of particle X */

Step 2: Start Sort of the search vector \mathbf{X} (see Figure 2 to Figure 5).

Step 3: in the present work, Equation 28 is developed to calculate the obtained energy. To speed up the programme, the calculation is made with only one year to work with less data.

$$U_{i=1} = E_{(Y=1)}[kWh] = \frac{\sum_{m=1}^{m=365} \sum_{h=H_{Sem}}^{h=H_{Sem}} P_p}{1000}$$
(28)

Step 4: in the present work, Equation 29 and Equation 30 calculate the angular movement of the tracker tilt and orientation respectively (see Figure 1 to Figure 5, Section 2.2.1 and Appendix A Section A.1). Equation 31 calculates the total energy consumed by this angular movement $\Delta E_{I(Y=1)}[u]$. To speed up the program, it is

made with only one year to work with less data. The factors $\frac{\Delta\beta}{180\ 365}[u]$ and $\frac{\Delta\gamma}{360\ 365}[u]$ are the proportion of energy expended, including the return to the starting point. It is estimated that the maximum energy invested should be 12% of the total energy produced. In addition, the movement of β represents 40% of the energy cost, while the movement of γ represents 80% of the energy cost.

$$\Delta \beta_{(Y=1)} [\circ] = \sum_{m=1}^{365} \left(\sum_{H_{Sem}+1}^{H_{Sem}} \left(\left| \beta_{m,h} - \beta_{m,h-1} \right| + \left| \beta_{m,H_{Sem}} - \beta_{m,H_{Sem}} \right| + \left| \beta_{m,H_{Sem}} - \beta_{m,H_{Sem}} \right| \right) + \left| \beta_{m,H_{Sem}} - \beta_{m-1,H_{Sem}} \right| \right) + \left| \beta_{m,H_{Sem}} - \beta_{m-1,H_{Sem}} \right| \right) + \left| \beta_{m,H_{Sem}} - \beta_{m-1,H_{Sem}} \right|$$

$$\left| \beta_{1,H_{Sel}} - \beta_{365,H_{Se365}} \right|$$
(29)

$$\Delta \gamma_{\left(Y=1\right)} \left[\circ \right] = \sum_{m=1}^{365} \left(\left| \frac{H_{Stm}}{H_{Sem}} \left(\left| \gamma_{m,h} - \gamma_{m,h-1} \right| + \left| \gamma_{m,H_{Sem}} - \gamma_{m,H_{Stm}} \right| \right) + \left| \gamma_{m,H_{Sem}} - \gamma_{m-1,H_{Sem}} \right| \right) + \left| \gamma_{1,H_{Se1}} - \gamma_{365,H_{Se365}} \right|$$
(30)

$$U_{2}[u] = \Delta E_{I(Y=1)}[u] = \frac{0.12}{180 \ 365} \left[\Delta \beta_{(Y=1)} \quad \frac{\Delta \gamma_{(Y=1)}}{2} \right] \begin{bmatrix} 0.4\\0.6 \end{bmatrix}$$
(31)

Step 5: in the present work, Equation 32 is improved to calculate the Net Present Value in 10 years (see Section 2.2.1). In this equation, $Y \begin{bmatrix} year \end{bmatrix}$ are the years, $t_d \begin{bmatrix} u \end{bmatrix}$ is the discount rate and $UL \begin{bmatrix} year \end{bmatrix}$ represents the life of the project. In addition, $ECO \begin{bmatrix} u \end{bmatrix}$ represents the economic investment cost overhead compared to a fixed solar system and $C_G \begin{bmatrix} USD \end{bmatrix}$ is the annual operating and maintenance cost. Finally, the panel loses 0.65% of energy produced per year (see Figure 1 to Figure 5 and Section 2.2.1. to Section 2.2.4.).

$$U_{3}[USD] = NPV = -C_{I}(1 + ECO) + \sum_{Y=1}^{10} \left[\left(\frac{1 + t_{i}}{1 + t_{d}} \right)^{Y} \left(E_{Y} \ p_{g} \left(1 - \Delta E_{I} \right) \left(1 - 0.0065 \right)^{Y} - C_{G} \left(1 + \Delta E_{I} \right) \right) \right]$$
(32)

Step 6: in the present work, the term $(U_5 = U_4 = X(\beta, \gamma))$ is the index related to the particle search vector which is used to obtain the hybrid dynamic space constraint (see Figure 1 to Figure 5).

2.2.9. Sort of particle X program

The Sort of particle X (see Section 2.2.11) program arranges the particle to obtain increasing or decreasing hourly angles as appropriate and to avoid unnecessary oscillations, advances or retreats. In addition, the inclination β and orientation γ angles are sorted according to the corresponding seasons of the year (see Figure 1 to Figure 5 and Appendix A Section A.1.1).

BEGIN /* Sort of particle X */

Input: Particle X corresponding to swarm (tilt β and orientation γ).

Output: Sort of particle X_{Sort} corresponding to swarm (tilt β and orientation γ).

Step 1: Obtain the tilt β and orientation γ from the search vector X. Then, in the present work, Equation 33 sorts the tilt β and Equation 34 sorts the orientation γ from the search vector X.

$$\gamma_{sort} = \begin{cases} sort(\gamma, decrease), & (\varphi < 0) \cap ((0 < m < 183) \cup (H_{Sem} \le h \le H_{Stm})) \\ sort(\gamma, increase), & (\varphi < 0) \cap ((183 < m < 365) \cup (H_{Sem} \le h \le H_{Stm})) \end{cases}$$
(33)

$$\beta_{sort} = \begin{cases} sort(\beta, increase), & (\varphi < 0) \land ((183 < m < 363) \cup (H_{Sem} \le h \le H_{Stm})) \end{cases}$$

$$\beta_{sort} = \begin{cases} sort(\beta, increase), & (\varphi < 0) \land ((0 < m < 183) \cup (H_{Snm} \le h \le H_{Stm})) \end{cases}$$

$$sort(\beta, decrease), & (\varphi < 0) \land ((183 < m < 365) \cup (H_{Sem} \le h \le H_{Snm})) \end{cases}$$

$$(34)$$

Step 2: The tilt β_{sort} and orientation γ_{sort} are saved in the sorted search vector of PSO particle X_{Sort}

2.2.10. Fuzzy decision making and fuzzy inference system programs

Fuzzy decision making: This program implements a fuzzy decision making approach to optimise a power generation system using lower and upper bounds on pre-defined objective and constraint indices. The $\mu_i(X_{\beta,\gamma},\xi_i)$ states are computed using an auxiliary variable ξ_i that depends on whether it is a decrease or an increase. Then the search space bounds are computed at levels m=4 and m=5. Next, the objective function f(X) is computed using the t-norm algebraic product, taking into account objectives such as net present value (NPV), energy gained, energy invested, and the upper and lower constraints of slope (β) and orientation (γ) . Finally, the fitness f(X) is returned, reflecting the optimisation of the system based on the fuzzy decisions.

BEGIN /* Fuzzy decision making with this new methodology */

Data: the lower U^{Low} and upper U^{Up} limits of the objective and constraint indices U_m , Exponential Weights EW_m (AHP) and their maximisation ($\xi=1$) or minimisation ($\xi=0$) are defined according to Table 3 (see Section 2.2.1.).

Input: the objective and constraint indices U (see Section 2.2.8).

Output: the fitness f(X) is returned, reflecting the optimisation of the system based on the fuzzy decisions. FOR (i=1:5) DO

Step 1: Equation 35 calculates the fuzzy function μ_{m^*}

$$\mu\left(X_{\beta,\gamma},\xi_{i}\right)_{i} = \begin{cases} \frac{1-\xi_{i}}{\left(U_{i}^{Up} - U\left(\mathbf{X}_{\beta,\gamma}\right)_{i}\right)\left(1-\xi_{i}\right) + \left(U\left(\mathbf{X}_{\beta,\gamma}\right)_{i} - U_{i}^{Low}\right) \xi_{i}}{U_{i}^{Up} - U_{i}^{Low}} \\ \xi_{i} \end{cases} EW_{i} , U_{i}^{Low} \geq U\left(\mathbf{X}_{\beta,\gamma}\right)_{i} \leq U_{i}^{Up} \\ , U_{i}^{Low} \leq U\left(\mathbf{X}_{\beta,\gamma}\right)_{i} \leq U_{i}^{Up} \\ , U_{i}^{Up} \leq U\left(\mathbf{X}_{\beta,\gamma}\right)_{i} \end{cases}$$
(35)

Step 6: Equation 36 calculates the search space restriction for the attributes or objectives i = 4 and i = 5 where the t-norm is used in an algebraic sum.

$$\mu_{i} = \frac{1}{365} \sum_{m=1}^{m=365} \left(\sum_{H_{Sem}}^{H_{Stm}} \left(\frac{\mu_{imh}}{H_{Stm} - H_{Sem}} \right) \right)$$
(36)

Step 3: Equation 37 calculates the fitness fuzzy function f(X) using the algebraic product t-norm. The objectives are: NPV (1), energy obtained (2), invested energy (3), upper and lower constraints of β (4) and γ (5).

$$f(X) = \mu_1 \,\mu_2 \,\mu_3 \,\mu_4 \,\mu_5 \tag{37}$$

The Fuzzy inference system algorithm program (see Section 2.2.9. and Appendix A Sections A.2) takes two inputs: the day (m) and the hour (h). Firstly, the tilt angle should be smaller in summer than in winter. Secondly, the tilt angle should start high at dawn, decrease at midday and increase at dusk. Thirdly, the orientation of the panel should start with a negative angle towards the east and move to a positive angle towards the west.

It transforms these crisp inputs into fuzzy values using sigmoidal membership functions with categories such as very low, low, medium, high and very high. Fuzzy rules are then applied to combine the membership degrees of the inputs and generate fuzzy outputs for the tilt angle (β) and orientation angle (γ) . The results are combined using the minimum fuzzy operator and finally obtained using the centroid method (Figure 1 to Figure 5).

BEGIN /* Fuzzy inference system algorithm */

Data: The centre parameters and standard deviations of the Gaussian function (see Appendix A Section A.2, Table A.1, Table A.2 and Table A.3). These are obtained through a process of trial and error and statistical data.

Input: day $m \mid d \mid$ and hour $h \mid h \mid$.

Output: Tilt angle $(\beta \lceil rad \rceil)$ and Orientation angle $(\gamma \lceil rad \rceil)$.

Step 1: Equation 38 calculates the Gaussian fuzzy membership function (for the hour h) $\mu_{FIS}\left(h,\sigma_h,H^{Low},H^{Up}\right)$ and (for the day) $m\,\mu_{FIS}\left(m,\sigma_h,H^{Low},H^{Up}\right)$. Each input has a membership subjective valuation in categories (see Table A2 and Table A3 of Appendix A Section A.2).

$$\mu_{FIS}\left(X,\sigma_{X},X^{Low},X^{Up}\right) = \begin{cases} 0\\ -\frac{\left(x-Centre\right)^{2}}{2\left(\sigma_{X}\right)^{2}} \end{cases}, X^{Low} \ge x\\ 0, X^{Low} \le x \le X^{Up}\\ 0, X^{Up} \le x \end{cases}$$
(38)

Step 2: The system's rules are applied to combine the membership degrees of the inputs within each category (see Table A2), generating fuzzy output results for each one. These results are then combined using a minimum fuzzy logic operator.

Step 3: Finally, the fuzzy output values are transformed back into crisp values using a defuzzification method. The Centroid (Centre of Mass) calculates the centre of gravity of the fuzzy curve.

2.2.11. Hybrid fuzzy-rigid constraint particle swarm optimisation with constriction factor

This program implements a Hybrid Fuzzy-Rigid Constraint Particle Swarm Optimisation with Constriction Factor to optimise the proposed problem. It starts by initialising the positions $X_i^{\left[k\right]}$, the best local positions b_i and the best global position b_G , assigning random values or good initial values according to the designer's criteria. For 200 iterations and 130 particles, a motion rule is applied to update the particle positions and velocities, constrained according to the search space constraints. At each iteration, the fitness functions $f(X_i^{\lfloor k \rfloor}), f(b_i)$

and $f(b_G)$ are calculated, evaluating the performance of the system and updating these positions based on these values. Finally, the programme returns the global best position, b_G , found by the swarm. All of these parameters are calibrated through a process of trial and error, based on statistical studies of the solutions obtained (see Figures 1 to 5). This is not developed here for reasons of space, but will be extended in future work.

BEGIN /* Hybrid Fuzzy-Rigid Constraint Particle Swarm Optimisation with Constriction Factor */

Data: weights $w_l = 0.999$, $w_C = w_S = 2.049$ and $\chi = 0.729$ which are obtained by iterative trial and error. w_{ICS} serve to enhance the vector components of the velocity and the parameter \mathcal{X} limits the resultant to achieve stability and convergence to good solutions (see Section 2.2.1.).

Input: Particle X (tilt β and orientation γ).

Output: global best solution b_G and its fitness function $f(b_G)$.

Step 1: Initialize $X_i^{\lfloor k \rfloor}$, b_G , b_i at zero, random values or a good value according to the designer's criteria. BEGIN /* Fuzzy fitness function */

Step 2: Start Fuzzy fitness function program and calculate fitness functions $f\left(X_i^{\left[k\right]}\right)$, $f\left(b_i\right)$ and $f\left(b_G\right)$. FOR $((k=1:200)\cap(i=1:130))$ DO Step 3: Equation 39 calculates the of motion of the particles $X_i^{\left[k\right]}$ in each iteration k and the next iteration

k+1. These values are constrained by boundary mechanisms.

$$V_{i}^{\left[k+1\right]} = \chi w_{\overline{l}i}^{\left[k\right]} V_{i}^{\left[k\right]} + \chi w_{Ci}^{\left[k\right]} \left(b_{i} - X_{i}^{\left[k\right]}\right) + \chi w_{Si}^{\left[k\right]} \left(b_{G} - X_{i}^{\left[k\right]}\right) \Rightarrow X_{i}^{\left[k+1\right]} = X_{i}^{\left[k\right]} + V_{i}^{\left[k+1\right]}$$

$$(39)$$

Step 4: Apply both rigid and soft constraints to the particles, as illustrated in the Figure 1 to Figure 5.

BEGIN /* Fuzzy fitness function */

Step 5: Calculate fitness functions $f\left(X_i^{\left[k\right]}\right)$, $f\left(b_i\right)$ and $f\left(b_G\right)$ (see Section 2.2.10.). Step 6: Equation 40 updates (if necessary) the best positions seen by the particles $b_i^{\left[k\right]}$ and by the swarm $b_G^{\left[k\right]}$.

$$\left(f\left(X_{\bar{i}}^{\left[k\right]}\right) > f\left(b_{\bar{i}}\right) \Rightarrow b_{\bar{i}} = X_{\bar{i}}^{\left[k+1\right]}\right) \cup \left(f\left(X_{\bar{i}}^{\left[k\right]}\right) > f\left(b_{G}\right) \Rightarrow b_{G} = X_{\bar{i}}^{\left[k\right]}\right)$$

$$(40)$$

2.3. Practical contributions of the proposed methodology

2.3.1. Simulation of the climatic conditions

Figure 7 in this section shows the hourly and seasonal variations in key meteorological data (average temperature, relative humidity and atmospheric pressure) for the provinces of La Rioja (LR), San Juan (SJ) and Entre Ríos (ER) over a ten-year period, as determined by the Radial Basis Function method (see Appendix A Section A.2.1.).

Figure 8 shows the hourly and daily changes in the atmospheric transmission coefficient (K_T) and solar azimuth angle (θ_z) in the aforementioned three provinces: La Rioja (LR), San Juan (SJ) and Entre Ríos (ER). As the temperature rises around midday, atmospheric pressure tends to decrease due to solar heating, as does relative humidity. This trend is more pronounced in the drier regions of LR and SJ, where temperature peaks are higher and there are stronger diurnal fluctuations in pressure and relative humidity. ER, by contrast, experiences more stable conditions, with higher average humidity and less variability in temperature and pressure. Based on the temperature map, ER has the lowest temperatures, followed by SJ. LR has the highest temperatures. In terms of atmospheric pressure, LR shows the lowest values, followed by SJ, with ER showing the highest. LR has the driest conditions in terms of relative humidity, with SJ intermediate and ER the wettest (see Table 5). These meteorological patterns significantly impact solar panel performance and are therefore incorporated into models of irradiance, energy yield, and dynamic optimisation constraints.

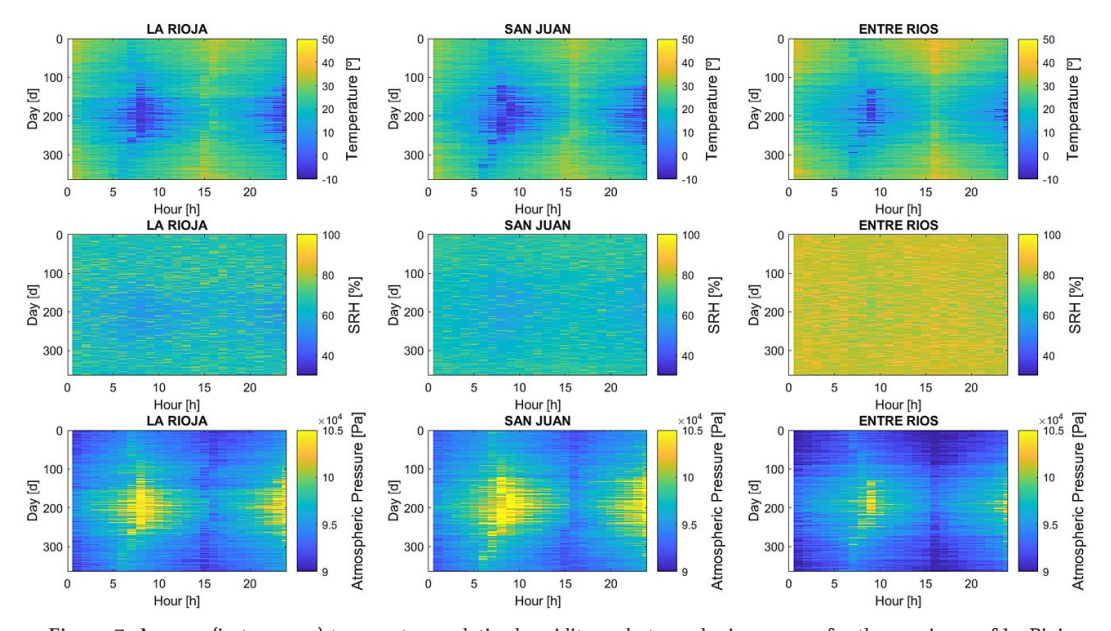


Figure 7. Average (in ten years) temperature, relative humidity and atmospheric pressure for the provinces of La Rioja, San Juan and Entre Ríos.

Source: The authors.

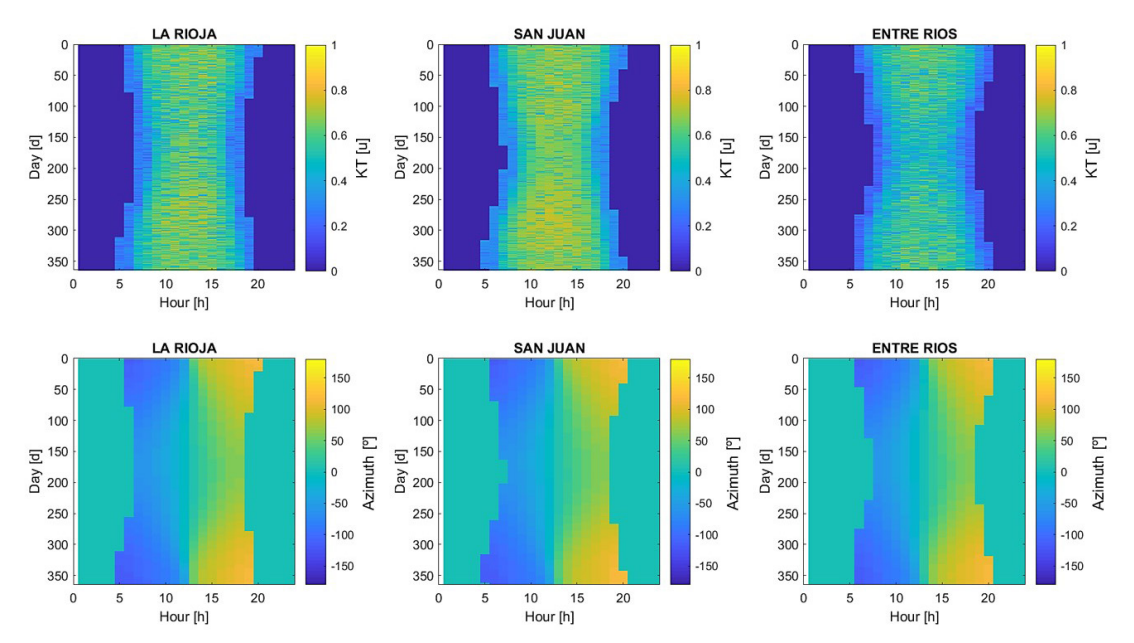


Figure 8. Hourly and daily fluctuations in the atmospheric transmission coefficient and solar azimuth angle for the provinces of La Rioja, San Juan and Entre Ríos.

The top row shows the K_T values, which represent the proportion of extraterrestrial solar radiation that reaches the surface. These values have been adjusted to account for cloudiness, providing a more accurate reflection of actual atmospheric transmissivity conditions. SJ has the highest average K_T values, suggesting clearer skies and lower cloud cover. LR follows, and ER exhibits the lowest values, indicating more diffuse radiation. The bottom row shows the annual evolution of the solar azimuth angle. The general pattern remains consistent across the provinces, with the azimuth reaching its maximum positive and negative values at around solar noon in summer and winter, respectively. However, there are slight regional differences in azimuth behaviour, particularly in SJ, due to its geographic location and solar geometry. These variables are crucial for determining the optimal orientation of solar panels and for accurately modelling solar tracking systems.

2.3.2. Tilt angle (β) and Orientation angle (γ) of the solar panels

This section shows the colour bar graphs of tilt angle $\beta[\circ]$ and orientation angle $\gamma[\circ]$ of the solar panels for each day and each hour for the provinces of La Rioja (LR), San Juan (SJ) and Entre Rios (ER), as well as for the different scenarios analysed (see Section 2.2.1.). All of these plotted angles adhere to the constraints set out in Section 2.2.9 and Appendix A Section A.1.1. This enables viable and feasible solutions to be analysed for the three provinces in question. For reasons of space, the cases or scenarios have not been plotted at fixed angles. Angles are given in degrees for ease of understanding.

The cases or scenarios plotted in this section are the follows (see Table 4 in Section 2.3.4.):

- Case 5: Figure 9 shows a mixed case with manual movement of the panel inclination but automatic movement of the panel orientation at 15°, 30° and 45° and variable orientation according to the zenith angle of the sun A_z $\lceil \circ \rceil$.
- Case 6: Figure 10 shows the case of a variable tilt angle and orientation according to the incidence angle θ_z [°] zenith angle of the sun A_z [°]. This case represents the automated control of the tracking system by complex embedded systems. This is the most efficient alternative (see Appendix A Section A.1.12) but, as will be shown, the most expensive.
- Case 7: Figure 11 shows a variable tilt angle and orientation according to a fuzzy inference system based on the developed fuzzy decision theory. This is an artificial intelligence-based system that takes into account the time of day. This system is simpler and cheaper than (3), and allows for less movement (see Section 2.3.4). Consequently, it will demonstrate lower energy consumption than the previous case.

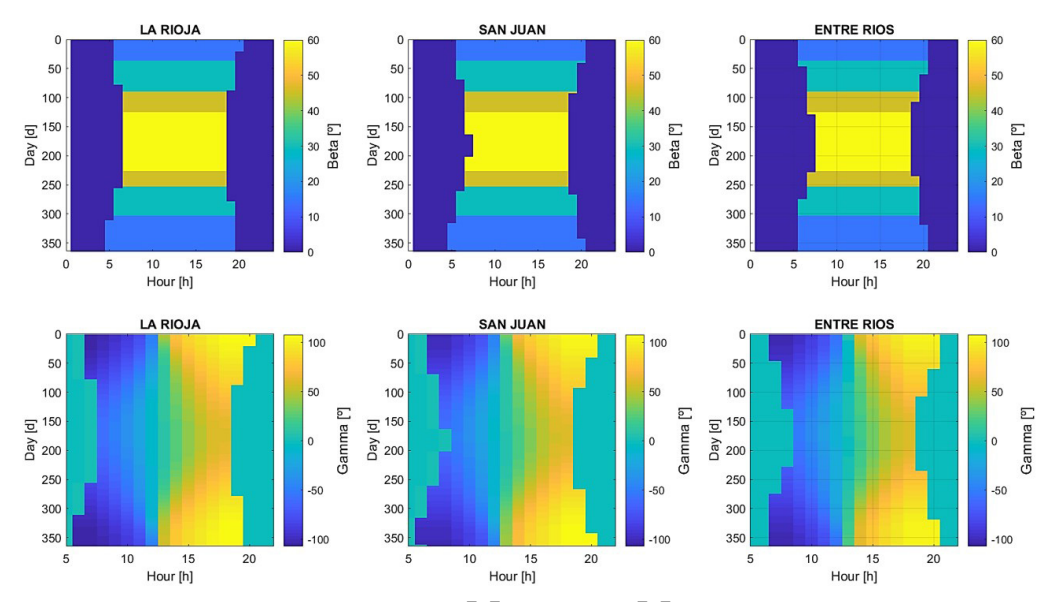


Figure 9. Case 5: Mixed fixed β [°] and variable γ [°] angles for all provinces. Source: The authors.

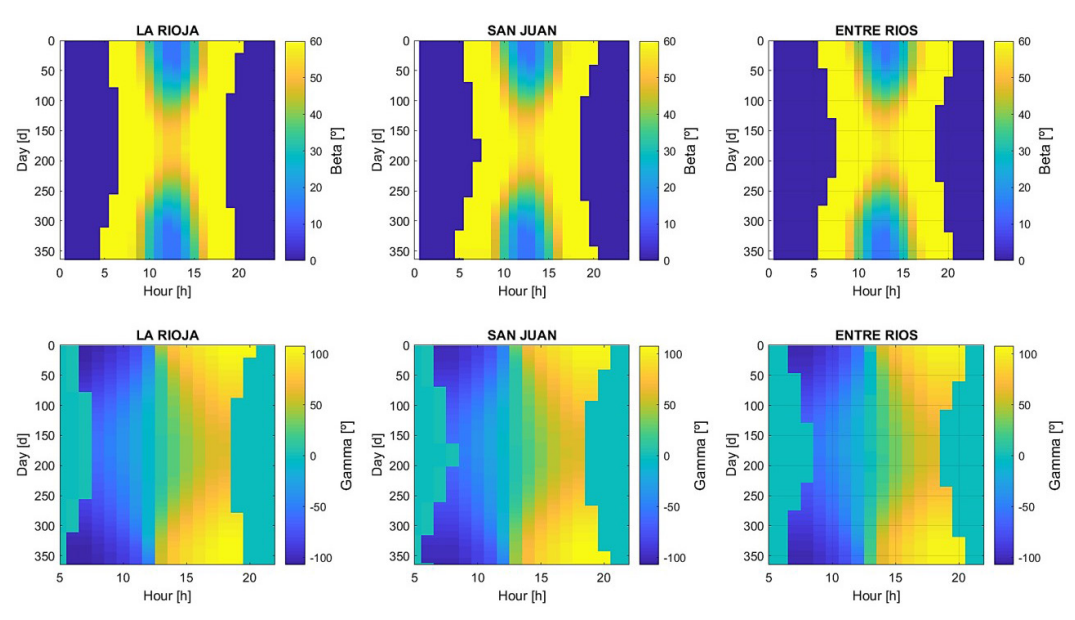


Figure 10. Case 6: Variable $\beta[\circ]$ and $\gamma[\circ]$ angles according to sun trajectory for all provinces. Source: The authors.

- Case 8: Figure 12 illustrates a variable tilt angle and orientation based on a Gaussian Neural Network system. As in the previous case, this is an artificial intelligence-based system implemented according to day and time. This system is simpler and cheaper than (3) and allows less movement (see Section 2.3.4). Consequently, it will demonstrate lower energy consumption than the previous case.
- Case 9: Figure 13 shows a variable tilt angle and orientation according to the multi-objective fuzzy model that was proposed and solved using Particle Swarm Optimisation (PSO). As in the previous case, this implementation of a swarm technique is based on artificial intelligence and day and time. This system is simpler and cheaper than (3) and allows for less movement (see Section 2.3.4). Consequently, it will demonstrate lower energy consumption than the previous case.

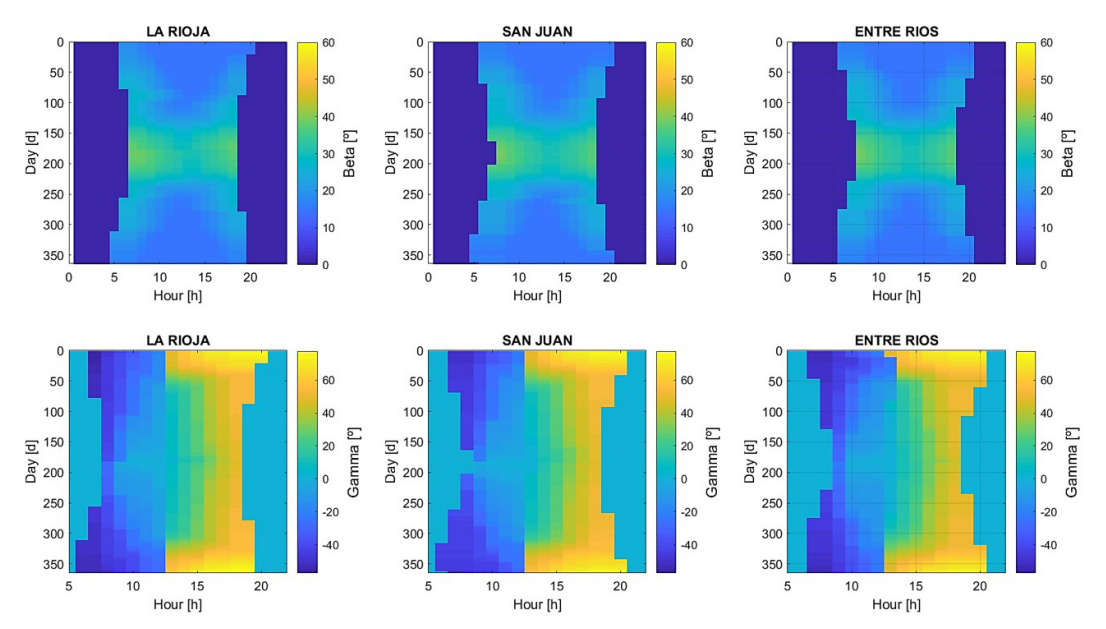


Figure 11. Case 7: Variable $\beta[\circ]$ and $\gamma[\circ]$. angles according to a fuzzy inference system for all provinces. Source: The authors.

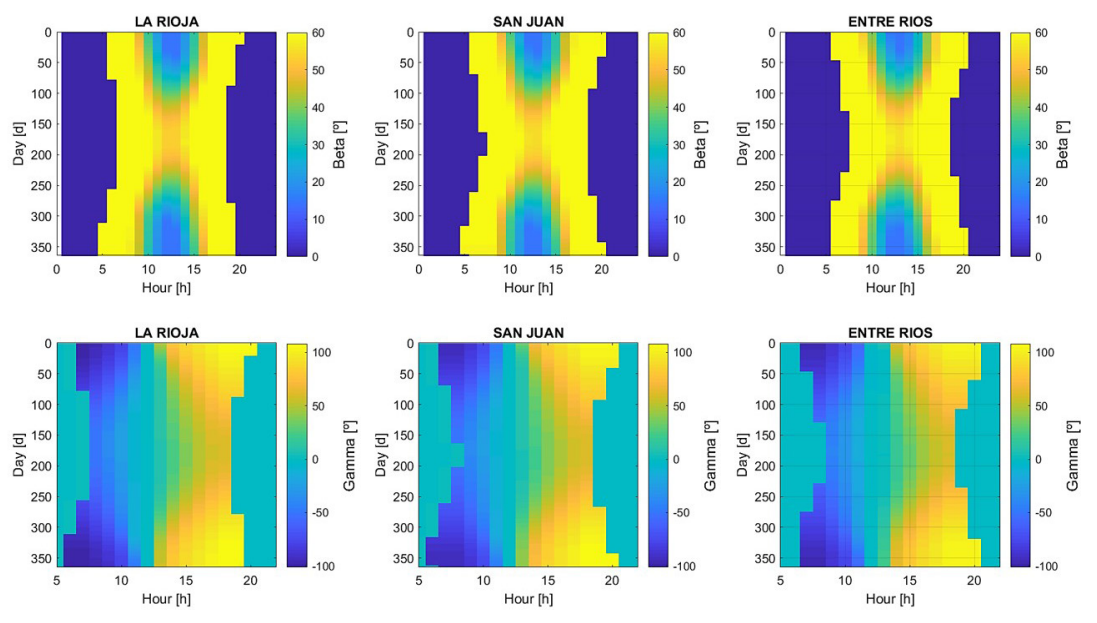


Figure 12. Case 8: Variable $\beta[\circ]$ and $\gamma[\circ]$ angles according to a Gaussian neural network for all provinces. Source: The authors.

The radial neural network-based scenario (see Figure 12) is similar to the continuous motion scenario (see Figure 10), as both produce the most energy and therefore generate similar motions with some adjustments (see Section 2.2.2 and Section 2.2.4). Figure 13 shows the optimal scenario obtained using the fuzzy multi-objective model, which was solved using a hybrid constraint PSO with a constriction factor.

This scenario aims to maximise energy production while minimising motion and cost, in order to achieve the best possible net present value. Regarding the provinces, Figures 9 to 13 show that SJ has the greatest movement, followed by LR and ER, which exhibit similar levels of movement.

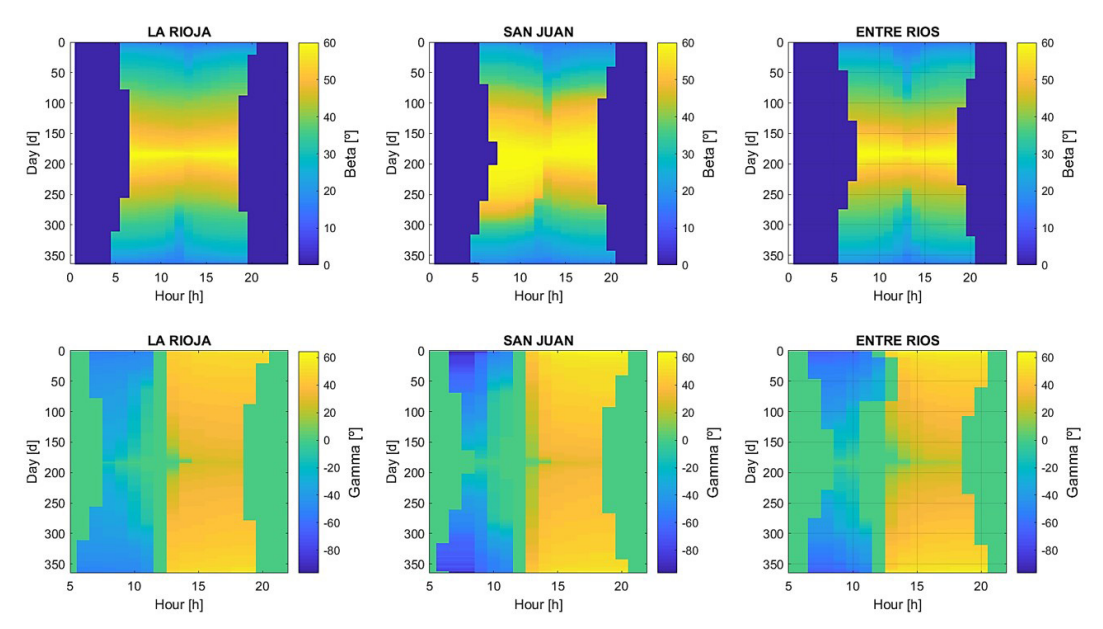


Figure 13. Case 9: Variable $\beta[\circ]$ and $\gamma[\circ]$ angles according to fuzzy multi-objective with hybrid constraint PSO with a constriction factor.

Source: The authors.

This is because SJ has higher solar irradiance, so the metaheuristic deems it more profitable for the system to have greater movement. This will be demonstrated in the following sections. The results are logical and satisfactory, and are in line with reality. The equations developed in Sectn 2.3.4 are also verified.

2.3.3. Cosine of incidence angle and total solar irradiance

This section presents the colour bar graphs of
$$\cos(\theta)[u]$$
, $G_{\beta,\gamma}\left[\frac{kW}{m^2}\right]$ and $R_{\beta,\gamma}[u]$ (see Section 2.2.5.

to Section 2.2.6.) for each hour h and day m, with the corresponding inclination and orientation, from which the total solar irradiance for each city (La Rioja LR, San Juan SJ and Entre Ríos ER) is calculated. Angles are expressed in degrees for ease of understanding. These figures show the cosine of the angle of incidence $\cos(\theta)$ for each case studied, which depends on the angles of inclination β and orientation γ , and which is proportional to proportional to the total solar irradiance $G_{\beta,\gamma}$ (see Equation 29). The cases or scenarios are the follows (see Table 4 in Section 2.3.5.):

- Case 1: Figure 14 shows the case of a horizontal panel facing north.
- Case 2: Figure 15 shows the case of a panel at 15° and facing north.
- Case 3: Figure 16 shows the specific case of the voltage, current and power for a panel at 30° and facing north.
- Case 4: Figure 17 shows the case of a panel at 45° and facing north.
- Case 5: Figure 18 shows a mixed case with manual movement of the panel inclination but automatic movement of the panel orientation at 15°, 30° and 45° and variable orientation according to the zenith angle of the sun $A_z \lceil \circ \rceil$.
- Case 6: Figure 19 shows the case of a variable tilt angle and orientation according to the incidence angle of horizontal panel $(\theta_z \lceil \circ \rceil)$ zenith angle of the sun $(A_z \lceil \circ \rceil)$.
- Case 7: Figure 20 shows the case of a variable tilt angle and orientation according to a fuzzy inference system according to the developed fuzzy decision theory.
- Case 8: Figure 21 shows the case of a variable tilt angle and orientation according to a Gaussian Neural Network system.
- Case 9: Figure 22 shows the case of a variable tilt angle and orientation according to the multi-objective fuzzy model proposed and solved by the Particle Swarm Optimisation (PSO).

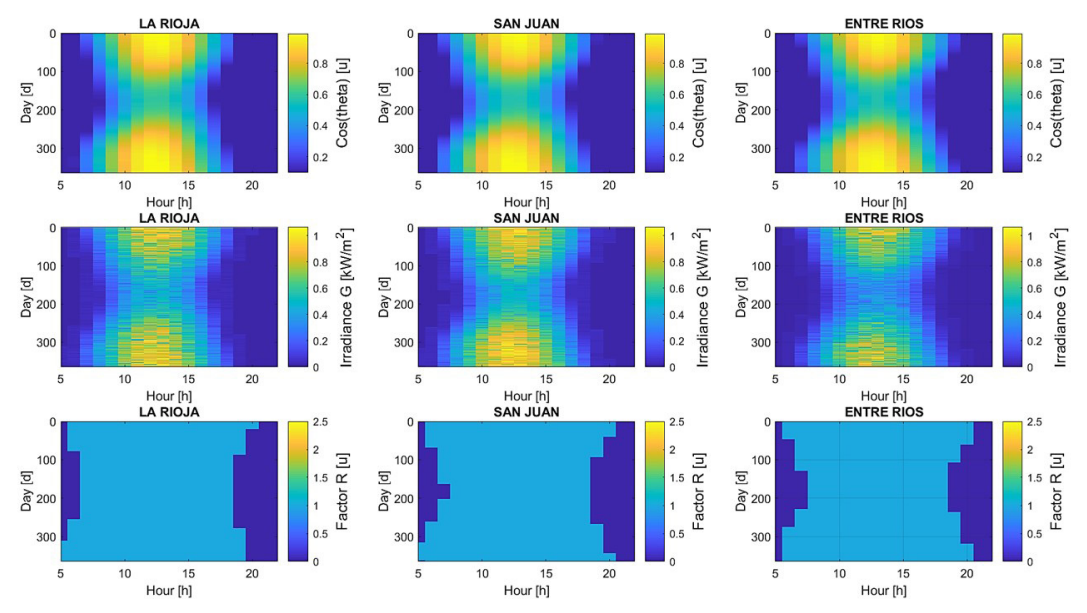


Figure 14. Case 1: $\cos(\theta)[u]$, $G_{\beta,\gamma}\left[\frac{kW}{m^2}\right]$ and $R_{\beta,\gamma}[u]$ for all provinces. Source: The authors.

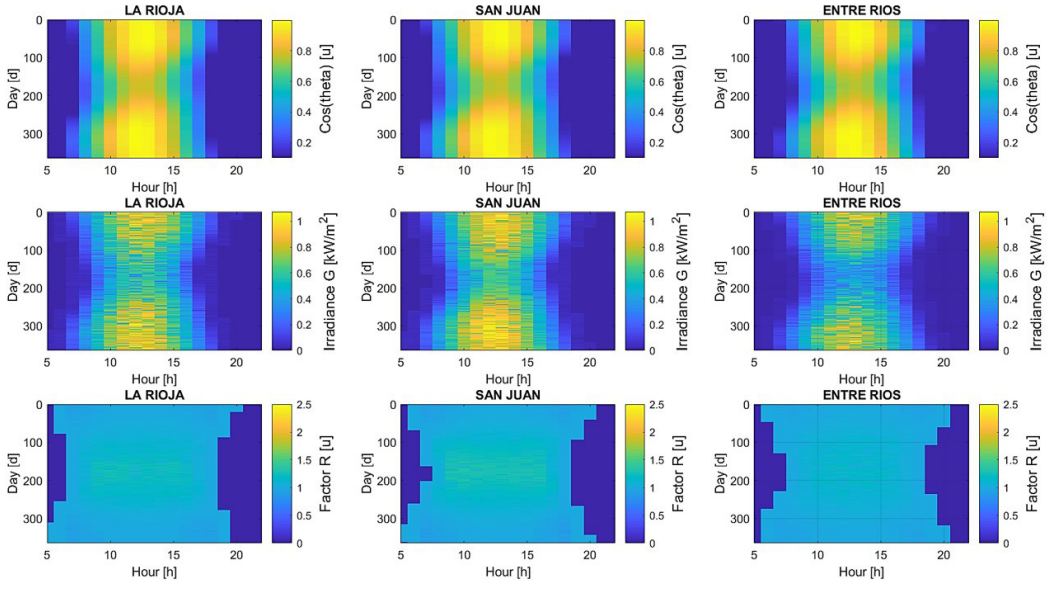


Figure 15. Case 2: $\cos(\theta) [u]$, $G_{\beta,\gamma} \left[\frac{kW}{m^2} \right]$ and $R_{\beta,\gamma} [u]$ for all provinces. Source: The authors.

The value of $\cos(\theta)$ is fundamental in understanding how a solar panel receives solar radiation. A high $\cos(\theta)$ indicates that radiation is striking the panel more directly (higher irradiance $G_{\beta,\gamma}$), which translates to higher efficiency. In this sense, a panel with a low tilt β (Case 1 or Case 2) will have a low $\cos(\theta)$ (and low irradiance $G_{\beta,\gamma}$), especially in winter when the sun is lower in the sky. On the other hand, a panel with a higher tilt β (Case 3 or Case 4) will have a higher $\cos(\theta)$ when the sun is closer to its zenith, such as in summer (see Section 2.2.6. to Section 2.2.8.).

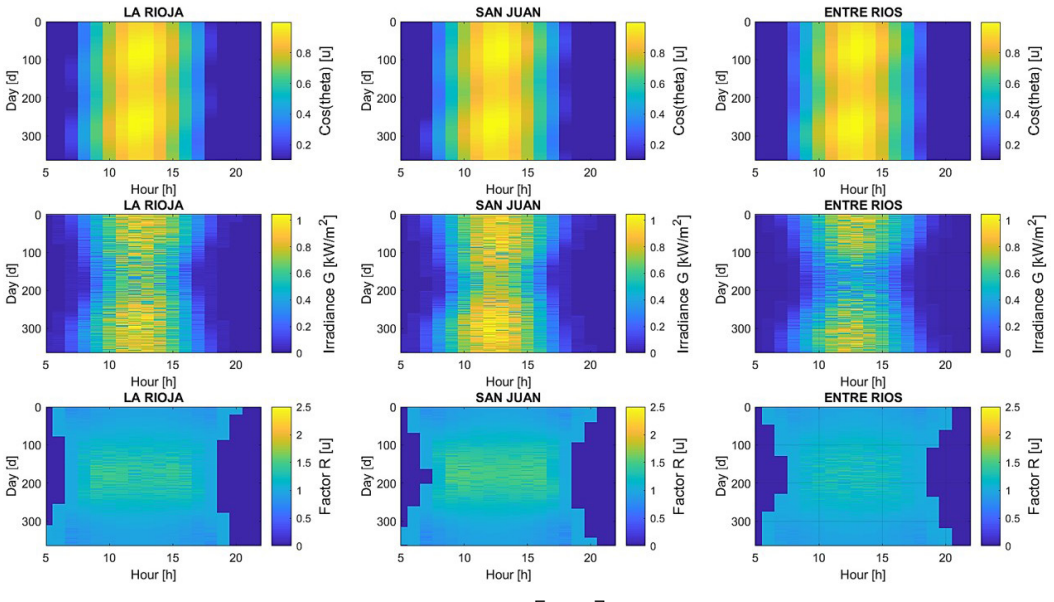


Figure 16. Case 3: $\cos(\theta)[u]$, $G_{\beta,\gamma}\left[\frac{kW}{m^2}\right]$ and $R_{\beta,\gamma}[u]$ for all provinces.

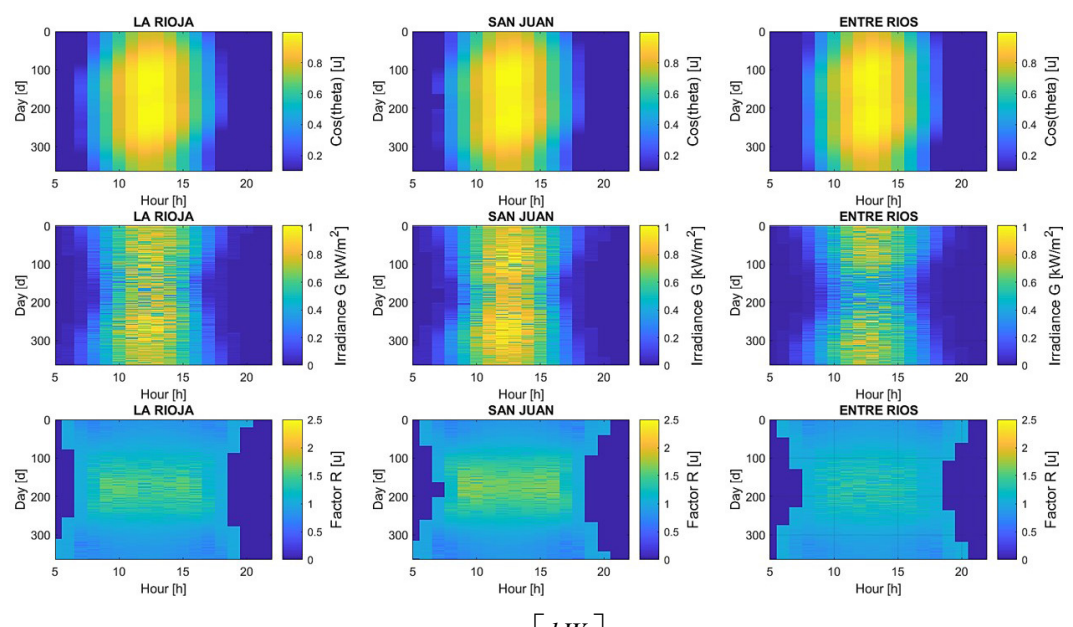


Figure 17. Case 4: $\cos(\theta)[u]$, $G_{\beta,\gamma}\left[\frac{kW}{m^2}\right]$ and $R_{\beta,\gamma}[u]$ for all provinces.

Source: The authors.

The factor $R_{\beta,\gamma}[u] = \frac{G_{\beta,\gamma}}{H_0}$ (see Section 2.2.6.), which is the ratio between the irradiance in a particular scenario and the irradiance of a panel with no tilt and a north orientation (Case 1), shows how the tilt and orientation impact the panel's efficiency. In Case 1 the value of the ratio is $R_{\beta,\gamma} = 1$, indicating relatively low efficiency.

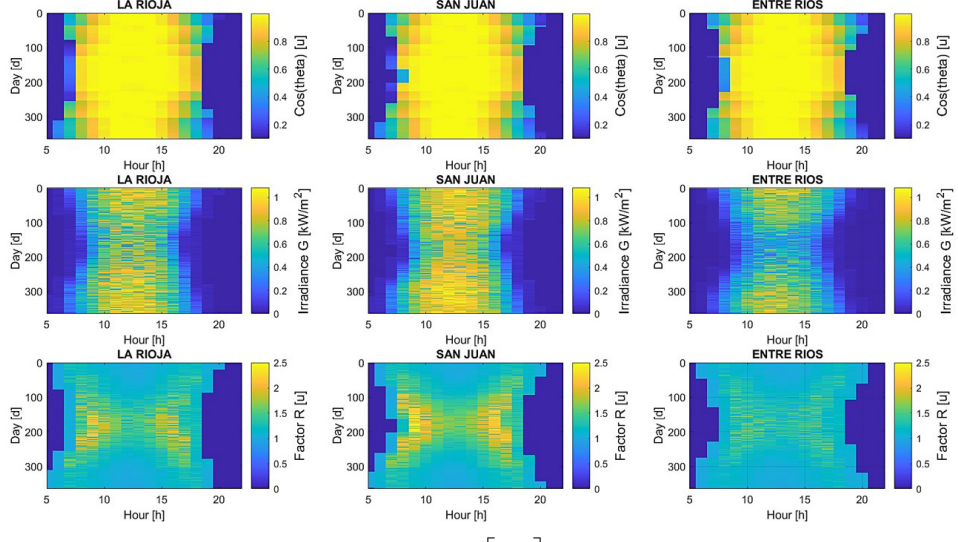


Figure 18. Case 5: $\cos(\theta)[u]$, $G_{\beta,\gamma}$ and $R_{\beta,\gamma}[u]$ for all provinces. Source: The authors.

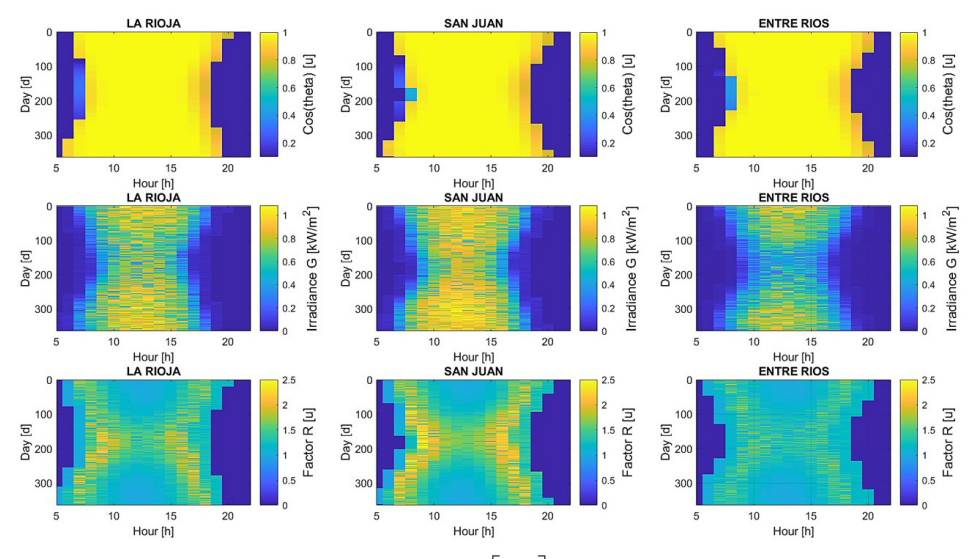


Figure 19. Case 6: $\cos(\theta)[u]$, $G_{\beta,\gamma}$ and $R_{\beta,\gamma}[u]$ for all provinces.

On the other hand, in Case 2 to Case 9, the values of $R_{oldsymbol{eta},\gamma}$ tend to be higher in winter due to the smaller angle of incidence, and lower in summer when the radiation is more direct. Therefore, the effect of tilting and orienting the panel has repercussions on these three variables, increasing or decreasing them at each point according to whether the solar panel is well directed.

The cases in which the panel is oriented_according to the sun's path have a better efficiency with respect

to this variable (Case 5 and Case 6). $R_{\beta,\gamma}[u]$ is low in summer and high in winter for all cases except in Case 1 (where $R_{\beta,\gamma}[u] = \frac{G_{\beta,\gamma}}{H_{0\beta,\gamma}} = 1$). This is because the $\cos(\theta)$ and the irradiance $G_{\beta,\gamma}$ are high in summer

and low in winter due to the effect of solar declination $\delta.$

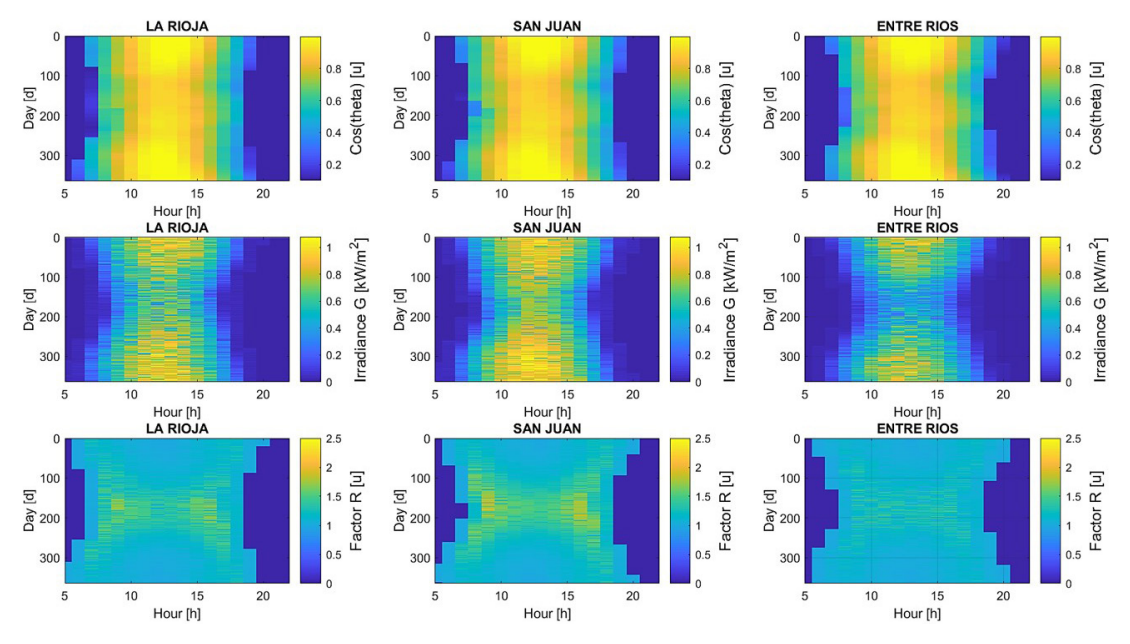


Figure 20. Case 7: $\cos(\theta)[u]$, $G_{\beta,\gamma}\left[\frac{kW}{m^2}\right]$ and $R_{\beta,\gamma}[u]$ for all provinces.

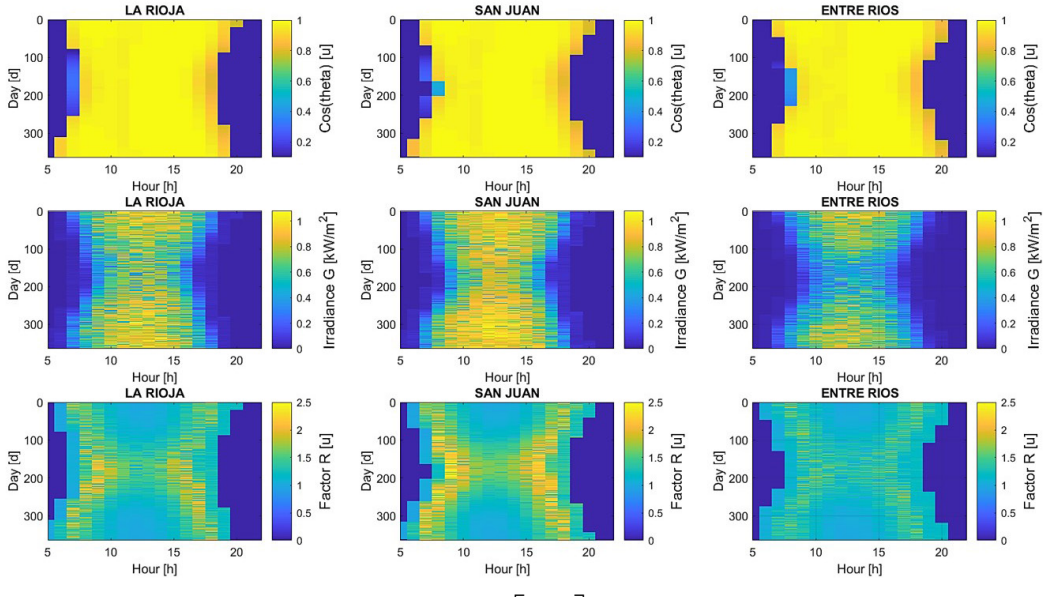


Figure 21. Case 7: $\cos(\theta)[u]$, $G_{\beta,\gamma}\left[\frac{kW}{m^2}\right]$ and $R_{\beta,\gamma}[u]$ for all provinces.

Source: The authors.

Diffuse and albedo radiation also play a role and slightly offset this effect. As a result, the best case of the proposed scenarios is the Case 6 (see Figure 19), although this is the case with the highest costs and the Case 1 (see Figure 14) gives the three worst factors and therefore the worst profitability. Seasonality also plays a significant role, as solar declination changes throughout the year, affecting both $\cos(\theta)$ and irradiance.

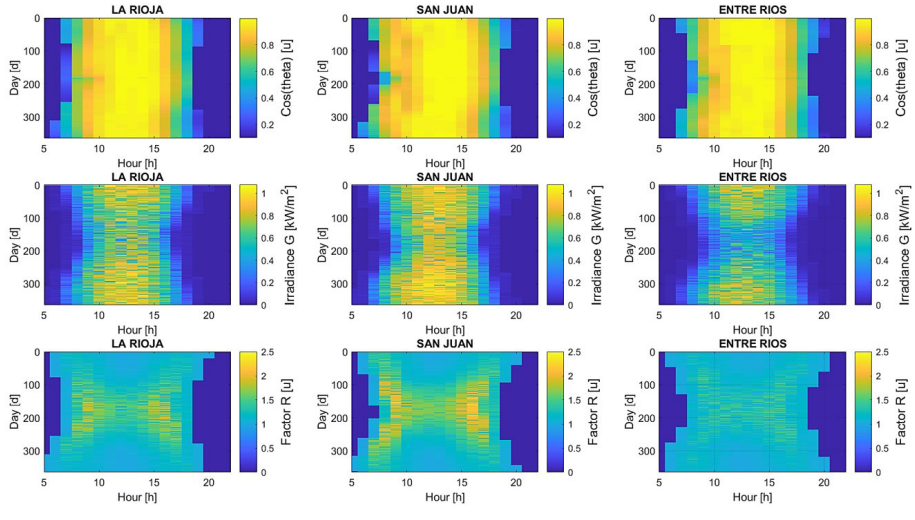


Figure 22. Case 9: $\cos(\theta)[u]$, $G_{\beta,\gamma}\left[\frac{kW}{m^2}\right]$ and $R_{\beta,\gamma}[u]$ for all provinces.

In winter, the sun is lower in the sky, reducing $\cos(\theta)$ and consequently irradiance. In summer, however, the sun is higher in the sky, increasing $\cos(\theta)$ and irradiance $G_{\beta,\gamma}$. This seasonal pattern directly influences the values of $R_{\beta,\gamma}$, which tend to be lower in summer and higher in winter due to the variation in the angle of incidence of solar radiation (see Section 2.2.6.).

In addition, the geographical location influences these variables and is critical in determining the optimal tilt and orientation angles for each site. These are latitude and longitude and their corresponding time difference), altitude, temperature and pressure (see Section 2.2.6. to Section 2.2.8.). Entre Rios is closer to the equator and has the higher $\cos(\theta)$. However, it has denser clouds and lower altitude, so solar irradiance $G_{\beta,\gamma}$ is lower throughout the year. LR (and SJ compared to these two cases) is less close to the equator and has a lower $\cos(\theta)$. However, LR (and SJ compared to these two cases) has denser clouds and a higher altitude, so the solar irradiance $G_{\beta,\gamma}$ is lower throughout the year. Then, the panels in SJ and LR will be more efficient than those in Entre Rios, due to the greater amount of solar irradiance $G_{\beta,\gamma}$, especially during the summer (see Section 2.3.4.). As in Section 2.3.2, the boundaries defined by the calculated sunrise and sunset times are visible in all these figures. These times are calculated as discrete values because they have been rounded for use in the algorithms and they differ for the three provinces due to their different latitudes and longitudes (see Section 2.3.4.).

Taking into account these analyses and comparing the scenarios for the analysed provinces, the following results are obtained. Case 7 related to the fuzzy inference system (see Figure 20) provides intermediate values between the best and the worst scenario, aiming at a more balanced solution and is an intermediate scenario between the best and the worst scenario. Case 8 related to the radial basis neural network (see Figure 21) produced results similar to Case 6 related to the continuous motion (see Figure 19). Case 9, related to the HFRCPSO-CF (see Figure 22), optimises multiple objectives simultaneously and produces solutions very close to the optimal ones, but at a lower cost compared to continuous solar tracking systems (see Figure 19). These optimisation systems improve the performance of the solar panels by approaching the ideal results without the high costs associated with continuous solar tracking systems. Then, Case 9 provides an intermediate case, although, as will be shown in the following sections, it is very close to the best scenarios. It's also important to note that at dawn and dusk, $\cos(\theta)$ tends to zero, and hence $R_{\theta,\gamma}$ would tend to infinity. Then, it is limited to a minimum value of 0.1 (see Section 2.3.4.).

2.3.4. Voltage, current and power

In this section, Figure 17 to Figure 25 analyse the colour bar graphs for the variables Voltage [V], Current [A] and Power [W] for each hour h and day m (see Section 2.2.5. to Section 2.2.7.). It is with the corresponding tilt $\beta[\circ]$ and orientation $\gamma[\circ]$, from which the total solar irradiance is obtained for each case and city (La Rioja LR, San Juan SJ and Entre Rios ER). Angles are expressed in degrees for ease of understanding. The cases or scenarios are the follows (see Table 4 in Section 2.3.5.):

- Case 1: Figure 23 shows the case of a horizontal panel facing north.
- Case 2: Figure 24 shows the case of a panel at 15° and facing north.
- Case 3: Figure 25 shows the specific case of the voltage, current and power for a panel at 30° and facing north.
- Case 4: Figure 26 shows the case of a panel at 45° and facing north.
- Case 5: Figure 27 shows a mixed case with manual movement of the panel inclination but automatic movement of the panel orientation at 15°, 30° and 45° and variable orientation according to the zenith angle of the sun A_{τ} \circ .

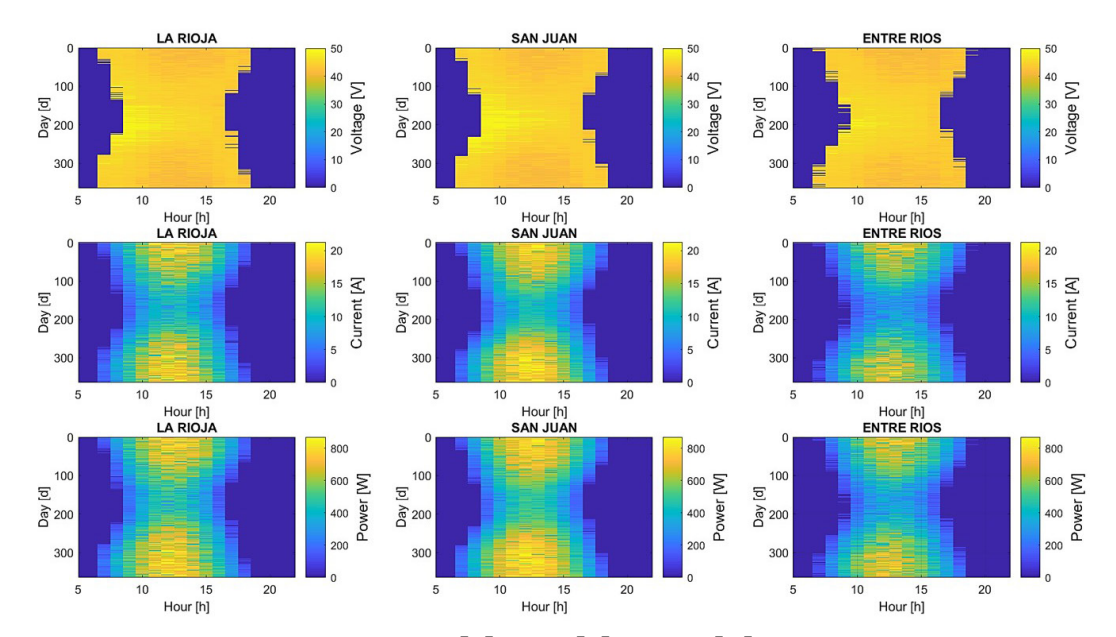


Figure 23. Case 1: Voltage [V], Current [A] and Power [W] for all provinces. Source: The authors.

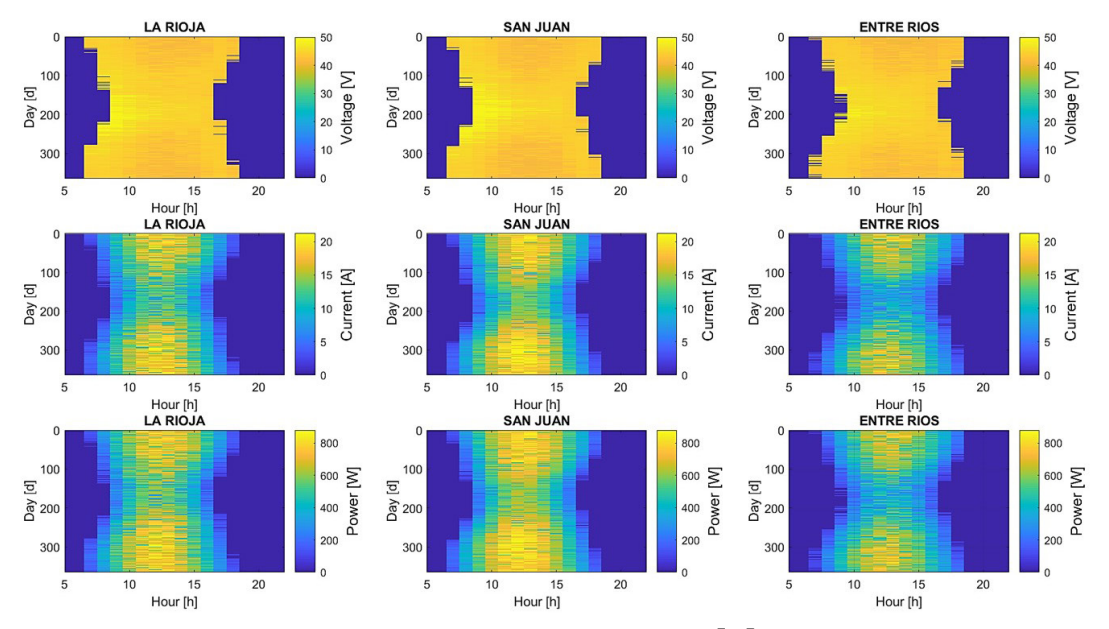


Figure 24. Case 2: Voltage [V], Current [A] and Power [W] for all provinces. Source: The authors.

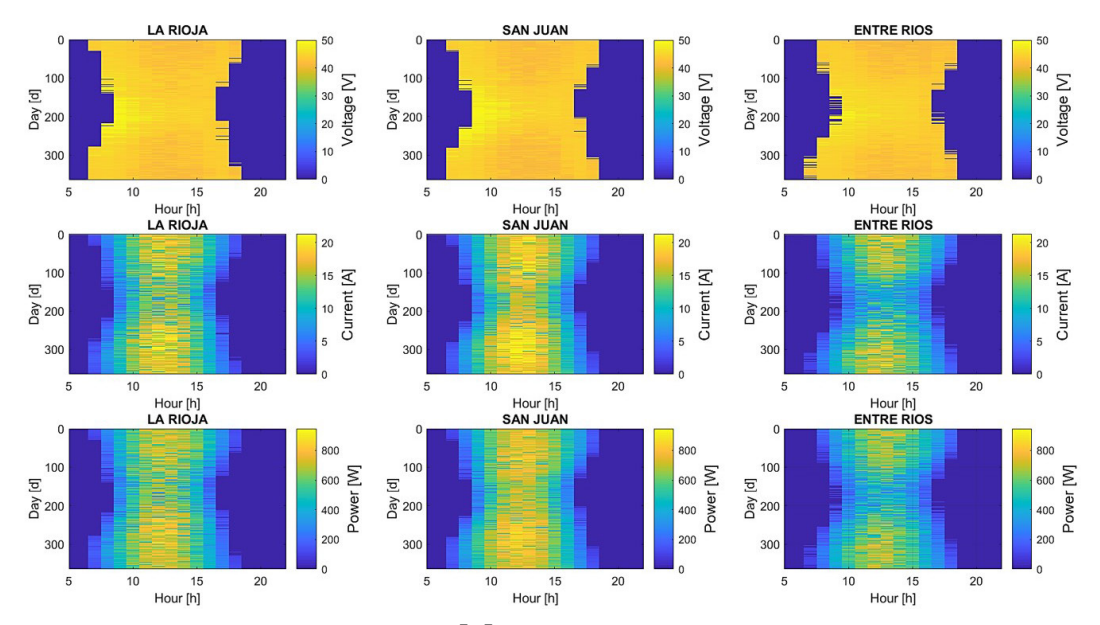


Figure 25. Case 3: Voltage [V], Current [A] and Power [W] for all provinces. Source: The authors.

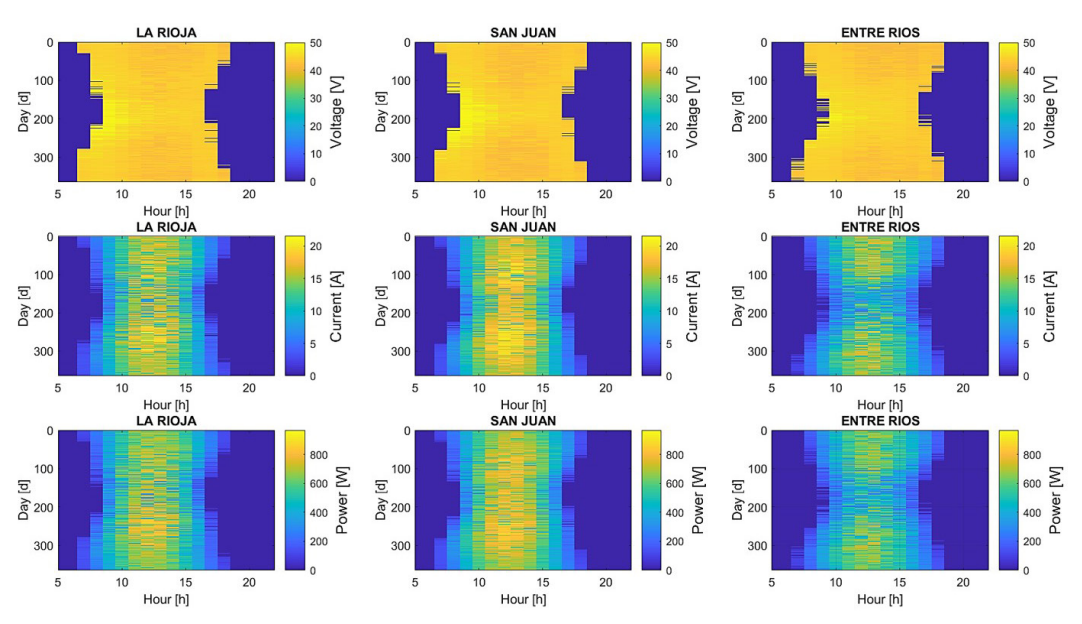


Figure 26. Case 4: Voltage [V], Current [A] and Power [W] for all provinces. Source: The authors.

- Case 6: Figure 28 shows the case of a variable tilt angle and orientation according to the incidence angle of horizontal panel θ_z [°] zenith angle of the sun A_z [°].
- Case 7: Figure 29 shows the case of a variable tilt angle and orientation according to a fuzzy inference system according to the developed fuzzy decision theory.
- Case 8: Figure 30 shows the case of a variable tilt angle and orientation according to a Gaussian Neural Network system.
- Case 9: Figure 31 shows the case of a variable tilt angle and orientation according to the multi-objective fuzzy model proposed and solved by the Particle Swarm Optimisation (PSO).

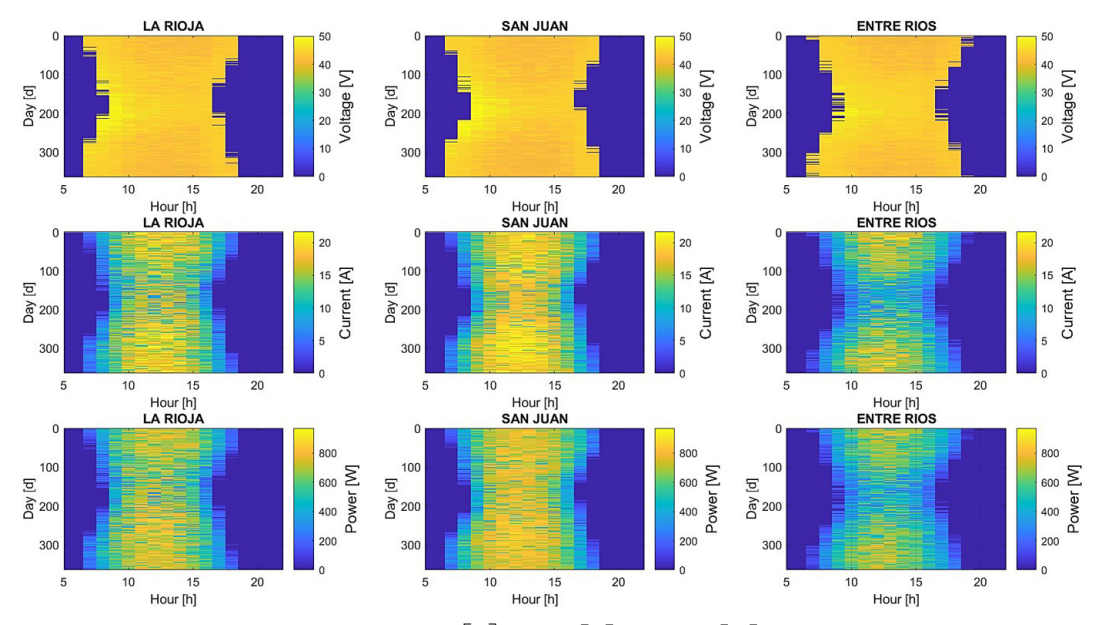


Figure 27. Case 5: Voltage [V], Current [A] and Power [W] for all provinces. Source: The authors.

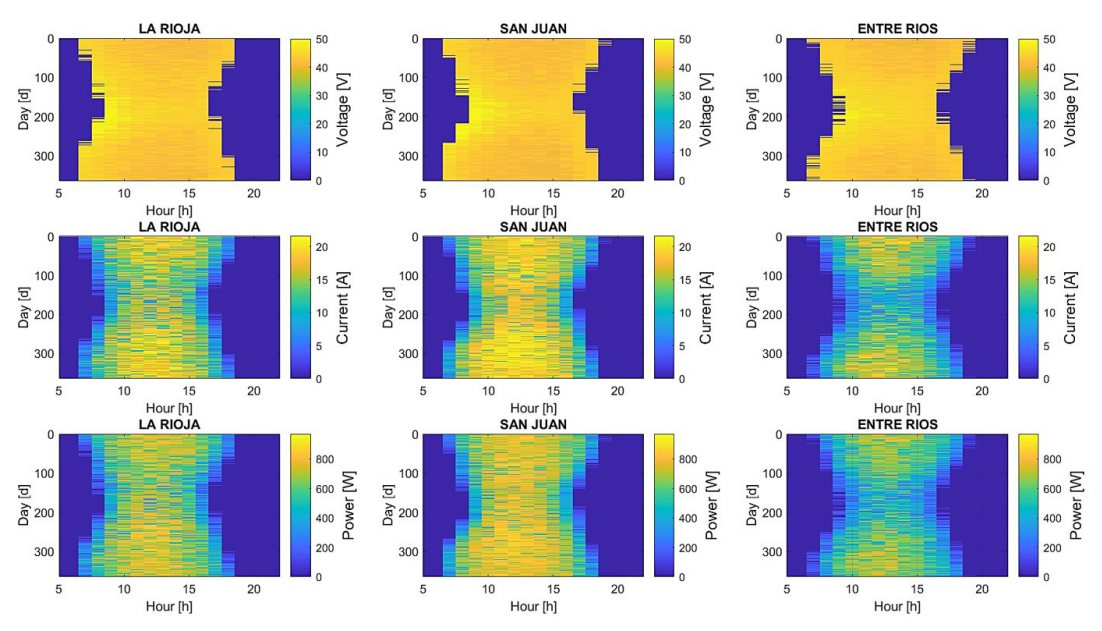


Figure 28. Case 6: Voltage [V], Current [A] and Power [W] for all provinces. Source: The authors.

It can be seen from the figures that the Voltage $\begin{bmatrix} V \end{bmatrix}$ is relatively stable, with some fluctuations due to the climate, and varies slightly with the seasons, being low in summer due to the effect of the high ambient temperature T_e and the increased temperature due to total solar irradiance $G_{\beta,\gamma}$ (see Section 2.2.5. to Section 2.2.7.), as well as the influence of the ambient humidity $SRH \begin{bmatrix} \% \end{bmatrix}$ taken into account. The Current $\begin{bmatrix} A \end{bmatrix}$ and Power $\begin{bmatrix} W \end{bmatrix}$ are therefore approximately proportional to the total irradiance (see Section 2.2.7.) and therefore to the $\cos(\theta)$, which varies according to these two parameters and is influenced by cloud cover and the surrounding climate.

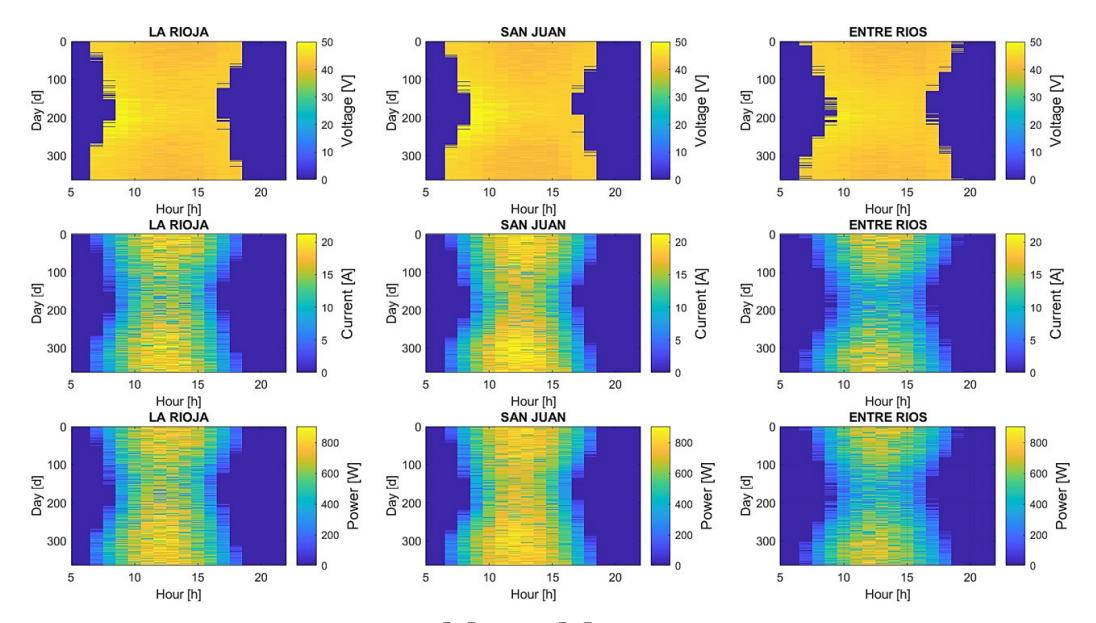


Figure 29. Case 7: Voltage [V], Current [A] and Power [W] for all provinces. Source: The authors.

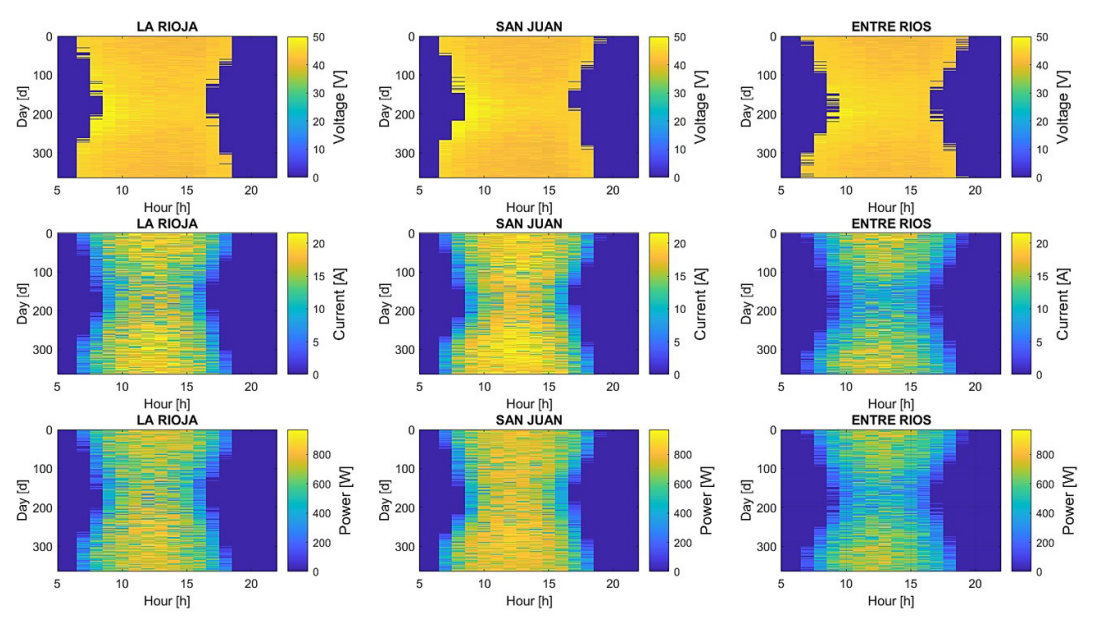


Figure 30. Case 8: Voltage [V], Current [A] and Power [W] for all provinces. Source: The authors.

The maximum current (and therefore power and energy) in all scenarios is higher in summer ($20 \lfloor A \rfloor$ in Case 1) than in winter ($10 \lceil A \rceil$ in Case 1).

However, by increasing the inclination without changing the orientation, the summer maximum is reduced and the winter minimum is increased, thus balancing the energy production curve and obtaining a stable production between 30° and 45°. This is because the angle of declination changes throughout the year, altering the angle of incidence and therefore solar energy production. Therefore, lower tilt angles are required in summer and higher tilt angles are required in winter, which was supported by the additional HFRCPSO-CF search space constraints.

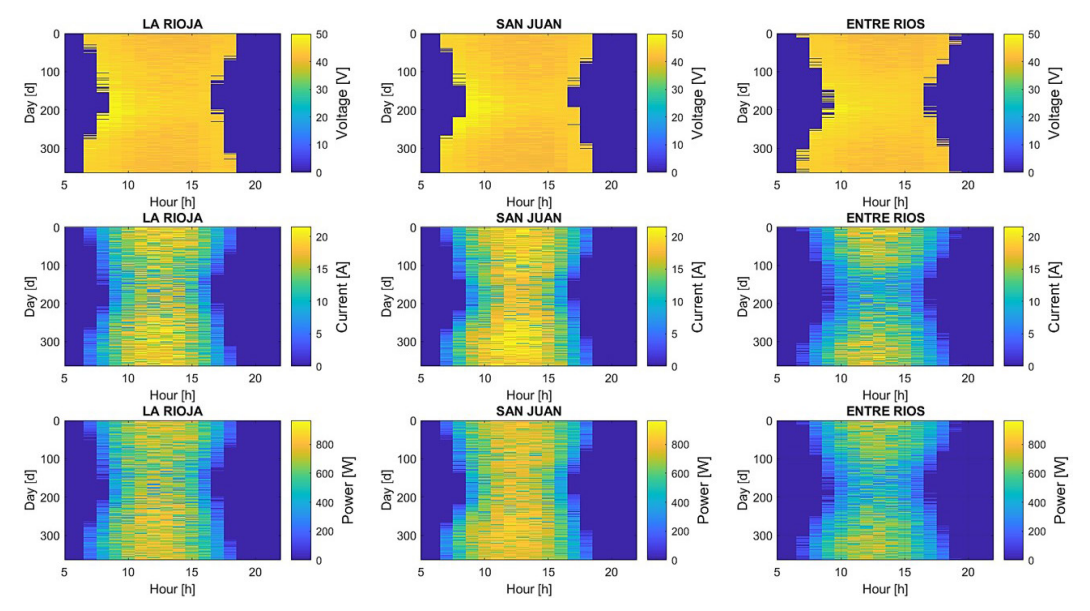


Figure 31. Case 9: Voltage [V], Current [A] and Power [W] for all provinces. Source: The authors.

As can be seen from these figures, the higher the cloud cover (see Section 2.3.1.), the lower the energy and power production, which has a direct impact on the efficiency and energy output of the system (see Section 2.2.5. to Section 2.2.7.). This highlights the importance of considering weather patterns and seasonal changes when designing and optimising solar energy systems, and the production system must take this into account when planning how to meet its energy needs based on this system. In regions such as ER, which have the lowest irradiance levels, higher temperatures and higher humidity, energy production is naturally reduced. The combination of climatic fluctuations and cloud cover also contributes to the variation in power output.

These factors need to be taken into account when planning how a solar system will meet energy needs, as fluctuations in weather patterns can lead to periods of underperformance. This highlights the need for effective forecasting tools and energy storage solutions to ensure a reliable energy supply, especially in regions with highly variable weather.

SJ has a higher and more consistent average yield throughout the year due to less influence from rainfall and weather variability. And LR has an intermediate production due to higher rainfall, rain, humidity and climatic fluctuations than SJ, although much less influence than ER. The mixed Case 5 (see Figure 27) of varying tilt angles by season follows this logic and improves production. The one with the best production (see Figure 28) is the one where the panel moves continuously according to the horizontal panel incidence angle and the azimuthal angle, as expected, although it is obviously the one with the highest associated energy and economic costs.

In the Case 7, the fuzzy inference system (see Figure 29) mimics this reasoning by looking for less motion and therefore lower energy cost, although it does not produce as stable an output as in Figure 28. Similarly, the radial based neural network (see Figure 30) presents an almost identical scenario to Figure 30, but with some adjustments. In the case of multi-objective particle swarm optimisation with fuzzy decision making (see Figure 31), an intermediate result of high and stable current, power and energy production is obtained. The HFRCPSO-CF searched for the best positioning for each day and time, which was as close as possible to the ideal case and minimised the proposed objective functions. As before, the three scenarios give similar results, with production varying due to weather conditions which impact current and power production.

The voltage also remained stable in all provinces and sceneries, regardless of the weather conditions, fluctuating between $45 \left[V\right]$ and $50 \left[V\right]$ in the three provinces. All scenarios give similar results, with production varying due to weather conditions which impact current and power production. Thus, good results are obtained for the variables analysed, which will be confirmed in Section 2.3.4. Future work can improve this proposal so that it deviates more from the ideal scenario, taking into account the other cases.

2.3.5. Comparison of attributes for each case and city

Firstly, this section presents a comparison of attributes for each case and city: San Juan (SJ), La Rioja (LR) and Entre Rios (ER). First, Figure 32 shows the irradiance $G_{\beta,\gamma}$ (see Section 2.2.6.) for the first six cases, excluding the effect of cloud cover (see Section 2.3.1). If the panel is not tilted and faces north, in summer and without weather variations, SJ has the highest maximum average daily irradiance with $0.48 \left[\frac{kW}{m^2}\right]$, followed by LR with $0.45 \left[\frac{kW}{m^2}\right]$ and ER with $0.42 \left[\frac{kW}{m^2}\right]$.

In winter and without weather variability, LR has the highest minimum average daily irradiance with $0.12 \left[\frac{kW}{m^2}\right]$, followed by SJ with $0.45 \left[\frac{kW}{m^2}\right]$ and ER with $0.10 \left[\frac{kW}{m^2}\right]$. Secondly, Figure 33 then shows the irradiance $G_{\beta,\gamma}\left[\frac{kW}{m^2}\right]$ for these six cases, including cloud cover. If the panel is not tilted and faces north, in summer and with weather variations, SJ has the highest maximum average daily irradiance with $0.32 \left[\frac{kW}{m^2}\right]$, followed by LR with $0.3 \left[\frac{kW}{m^2}\right]$ and ER with $0.27 \left[\frac{kW}{m^2}\right]$. In winter and with weather variability, LR has the highest minimum average daily irradiance with $0.13 \left[\frac{kW}{m^2}\right]$, followed by SJ with $0.12 \left[\frac{kW}{m^2}\right]$ and ER with $0.08 \left[\frac{kW}{m^2}\right]$.

Thirdly, Figure 34 shows the irradiance $G_{\beta,\gamma}\left[\frac{kW}{m^2}\right]$ for all cases, including the effect of cloud cover.

The presence of cloud cover reduces the solar energy by approximately 33%, adding to the variability and complicating the analysis. In addition, climatic factors add a noise to the average irradiance curve of about 5 to 10%.

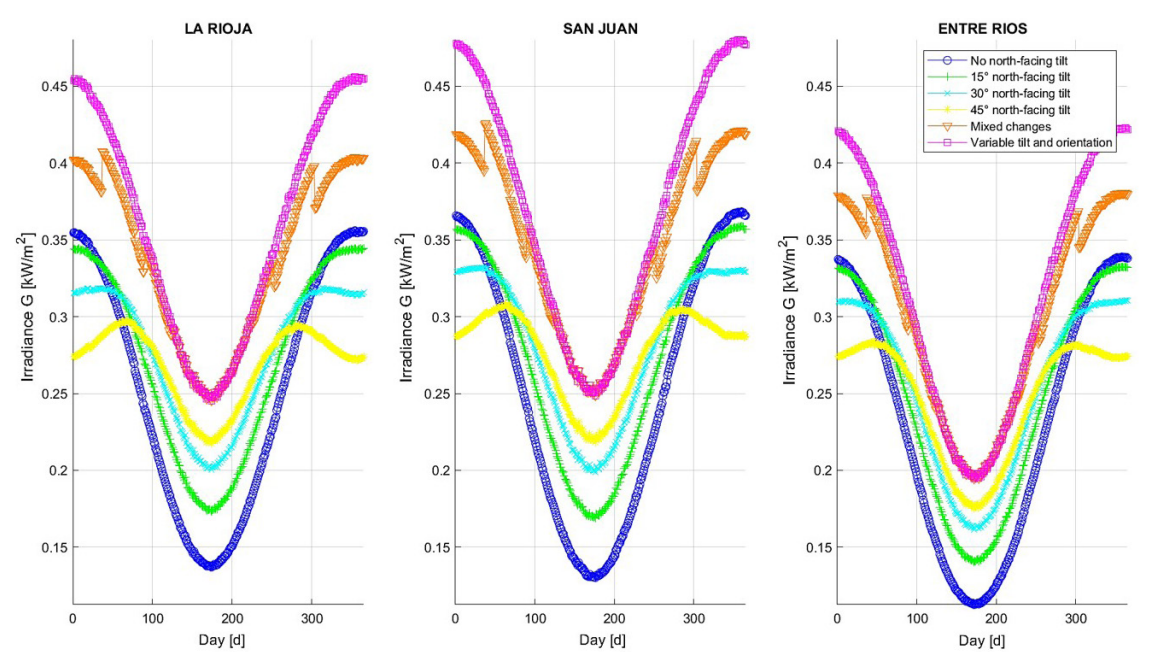


Figure 32. Daily solar irradiance $G_{\beta,\gamma}$ without weather variability. Source: The authors.

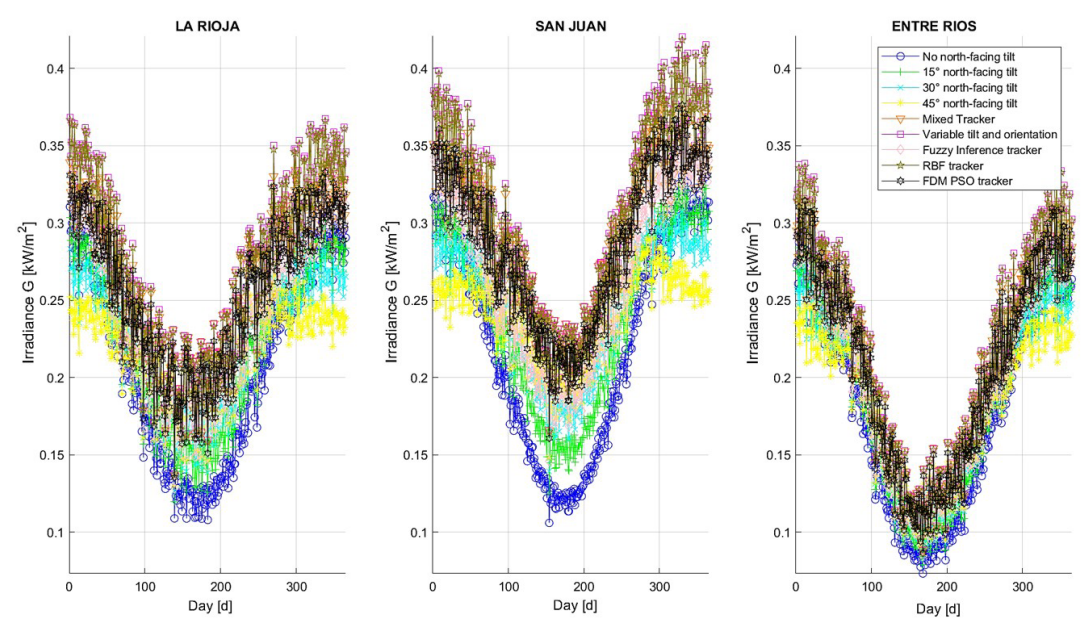


Figure 33. Daily solar irradiance $G_{\beta,\gamma}$ with weather variability. Source: The authors.

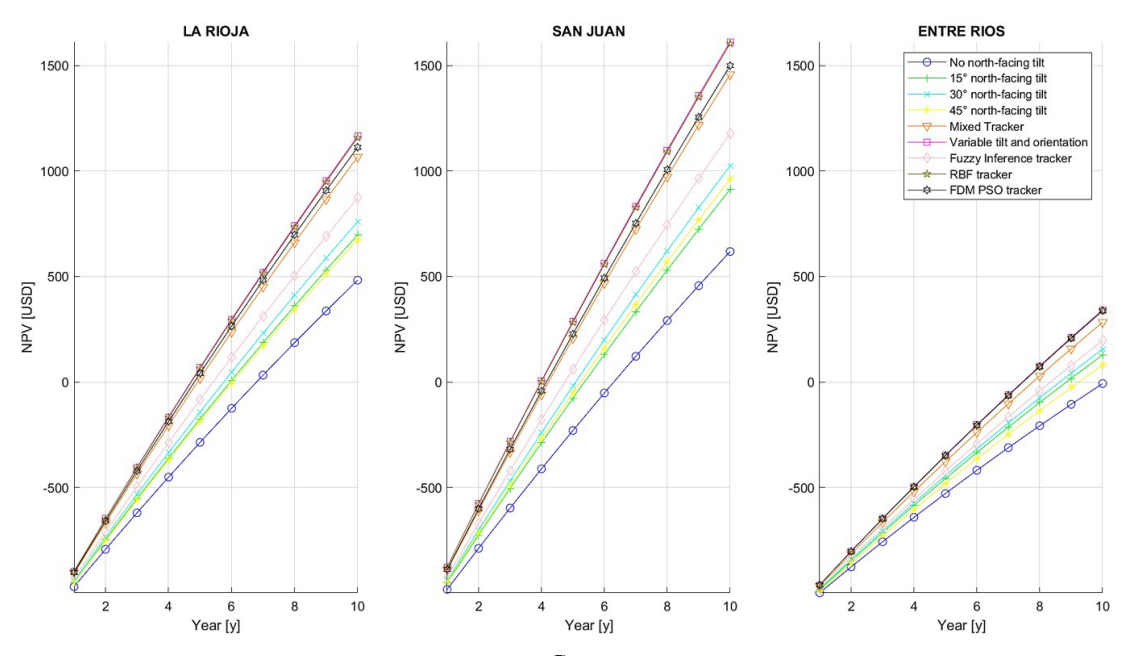


Figure 34. Daily solar irradiance $G_{m{eta}, \gamma}$ of all cases with weather variability. Source: The authors.

Fourthly, these scenarios are then analysed in detail using a Net Present Value (NPV) to assess their economic desirability (see Figure 35). The NPV is in turn related to total irradiance and climatic factors. As noted earlier, increasing the tilt angle without adjusting the orientation reduces the summer maximum irradiance but increases the winter minimum irradiance, resulting in a more stable energy production curve between 30° and 45° tilt (Figure 27 and Figure 28). This is due to the changing angle of solar declination throughout the year, which changes the angle of incidence and therefore solar energy production.

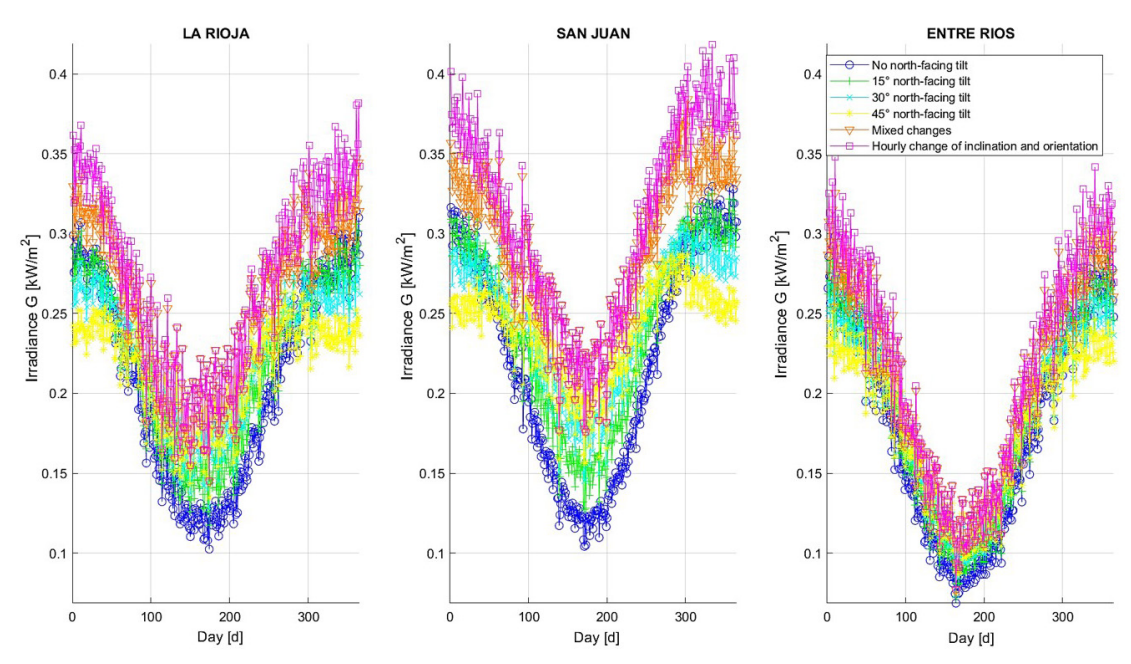


Figure 35. Net Present Value of all cases with weather variability.

Source: The authors.

Therefore, smaller tilt angles are more effective in summer, while larger angles are better for winter, a finding supported by the PSO and further refined by additional search space constraints.

Fifthly, Table 7 compares all cases (see Section 2.3.2) and all provinces (all analysed cases across the provinces of SJ, LR and ER, under weather variability. It shows the absolute values of the OE, the IE and the NPV for all the cases proposed under weather variability across the three Argentinian provinces: SJ, LR and ER. Fixed-panel configurations (Cases 1 to 4) incur no investment costs (IE = 0%), but deliver lower OE and NPV. In contrast, the dynamic cases (Cases 5 to 9) incorporate solar tracking and artificial intelligence-based strategies, leading to substantial increases in energy production (see Table 7). Of these cases, Cases 6 (variable movement) and 8 (RBF) achieve the highest OE and NPV values across most provinces, albeit with moderate investment percentages (around 6%). Case 9 (HFRCPSO-CF) offers a favourable balance between performance and investment, with slightly lower costs and a high NPV. Notably, economic viability is strongly region-dependent: SJ and LR demonstrate significant economic returns under tracking systems, whereas ER, with lower irradiance, exhibits more modest gains, albeit still improved under intelligent tracking. Overall, this table highlights the effectiveness of adaptive tracking strategies in improving both OE and NPV.

Table 7 provides a summary of the relative percentage changes in relation to Case 1 (fixed horizontal panels) for all analysed cases across the provinces of SJ, LR and ER under weather variability. The attributes compared are OE, IE and NPV. It can be seen that energy output (OE) consistently increases with tracking strategies, especially in Cases 6 (variable movement), 8 (RBF) and 9 (HFRCPSO-CF), which show the greatest improvement. IE remains constant at 100% for all advanced cases relative to the fixed baseline, indicating that additional investment is required for movable systems. In terms of economic performance, the NPV significantly improves across all dynamic cases, particularly in SJ and LR, with gains of over 50% in most scenarios. ER shows a smaller, yet still positive, economic impact, likely due to its lower solar resource availability. Overall, the data demonstrates that incorporating intelligent and adaptive tracking strategies leads to substantial energy and economic benefits compared to the fixed-panel baseline.

From all these results, the following analyses are carried out, which are summarised in the conclusions.

Angles and irradiance: Figures 33 to Figure 35, Table 6 and Table 7 show that increasing the tilt angle reduces irradiance in summer and increases it in winter. This is due to the effect of solar declination caused by the movement of the Earth's axis of rotation (see Section 2.3.1 to Section 2.1.2.). Among the fixed angles, Case 3 (inclination of 30°) has the best values that correspond to reality, as it is the angle considered optimal for these latitudes and it is also the one used for the installation of fixed solar panels. On the other hand, Case 5 (mixed changes) increases the energy produced by between 25% and 30% compared to Case 1 (horizontal panel).

Table 7. A comparison summary of all cases and all provinces with weather variability, showing values and relative percentage change:

Obtained energy (OE), invested energy (IE) and net present value (NPV) for all cases and provinces.

Summary of values comparison											
City	Attributes	Case 1 0º	Case 2 15º	Case 3 30°	Case 4 45°	Case 5 mixed	Case 6 variable	Case 7 FIS	Case 8 RBF	Case 9	
SJ	OE [kWh]	1638.2	1.764.7	1.812.8	1.785.6	2.135.6	2.240.6	1.958.9	2.227.8	2.100.3	
LR	OE [kWh]	1544.1	1636.0	1662.8	1626.4	1922.1	1999.5	1790.0	1989.3	1875.2	
ER	OE [kWh]	1302.4	1360.7	1372.6	1340.1	1524.9	1575.0	1450.2	1567.0	1501.4	
SJ	1E [%]	0.00	0.00	0.00	0.00	6.5	6.5	3.8	6.1	3.6	
LR	1E [%]	0.00	0.00	0.00	0.00	6.67	6.67	4.01	6.35	3.06	
ER	1E [%]	0.00	0.00	0.00	0.00	6.4	6.4	3.8	6.1	3.1	
SJ	NPV [USD]	618.4	913.2	1025.3	961.7	1457.7	1612.7	1178.0	1603.8	1499.2	
LR	NPV [USD]	482.8	697.0	759.3	674.5	1066.2	1164.6	873.4	1157.6	1112.4	
ER	NPV [USD]	-7.5	128.3	155.9	80.2	282.9	341.3	196.4	337.3	338.3	
	Relative percentage change in relation to Case 1 (fixed horizontal panels).										
SJ	OE [%]	0.00	7.17	9.63	8.25	23.29	26.89	16.37	26.47	22.00	
LR	OE [%]	0.00	5.62	7.14	5.06	19.67	22.78	13.74	22.38	17.66	
ER	OE [%]	0.00	4.28	5.11	2.81	14.59	17.31	10.19	16.89	13.25	
SJ	1E [%]	0.00	0.00	0.00	0.00	100.00	100.00	100.00	100.00	100.00	
LR	1E [%]	0.00	0.00	0.00	0.00	100.00	100.00	100.00	100.00	100.00	
ER	1E [%]	0.00	0.00	0.00	0.00	100.00	100.00	100.00	100.00	100.00	
SJ	NPV [%]	0.00	32.28	39.69	35.70	57.58	61.65	47.50	61.44	58.75	
LR	NPV [%]	0.00	30.73	36.42	28.42	54.72	58.54	44.72	58.29	56.60	
ER	NPV [%]	0.00	105.85	104.81	109.35	102.65	102.20	103.82	102.22	102.22	

Source: The Authors.

However, Case 6 (continuous movement) receives the most solar radiation and therefore produces the most energy, increasing the energy produced by between 30% and 50% compared to Case 1 (horizontal panel). The cases based on Al techniques correspond to intermediate cases between these cases, where Case 8 (RBF) is closer to Case 6 (higher irradiance continuous motion). However, the HFRCPSO-CF obtains lower energy and economic profitability but invests less energy in turning the panels. This is interesting since it requires lower investment, operation and maintenance costs.

Regional analysis and climatic factors: Table 6 to Table 7 show the energy obtained (kWh), the energy invested (%) and the NPV (in USD) for three provinces (SJ, LR and ER) in different cases. For ease of reference, the abbreviations of these provinces are used. As explained in Section 2.3.2. and Section 2.3.3. geographical location influences energy production, depending on latitude, longitude, altitude, climatic factors, pressure, rainfall, etc (see Appendix A Section A.2.1.). In this sense, SJ has the highest energy obtained and the highest NPV compared to the other provinces, indicating a higher profitability. LR has intermediate results, with a lower energy yield and NPV than SJ. Finally, ER has the lowest values for energy produced and NPV, indicating lower profitability due to less favourable conditions. The variability of the invested energy ranges from 0% to 6.67% for all provinces. Radiation variability in LR, SJ and ER is influenced by climatic factors such as cloud cover, temperature, humidity and seasonal changes. SJ has a more stable and consistent energy production due to its lower climatic variability and minimal rainfall. LR has an intermediate energy production, as it is affected by higher rainfall and climatic fluctuations. ER, on the other hand, has the lowest solar energy production due to higher humidity, frequent rainfall and greater climatic instability, resulting in lower yields during certain periods. These variations highlight the need for reliable forecasting and energy storage solutions, particularly in regions with greater climatic uncertainty, to ensure a consistent energy supply.

Regional analysis and Net present value: Table 6 and Table 7 show that the most profitable case in terms of NPV (Figure 35) is continuous panel movement (Case 6), while the least profitable case is a static north-facing panel with no tilt. Increasing the tilt angle to 30° does not improve profitability because the energy gains in winter offset the losses in summer. Beyond this angle, however, summer energy losses outweigh winter gains, reducing overall profitability. This has significant implications for the economic viability of the analysed scenarios. SJ is the most profitable and has the shortest recovery time, followed by LR and then ER. These differences are due to the varying levels of irradiation, influenced by each region's geographical location and climatic conditions. Consequently, solar energy projects are more profitable in SJ and LR than in ER (see Appendix A Section A.2.1.).

Artificial Intelligence Analysis: Case 7 (FIS), Case 8 (RBF) and Case 9 (HFRCPSO-CF) show an interesting trend in the relationship between regions and attributes. SJ continues to show the highest performance in terms of energy obtained and net present value, compared to LR and ER, although the difference in energy obtained is reduced in the cases 8 and 9. The energy invested in these cases shows a slight variation in all provinces, with higher values in SJ and LR (6.1%-6.7%), as opposed to ER, which has lower values (3.1%-3.8%). Although ER has a relatively low yield in terms of NPV and energy obtained, the energy invested does not increase significantly, reflecting a lower efficiency in converting the energy invested into economic value. This suggests that climate and infrastructure conditions in ER may limit the performance of solar projects compared to the other regions, especially in Case 7, Case 8 and Case 9. The FIS (Case 7) and the RBF (Case 8) provide irradiance values ($G_{\beta,\gamma}$) that closely match the results obtained using continuous solar tracking.

The HFRCPSO-CF is the most satisfactory option, offering an intermediate solution that closely resembles higher energy production scenarios while minimising energy and economic costs (see Figure 27, Figure 28 and Figure 29, respectively). The HFRCPSO-CF offers a similar level of profitability to that of continuous motion, but at a lower cost for mixed motion tracking. It provides a balanced, intermediate solution that ensures stable, high energy production while minimising costs. In terms of energy invested, it effectively searches for optimal panel positioning each day and at each time by minimising objective functions. Additionally, it reduces energy investment by 48–52% compared to the other cases. However, the energy payback is 4–5% lower than for RBF (Case 8) and continuous motion (Case 6). In this sense, an improvement in profitability is observed in ER. Intermediate solutions are obtained using the HFRCPSO-CF, which can be modified by adjusting the EW constraints according to energy needs within the production chain. Consequently, the energy gains of the Al-based scenarios range from 13% to 22%, the economic benefits range from 56% to 102%, and the IE decreases by 48–52% compared to Case 1.

These results are consistent with existing data and software simulations (see Section 2.2.1), with an acceptable margin of error of 3–5%. Future work will employ statistical tests, such as the Wilcoxon signed-rank test. These will be used to compare the current proposals with other available and experimental artificial intelligence techniques at a given level of confidence. This was not done in the present proposal due to space limitations and the desire to provide a thorough explanation of the methodology. This will allow sensitivity, statistical analysis and further scenarios to be explored by varying these parameters and examining their impact on the results. While the enhancements solved the problem, they increased execution time by between 30% and 50%, and can be developed and improved in future research.

3. Conclusions

This paper presents an innovative multi-objective optimisation methodology using artificial intelligence techniques, applied to the optimal orientation and inclination of photovoltaic panels within the Argentinean production chain. It considers technical, economic and environmental aspects, all within a framework of uncertainty and hierarchical evaluation.

The proposed methodology addresses the next challenges (see Table 1 to Table 4):

- (1) The inadequate use of artificial intelligence tools in solar tracking optimisation has resulted in solutions that do not reflect decision-makers' preferences, handle uncertainty inadequately, and lack metric compatibility and hierarchical analysis across multiple indices.
- (2) Determining the optimal tilt and orientation of dual-axis solar tracking systems is difficult because of the dynamic inefficiencies involved, which significantly increase the complexity of mathematical modelling.
- (3) Standard PSO metaheuristics may converge on suboptimal solutions, or solutions that violate technical or economic constraints. This is particularly the case in the context of dual-axis tracking problems.
- (4) These limitations are inadequately addressed by existing studies, particularly in the analysed regions of Argentina.

Methodological originality (see Table 1 to Table 4): The novelty of the present methodology consists in:

- (1) It improves, combines and compares mathematical modelling, artificial and swarm intelligence for multi-criteria optimisation, as well as for metaheuristic models and embedding hybrid constraints and tracking cases.
- (2) It identifies and addresses theoretical, methodological and practical gaps in Argentina and other under-explored regions, providing decision-makers with a feasible, intermediate solution.

These two aspects are covered in the following points:

- The development and combination of different artificial intelligence techniques to optimise and compare scenarios applied to the motion of a solar system.
- The development and combination of available mathematical models with multiple indices and the metaheuristic program with a hybrid Particle Swarm Optimisation with Constriction Factor and Fuzzy Decision Making Optimisation.
- The previous points were used to obtain the parameters of the problem: weather conditions, generation costs and prices from the productive chain (see Figure 1 to Figure 5 and Section 2.3.1).
- Hybrid dynamic constraints and multi-objective fuzzy-guided feedback were incorporated both in the techniques used and in the models proposed in order to obtain technically and economically feasible solutions and to help the methodology to find better solutions.
- The combination of all these strategies, together with the models and results obtained, supports the novelty of the present proposal. The aim was to obtain quality solutions intermediate between the results obtained with horizontal panels (or the worst sceneries) and those obtained with automatic mobile panels (the best sceneries).

In summary, the proposed methodology not only improves the performance of solar systems under realistic conditions and multiple constraints, but also provides an adaptable framework for decision making under uncertainty. In the long term, this approach is expected to be extended to other energy sectors and regions, contributing to the development of intelligent decision support tools for sustainable energy planning in developing countries.

Research method (see Figure 1 to Figure 5 and Section 2.3.1):

- (1) Novel modelling, simulation and optimisation using multi-criteria metaheuristic optimisation techniques with scenario comparison and improvement, validation of provinces and extremal scenarios and dual-axis solar tracking mathematical model (fixed and mobile cases). A new methodology has been developed that incorporates a multi-criteria evaluation of this problem, as well as hybrid-optimised dynamic energy and economic constraints. It has been enhanced with an improved hybrid PSO based on constraints with boundary reflection.
- (2) Novel hybrid fuzzy decision models, analytic hierarchy process, radial basis function neural networks and particle swarm optimisation with a constriction factor, dynamic boundary constraints and reflection, as well as a hybrid fuzzy-guided feedback system for multi-criteria optimisation.
- Most studies use subjective and arbitrary weights or simplified cost models. In the present methodology, the
 parameters are determined iteratively and holistically by adjusting them and analysing the results obtained using
 the methodology.
- This is achieved within a unified system that dynamically adjusts solar tracking strategies based on weather data and input parameters. Future papers will expand on this by exploring more automated ways to adjust the parameters and identifying better solutions.
- The fuzzy decision-making system is enhanced with AHP weighting and hybridized multi-criteria hybrid PSO with neural networks and swarm intelligence, enabling adaptability and robust optimization in this complex problem. In this sense, our approach involves studying three cases of Argentine provinces, which makes the solutions more realistic and practical.
- (3) A survey based on data obtained through the present line of research: government and meteorological station data, manufacturer data and independent research. The data source used for the article was presented and figures were added based on the simulation of average meteorological conditions over ten years (not for all years, to avoid exceeding the page limit).

Main theoretical contributions (see Table 1 to Table 4):

This methodology not only improves the efficiency of Argentina's energy production, but also provides an adaptable framework for addressing global energy issues. It uses strategies based on swarm intelligence, techniques based on human reasoning and how the brain works to find the best solutions to difficult problems.

- 1) Artificial Intelligence: This study employed advanced artificial intelligence techniques to address the issue of optimising solar panel tilt angles and compare different scenarios. Specifically, swarm intelligence-based techniques were employed to direct the search process within the solution space, thereby minimising constraint violations over time. To this end, a hybrid PSO with a constriction factor and dynamic boundary reflection was employed to ensure convergence within feasible regions (see Figure 1 to Figure 5). Additionally, a fuzzy inference system was implemented to incorporate fuzzy constraints into the decision-making process, thereby improving the accuracy of the results. This combination of techniques enables more efficient, appropriate solutions to be found that can adapt to the dynamic conditions of the solar environment (see Figure 1 to Figure 5).
- 2) Mathematical modelling with algorithms and schematics of programs used with Al tools: Firstly, an exhaustive literature review was conducted to investigate the key equations governing the energy production and tilt angles of biaxial solar panels, focusing on the relationship between irradiance and both tilt and orientation angles. This analysis revealed the complexity of the relationship, largely due to inconsistent conventions for the signs and reference axes of the angles. Secondly, the equations were iteratively refined and verified using graphical methods with specially developed software. While existing models often depend on specific panel orientations and tracker types, this study developed a more general equation, deliberately omitting these specifics for clarity. Thirdly, mathematical modelling was used to identify optimisation indices, with a compromise solution achieved through fuzzy decision theory. The prioritisation of these indices was managed using exponential weightings, adjustable to meet different requirements. Fourthly, artificial intelligence techniques based on swarm intelligence and techniques based on human reasoning were integrated to optimise search and parameter tuning, significantly improving the accuracy of irradiance predictions and solar panel performance. In this sense, computational tools were further used to refine the models, with graphical verification to fine-tune the equations (see Figure 1 to Figure 5).
- 3) Mathematical Models and Optimisation of Indices in the Study: The mathematical models describing the relationship between irradiance and solar panel angles were derived and analysed in detail. A major focus was on optimising the indices governing these relationships to improve the performance of solar tracking systems. Instead of relying on the anisotropy index, simpler, more accessible indices were introduced to calculate total irradiance more efficiently. These models were adapted through an iterative process, incorporating various constraints and conditions to optimise tracking angles and maximise energy production. By refining the mathematical models and adjusting the indices accordingly, the overall performance and efficiency of the solar tracking system was significantly improved (see Figure 1 to Figure 5).
- 4) Incorporating Climatic Factors Using the Neural Network: The models were extended to include climatic factors such as temperature and relative humidity, which directly affect the efficiency of the solar panels. The neural network was used to integrate these factors into the mathematical models, allowing the performance coefficients and parameters of the solar panels to be adjusted. Temperature affects performance by changing voltage, current and power coefficients, while relative humidity affects efficiency through vapour saturation effects. By incorporating these factors into the model, more accurate approximations were achieved, allowing better simulation of real-world environmental conditions. The optimal results of artificial intelligence techniques lie between the worst and best scenarios (see Figure 1 to Figure 5).

Main practical results:

Parameters: The parameters used in this methodology were obtained from four clearly defined sources.

- (1) Government (Argentina, 2025a, b; Compañía Administradora del Mercado Mayorista Eléctrico, 2025) and data from governmental and private meteorological stations (Entre Ríos, 2025; La Rioja, 2025; San Juan, 2025; Meteored, 2025; Meteoblue, 2025; WeatherSpark, 2025; Straffelini et al., 2023; Ovando et al., 2021; Palmero et al., 2022).
- (2) Technical specifications from regional manufacturers, industry and software (Ichi, 2025; National Renewable Energy Laboratory, 2025; Hoseinpoor et al., 2020, National Instruments, 2025; Photovoltaic Geographical Information System, 2025; Ré et al., 2021; Ceballos et al., 2023; Ortega et al., 2024).
- (3) Results from our own experimental and methodologic work (Camargo, 2022; Camargo et al., 2024; Sarroca et al., 2024).
- (4) Reviewed literature, as clarified in the provided tables (see Table 1 to Table 4).

Comparison of Scenarios for Three Studied Provinces: Finally, comparisons were made between the scenarios studied in three different provinces (San Juan SJ, La Rioja LR and Entre Ríos ER) to evaluate how the results varied according to climatic conditions and different solar tracking models. The following cases or scenarios are studied for these provinces:

- Case 1 to Case 4 (fixed panels): North-facing horizontal panel (Case 1), 15° panel facing north (Case 2), 30° panel facing north (Case 3), 45° panel facing north (Case 4).
- Case 5: Mixed case with manually adjustable inclination and variable orientation according to the zenith angle of the sun A_7 .
- Case 6: a variable tilt angle and orientation according to the angle of incidence θ_{π} and zenith angle of the sun A_{π} .
- Case 7: a variable tilt angle and orientation according to a fuzzy inference system.
- Case 8: a variable tilt angle and orientation according to a Radial Basis Function (RBF) Neural Network system (see Section 2.2.2 and Section 2.2.4).
- Case 9: a variable tilt angle and orientation according to The multi-objective fuzzy-guided feedback system solved by the hybrid Fuzzy Particle Swarm Optimisation with constriction factor (HFRCPSO-CF).

For each scenario, various factors such as inclination and orientation angles, the cosine of the angle of incidence, irradiated energy, Obtained Energy (OE), Invested Energy (IE) and the Net Present Value (NPV) are analysed and compared. This comparison provided valuable insights into the effectiveness of the optimisation strategies and the impact of climatic factors on energy production. Climatic conditions were found by a RBF neural network to have a significant impact on system performance, highlighting the importance of tailoring models to the local characteristics of each city to achieve optimal results.

Firstly, Figures 9 to Figure 13 analyse the inclination and orientation for each hour and day, showing how the total irradiance is obtained. Secondly, Figure 14 to Figure 22 explore the cosine of the angle of incidence and the total irradiance on the panel, with corresponding inclination and orientation values for each hour and day. Thirdly, Figures 23 to 31 display the voltage, current, and power data for each hour and day, based on the inclination and orientation. Fourthly, Figures 32 to 35 summarize the main attributes for all cases and provinces analysed (LR, SJ and ER). Increasing the tilt angle improves the energy efficiency up to a tilt angle of 30° (Case 3), as the energy gain in winter compensates for the energy loss in summer (see Figure 35). Beyond 30°, however, this compensation effect diminishes and the energy loss in summer outweighs the energy gain in winter. This finding is crucial for assessing the economic viability of different tracking cases.

Climatic Factors and Regional analysis: This comprehensive analysis of solar energy production in different regions demonstrates the impact of climatic factors and tracking systems on solar performance. It also highlights the potential for optimisation and improvements to solar energy systems in the future. Although the inclusion of climatic factors is still under discussion, this study has incorporated estimates of factors such as humidity, pressure (due to altitude) and temperature variations into the model. These factors have been considered for their influence on energy production, and further investigation is warranted. Future research could build on this work by exploring additional models that better integrate these climatic aspects (see Section 3.2.1). Solar energy production in the LR, SJ and ER regions is significantly influenced by the variability of solar radiation, which is in turn influenced by climatic factors such as cloud cover, temperature and humidity. SJ has the most stable and consistent energy production due to its relatively low climatic variability. LR has intermediate energy production, influenced by higher rainfall and greater climatic variability. ER has the lowest solar energy production due to its high humidity and frequent rainfall, which cause greater climatic instability (see Appendix A Section A.2.1).

In terms of solar radiation and weather variations, if the panel is not tilted and faces north, SJ has the

highest maximum average daily irradiance in summer at $0.32 \left[\frac{kW}{m^2} \right]$, followed by LR at $0.3 \left[\frac{kW}{m^2} \right]$ and ER at

$$0.27 \left[\frac{kW}{m^2} \right]$$
. In winter, LR has the highest minimum average daily irradiance with $0.13 \left[\frac{kW}{m^2} \right]$, followed by SJ

with
$$0.12 \left[\frac{kW}{m^2} \right]$$
 and ER with $0.08 \left[\frac{kW}{m^2} \right]$. As can be seen in Figure 27 to Figure 29, the presence of cloud

cover reduces radiation by around 33%, adds variability to the analysis.

In terms of profitability and recovery time, SJ stands out with the highest profitability (Figure 35) and the shortest recovery time. LR follows, while ER has the lowest profitability due to lower solar radiation, higher humidity, frequent rainfall and increased cloud cover. Even in the optimal scenarios, solar energy projects are more profitable in SJ and LR than in ER. They highlight the importance of integrating forecasting tools and energy storage solutions, especially in areas such as ER, where high climatic variability makes it more difficult to maintain a stable energy supply. These results are consistent with real data validated by external studies and independent software tools (see Section 2.2.1.).

Energy and economic gain: The scenario involving continuous panel movement (Case 6) is the most energy-efficient (but most expensive), while the scenario involving a fixed north-facing panel with no tilt (Case 1) is the least efficient (but least expensive). The main results show that the HFRCPSO-CF (Case 9) significantly improves the energy efficiency, with increases ranging from 13% to 22% compared to the fixed horizontal panel (Case 1). Notable economic gains are also achieved in Case 9, with NPV increases ranging from 56% to 102%. Case 9 also reduces energy investment by between 48.2% and 51.8% compared to the other cases. However, the energy gain is approximately 4–5% lower than for the neural network (Case 8) and continuous motion (Case 6). The importance of reducing energy investment, even if this results in slightly lower energy gains, lies in the lower initial cost, which can be adapted to site-specific needs. Furthermore, energy investment was reduced more significantly than the slight losses in efficiency and profitability. Intermediate solutions were obtained using HFRCPSO-CF in this sense, and these can be adjusted by modifying the exponential weight constraints according to the user's energy priorities. These findings confirm the potential of Al-based techniques in dual-axis solar tracking systems in Argentina, providing valuable insights for theoretical advancement and practical deployment in the renewable energy sector.

Validation: The validation of the results obtained showed an error of between 3% and 5% with respect to alternative software (see Section 2.2.1.). For reasons of space, this analysis has not been included, but will be developed in future articles. The results of the analysis are logical, satisfactory and consistent with real data from the regions studied, validating the proposed methodology. On the other hand, Figures 33 to Figure 35, Table 6 and Table 7 show that increasing the tilt angle reduces the irradiance in summer and increases it in winter. This is due to the effect of solar declination caused by the movement of the Earth's axis of rotation. Of the cases with fixed angles, Case 3, with an inclination of 30°, has the best values. This corresponds to reality, as it is the angle considered optimal for these latitudes. It is also the one used for the installation of fixed solar panels. Case 5 (mixed changes) increases the energy produced by between 25% and 30% compared to Case 1 (horizontal panel). On the other hand, case 6 receives the most solar radiation and therefore produces the most energy, increasing the energy produced by between 30% and 50% compared to a horizontal panel (Case 1).

Advantages, disadvantages and limitations: The present methodology successfully incorporated several techniques to optimise and compare results for a complex problem, avoiding oversimplification. There was no need to transform the equations into linear functions, and the most accurate, cutting-edge models were employed. However, due to the nature of strategies based on swarm behaviour, several constraints had to be added to obtain simple, feasible solutions and guide the algorithm more effectively. Swarms tend to become trapped in local optima (good solutions, but not the best), from which it is difficult to escape. While the proposed improvements solved this problem, they also increased the length of the algorithm and its execution time by between 30% and 50%. The RBF is an additional optimisation that must be computed externally and only once to obtain the necessary parameters. Similarly, the RBF must be computed externally and only once to obtain the necessary parameters for the proposed multi-objective model. Otherwise, it would not be possible to execute the programme of the proposed methodology within a reasonable timeframe.

Despite its strengths, the proposed methodology has several limitations. Firstly, it is only applicable to the Argentinian regions that were studied, and adjustments may be required for different climates or regulatory contexts. The simulation does not consider climate change events. The focus is on dual-axis tracking systems. In this context, this model cannot be applied to single-axis systems without being redesigned first. Secondly, the adaptability of the model depends on the availability of local data and the preferences of decision makers, which may necessitate the re-training of neural networks and the recalibration of fuzzy weights. Thirdly, the methodology is computationally intensive due to the hourly simulations conducted and the hybrid nature of the metaheuristic. The methodology is applied to optimisation using hourly and daily data from the last 10 years. This requires significant computational resources for full optimisation. Therefore, for real-time applications, other methodologies can be used instead. Finally, while the model performs well in simulations, its effectiveness in real-world deployments has yet to be validated experimentally. The parameters and constraints used for the search space and HFRCPSO-CF may affect the outcome of the problem in question. Using these constraints may result in promising solutions for a given time and date being overlooked. However, the constraints successfully quided the algorithm to find feasible and viable solutions, eliminating the need for more complex strategies.

In this context, the scope, adaptability and computational demands of both the Gaussian FIS and the RBF are limited. Their accuracy depends on the availability and quality of climatic and operational data, and they require recalibration when applied to regions or conditions not represented in the training set. They are less adaptable when facing extreme or atypical scenarios, which can reduce performance. Furthermore, while inference times are low, the parameter tuning and training phases, especially when working with large datasets and multiple variables, are computationally intensive, which could restrict their use in real-time or in contexts with limited resources. Future work should therefore focus on improving robustness and adaptability to diverse environmental conditions, while reducing computational costs.

However, the method is flexible and scalable and can be applied to several related problems, as explained below.

Future Implications: This study presents a flexible and scalable methodology that can be applied to a variety of public and private energy projects. The aim is to accelerate the return on energy investments and reduce costs. Designed for the Argentine production system, the methodology incorporates advanced artificial intelligence tools to address complex energy challenges in different climates. This approach can also be adapted for use with other renewable energy applications, such as wind farms, hydroelectric generation and biomass. It has already been simplified and applied in related research to optimise investments across energy sources by integrating the production chain (Camargo, 2022). Future work will seek to refine this methodology by exploring new variants of swarm intelligence, incorporating more intricate models for solar irradiance estimation and leveraging real-time weather data to enhance optimisation. Statistical validation methods such as the Wilcoxon signed-rank test will be employed to compare the performance of the proposed methodology with that of alternative AI techniques at a given confidence level. Although this analysis is not included in the current version due to space limitations, it will be expanded in subsequent studies. All Al technique parameters were calibrated through trial and error based on a statistical evaluation of the solutions. Although not detailed here for brevity, future research will include sensitivity and statistical analyses to examine the impact of parameter variations and allow further scenario exploration. Weights used in the decision-making process can also be adjusted to reflect site-specific conditions and improve results further.

Acknowledgements

None.

Data availability

Research data is available in the body of the article.

References

- Ahamed, M. S., Guo, H., & Tanino, K. (2021). Cloud cover-based models for estimation of global solar radiation: A review and case study. *International Journal of Green Energy*, 19(2), 175-189. http://doi.org/10.1080/15435075.2021.1941043.
- Alizamir, M., Othman Ahmed, K., Shiri, J., Fakheri Fard, A., Kim, S., Heddam, S., & Kisi, O. (2023). a new insight for daily solar radiation prediction by meteorological data using an advanced artificial intelligence algorithm: deep extreme learning machine integrated with variational mode decomposition technique. *Sustainability*, *15*(14), 11275. http://doi.org/10.3390/su151411275.
- Argentina, Ministerio de Energía y Minería. (2025a). Datos energía. Retrieved in 2025, March 13, from http://datos.energia.gob.ar/
- Argentina, Secretaría de Energía de la Nación. (2025b). Datos energéticos abiertos de la República Argentina. Retrieved in 2025, March 17, from http://datos.energia.gob.ar/
- Azam, M. S., Bhattacharjee, A., Hassan, M., Rahaman, M., Aziz, S., Shaikh, M. A. A., & Islam, M. S. (2024). Performance enhancement of solar PV system introducing semi-continuous tracking algorithm based solar tracker. *Energy*, 289, 129989. http://doi.org/10.1016/j.energy.2023.129989.
- Camargo, F. G. (2022). Fuzzy multi-objective optimization of the energy transition towards renewable energies with a mixed methodology. *Production*, 32, e20210132. http://doi.org/10.1590/0103-6513.20210132.
- Camargo, F. G., Rossomando, F. G., Gandolfo, D. C., Sarroca, E. A., Faure, O. R., & Andrés Pérez, E. (2024). A novel methodology to obtain optimal economic indicators based on the Argentinean production chain under uncertainty. *Production*, *34*, e20230091. http://doi.org/10.1590/0103-6513.20230091.
- Cao, J., Zhou, T., Zhi, S., Lam, S., Ren, G., Zhang, Y., Wang, Y., Dong, Y., & Cai, J. (2024). Fuzzy inference system with interpretable fuzzy rules: Advancing explainable artificial intelligence for disease diagnosis: a comprehensive review. *Information Sciences*, 662, 120212. http://doi.org/10.1016/j.ins.2024.120212.
- Ceballos, J. C., Forciniti, J. D., & Molina, M. L. (2023). Algunas características del régimen de radiación solar global en el Noroeste Argentino, período 2017-2021. *Avances en Energías Renovables y Medio Ambiente*, *26*, 345-356. Retrieved in 2025, March 17, from https://portalderevistas.unsa.edu.ar/index.php/averma/article/view/3848
- Chrifi-Alaoui, C., Bouhaddou, I., Benabdellah, A. C., & Zekhnini, K. (2025). Industry 5.0 for sustainable supply chains: a fuzzy AHP approach for evaluating the adoption barriers. *Procedia Computer Science*, 253, 2645-2654. http://doi.org/10.1016/j.procs.2025.01.324.

- Compañía Administradora del Mercado Mayorista Eléctrico CAMMESA. (2025). Retrieved in 2025, March 17, from https://cammesaweb.cammesa.com/
- Cuevas, E., Ascencio-Piña, C. R., Pérez, M., & Morales-Castañeda, B. (2024). Considering radial basis function neural network for effective solution generation in metaheuristic algorithms. *Scientific Reports*, *14*(1), 16806. http://doi.org/10.1038/s41598-024-67778-0. PMid:39039169.
- Entre Ríos. (2025). Estación meteorológica automática Concordia (Uruguay). Retrieved in 2025, March 17, from https://www.hidraulica.gob.ar/ema.php?station=curuguay
- Güler, N., Hazem, Z. B., & Gunes, A. (2025). Optimizing solar PV systems using fuzzy logic for Climate-Resilient Healthcare infrastructure in Kyrgyzstan. *Green Technologies and Sustainability*, 3(3), 100190. http://doi.org/10.1016/j.grets.2025.100190.
- Hadroug, N., Iratni, A., Hafaifa, A., Boudjemline, A., Alshammari, O. S., Jerbi, H., Colak, I., & Chen, X. Q. (2023). Energy efficiency improvement in photovoltaic installation using a twin-axis solar tracking mechanism with LDR sensors compared with neuro-fuzzy adaptive inference structure. *Journal of Electrical Engineering & Technology*, 18(4), 2943-2967. http://doi.org/10.1007/s42835-023-01411-4.
- Hammi, Z., Labjar, N., Dalimi, M., El Hamdouni, Y., Lotfi, E. M., & El Hajjaji, S. (2024). Green hydrogen: A holistic review covering life cycle assessment, environmental impacts, and color analysis. *International Journal of Hydrogen Energy*, *80*, 1030-1045. http://doi.org/10.1016/j.ijhydene.2024.07.008.
- Hoseinpoor, M., Prošek, T., Babusiaux, L., & Mallégol, J. (2020). Toward more realistic time of wetness measurement by means of surface relative humidity. *Corrosion Science*, 177, 108999. http://doi.org/10.1016/j.corsci.2020.108999.
- Hraich, A., & Haddi, A. (2025). Energy optimization and digitization of the PV energy balance between production and consumption. *e-Prime-Advances in Electrical Engineering, Electronics and Energy, 11*, 100883. http://doi.org/10.1016/j.prime.2024.100883.
- lchi. (2025). Posición de Python Sun para la investigación y la energía solar. Retrieved in 2025, March 17, from https://ichi.pro/es/posicion-de-python-sun-para-la-investigacion-y-la-energia-solar-134478336890743
- Kazem, H. A., Chaichan, M. T., Al-Waeli, A. H., & Sopian, K. (2024). Recent advancements in solar photovoltaic tracking systems: an in-depth review of technologies, performance metrics, and future trends. Solar Energy, 282, 112946. http://doi.org/10.1016/j. solener.2024.112946.
- Kizielewicz, B., Tomczyk, T., Gandor, M., & Sałabun, W. (2024). Subjective weight determination methods in multi-criteria decision-making: a systematic review. *Procedia Computer Science*, 246, 5396-5407. http://doi.org/10.1016/j.procs.2024.09.673.
- Koshkarbay, N., Mekhilef, S., Saymbetov, A., Kuttybay, N., Nurgaliyev, M., Dosymbetova, G., Orynbassar, S., Yershov, E., Kapparova, A., Zholamanov, B., & Bolatbek, A. (2024). Adaptive control systems for dual axis tracker using clear sky index and output power forecasting based on ML in overcast weather conditions. *Energy and Al, 18*, 100432. http://doi.org/10.1016/j.egyai.2024.100432.
- Kuttybay, N., Mekhilef, S., Koshkarbay, N., Saymbetov, A., Nurgaliyev, M., Dosymbetova, G., Orynbassar, S., Yershov, E., Kapparova, A., Zholamanov, B., & Bolatbek, A. (2024). Assessment of solar tracking systems: a comprehensive review. *Sustainable Energy Technologies and Assessments, 68*, 103879. http://doi.org/10.1016/j.seta.2024.103879.
- La Rioja. (2025). Red de estaciones agroclimáticas SIAR. Retrieved in 2025, March 17, from https://www.larioja.org/agricultura/es/informacion-agroclimatica/red-estaciones-agroclimaticas-siar
- Lu, N., & Qin, J. (2024). Optimization of tilt angle for PV in China with long-term hourly surface solar radiation. *Renewable Energy*, 229, 120741. http://doi.org/10.1016/j.renene.2024.120741.
- Meteoblue. (2025). Tiempo. Retrieved in 2025, March 17, from https://www.meteoblue.com/
- Meteored. (2025). Pronóstico del tiempo 14 días. Retrieved in 2025, March 17, from https://www.meteored.com.ar/
- Molu, R. J. J., Tripathi, B., Mbasso, W. F., Naoussi, S. R. D., Bajaj, M., Wira, P., Blazek, V., Prokop, L., & Misak, S. (2024). Advancing short-term solar irradiance forecasting accuracy through a hybrid deep learning approach with Bayesian optimization. *Results in Engineering*, 23, 102461. http://doi.org/10.1016/j.rineng.2024.102461.
- National Instruments. (2025). Descargar Multisim. Retrieved in 2025, March 17, from https://www.ni.com/es/support/downloads/software-products/download.multisim.html
- National Renewable Energy Laboratory NREL. (2025). Solar position algorithm for solar radiation applications. Retrieved in 2025, March 17, from https://www.nrel.gov/docs/fy08osti/34302.pdf
- Ortega, A., Kurbán, A., & Montilla, E. (2024). Estadística climática año 2023 área metropolitana de San Juan: registros horario, estadística mensual, estacional y anual. Retrieved in 2025, March 17, from http://huru.unsj.edu.ar/handle/123456789/382
- Ovando, G., Sayago, S., Bellini, Y., Belmonte, M. L., & Bocco, M. (2021). Precipitation estimations based on remote sensing compared with data from weather stations over agricultural region of Argentina pampas. *Remote Sensing Applications: Society and Environment*, 23, 100589. http://doi.org/10.1016/j.rsase.2021.100589.
- Palmero, F., Carcedo, A. J., Haro, R. J., Bigatton, E. D., Salvagiotti, F., & Ciampitti, I. A. (2022). Modeling drought stress impacts under current and future climate for peanut in the semiarid pampas region of Argentina. *Field Crops Research*, *286*, 108615. http://doi.org/10.1016/j.fcr.2022.108615.
- Photovoltaic Geographical Information System PVGIS. (2025). Retrieved in 2025, March 17, from https://pvgis.com/
- Praveen, P. N., & Menaka, D. (2024). A dual-axis solar tracking system with minimized tracking error through optimization technique. *Multimedia Tools and Applications*, 83(1), 58891-58914. http://doi.org/10.1007/s11042-023-17698-4.
- Ré, M. G., Mazzocco, M. P., & Filippín, C. (2021). Mejoras de eficiencia energética en calefacción: Potencial de intervención en edificio escolar existente del área metropolitana de San Juan, Argentina. *Revista Hábitat Sustentable*, 11(1), 20-31. http://doi.org/10.2232 0/07190700.2021.11.01.02.
- Sameera, T., Tariq, M., Rihan, M., & Ayan, M. (2024). A comprehensive review on the application of recently introduced optimization techniques obtaining maximum power in the solar PV system. *Renewable Energy Focus*, 49, 100564. http://doi.org/10.1016/j. ref.2024.100564.
- San Juan, Departamento de Hidráulica. (2025). Sistema Integrado de Información Hídrica. Retrieved in 2025, March 17, from https://hidraulica.sanjuan.gob.ar/sistemas/hidrico.php

- Saraji, M. K., Streimikiene, D., & Suresh, V. (2024). A novel two-stage multicriteria decision-making approach for selecting solar farm sites: a case study. *Journal of Cleaner Production*, 444, 141198. http://doi.org/10.1016/j.jclepro.2024.141198.
- Sarroca, E. A., Nieto, F. G., Sosa, G., Camargo, F. G., Douglas, G. N., Rossomando, F., & Arias, E. N. (2024). Diseño de prototipo de sistema de telemetría para sistema solar fotovoltaico. In Libro de Trabajos del Congreso Argentino de Sistemas Embebidos (CASE 2024). Ciudad Autónoma de Buenos Aires: ACSE. Retrieved in 2025, March 17, from https://case.ar/wp-content/uploads/2024/10/libro2024_C.pdf
- Sobirov, M. M., Rozikov, J. Y., Yusupova, D. A., & Ruziboev, V. U. (2023). The calculation of spectral and angular distribution of diffusely reflected, diffusely transmitted, and unscattered fluxes of solar radiation in atmospheric layers. *Applied Solar Energy*, *59*(5), 761-769. http://doi.org/10.3103/S0003701X23601187.
- Straffelini, E., Carrillo, N., Schilardi, C., Aguilera, R., Estrella Orrego, M. J., & Tarolli, P. (2023). Viticulture in Argentina under extreme weather scenarios: actual challenges, future perspectives. *Geography and Sustainability, 4*(2), 161-169. http://doi.org/10.1016/j. geosus.2023.03.003.
- Sun, L., Bai, J., Pachauri, R. K., & Wang, S. (2024). A horizontal single-axis tracking bracket with an adjustable tilt angle and its adaptive real-time tracking system for bifacial PV modules. *Renewable Energy*, 221, 119762. http://doi.org/10.1016/j.renene.2023.119762.
- WeatherSpark. (2025). Clima en Argentina. Retrieved in 2025, March 17, from https://es.weatherspark.com/countries/AR
- Wen, L., & Ajay, P. (2024). Solar PV tracking system using arithmetic optimization with dual axis and sensor. *Measurement: Sensors*, 33, 101089. http://doi.org/10.1016/j.measen.2024.101089.
- Wu, C. H., Wang, H. C., & Chang, H. Y. (2022). Dual-axis solar tracker with satellite compass and inclinometer for automatic positioning and tracking. *Energy for Sustainable Development, 66*, 308-318. http://doi.org/10.1016/j.esd.2021.12.013.
- Yadav, A. K., Khargotra, R., Lee, D., Kumar, R., & Singh, T. (2024). Novel applications of various neural network models for prediction of photovoltaic system power under outdoor condition of mountainous region. *Sustainable Energy, Grids and Networks, 38*, 101318. http://doi.org/10.1016/j.segan.2024.101318.
- Zou, Y., Qin, C., Liu, H., Zhang, B., & Wu, X. (2024). Concentrating photovoltaic systems: A review of temperature effects and components. *Journal of Thermal Analysis and Calorimetry*, 149(3), 1301–1329. http://doi.org/10.1007/s10973-023-12767-0.

Author Contributions

Federico Gabriel Camargo: Conceptualization, Data curation, Resources, Formal analysis, Investigation, Methodology, Project administration, Software, Validation, Visualization, Writing – original draft, Writing – review & editing

Francisco Guido Rossomando: Resources, Data curation, Software, Validation, Investigation, Project administration, Supervision

Daniel Ceferino Gandolfo: Resources, Data curation, Software, Validation, Investigation, Project administration, Supervision

Esteban Antonio Sarroca: Resources, Formal analysis, Data curation, Investigation, Methodology, Project administration, Software, Validation, Visualization, Writing – review & editing

Omar Roberto Faure: Resources, Data curation, Software, Validation, Investigation, Project administration, Supervision

Gonzalo Sosa: Resources, Data curation, Formal analysis, Investigation, Methodology, Software, Validation, Visualization

Appendix A. Mathematical modelling, Radial Basis Neural Networks and Gaussian Fuzzy Inference System parameters

A.1. Mathematical modelling

Mathematical modelling of the relationship between irradiation and solar panel tracking angles (tilt and orientation) reveals a significant divergence from the equations proposed in previous studies. Despite extensive efforts to develop accurate formulations, significant variability in the results is evident throughout the literature (Ahamed et al., 2021; Wu et al., 2022; Kuttybay et al., 2024; Zou et al., 2024; Sameera et al., 2024; Azam et al., 2024; Molu et al., 2024; Sobirov et al., 2023), highlighting the complexity of this interaction. The developments presented in this work and in the supplementary material are based on these references, while also incorporating mathematical improvements that enhance the models' accuracy and adaptability to different conditions. Due to space constraints, detailed derivations for each cited work are not included here, but their contributions are embedded within and expanded upon in the proposed methodology.

The main technical data of the solar system are as follows:

$$t_{d,i}$$
 Discount rate of the solar system: 0.08 (8%) and Annual inflation rate: 0.0065 (6.5%). $\begin{bmatrix} k_B, q \end{bmatrix}$ Bolztman constant: $0.0138 \begin{bmatrix} J \\ {}^{o}K \end{bmatrix}$ and Electron Charge: $1.602 \cdot 10^{-19} \begin{bmatrix} C \end{bmatrix}$. $\begin{bmatrix} a, N_s \end{bmatrix}$ Ideality factor (1.0531 $\begin{bmatrix} u \end{bmatrix}$) and Number of cells (132 $\begin{bmatrix} u \end{bmatrix}$). P_{max} Installed power of the solar system: $1000 \begin{bmatrix} W \end{bmatrix}$ with a Useful Life (*UL*) of $30 \begin{bmatrix} Years \end{bmatrix}$. $R_{\begin{bmatrix} s, sh \end{bmatrix}}$ Resistance Series $0.39381 \begin{bmatrix} Ohm \end{bmatrix}$ and Shunt resistance $313.05 \begin{bmatrix} Ohm \end{bmatrix}$. V Photovoltaic system voltage: between $0 \begin{bmatrix} V \end{bmatrix}$ and $50 \begin{bmatrix} V \end{bmatrix}$. $NOCT$ Nominal Operating Cell Temperature (45°C) when $G_{ref} = 1 \begin{bmatrix} \frac{kW}{m^2} \end{bmatrix}$, $T_e = 25$ °C and wind speed of $1 \frac{m}{s}$.

A.1.1. Direct and diffuse solar irradiance and dynamic search space constraint

Direct H_b and diffuse H_d solar irradiance: Equation A1 shows the rate f[u], clearness rate R_b and the index of anisotropy $A_i[u]$. Where H_b is the Direct Irradiance and H_d is the Diffuse Irradiance. The variable H_b is the amount of solar power that reaches a surface directly per unit area, without being scattered or absorbed by the atmosphere. H_d is solar energy that has been scattered by molecules, aerosols or clouds in the atmosphere coming from all directions in the sky. They depend on factors such as cloud cover, atmospheric conditions and latitude (Sobirov et al., 2023; Wu et al., 2022; Azam et al., 2024). In addition, a development is made that eliminates anisotropy A_i , which is very difficult to obtain.

$$\begin{pmatrix} f \\ R_b \\ A_i \end{pmatrix} = \begin{pmatrix} \sqrt{\frac{H_b}{H}} \\ \frac{H_{0\beta, \gamma}}{H_{0\beta=0, \gamma=0}} \end{pmatrix} = \begin{pmatrix} \sqrt{1 - \frac{H_d}{H}} \\ \frac{\cos(\theta)}{\cos(\theta_z)} \\ \frac{H_b}{H_0} \end{pmatrix} \cap \begin{pmatrix} \frac{1}{H_0} \begin{pmatrix} H_b + H_d A_i \\ H_d (1 - A_i) \end{pmatrix} = K_T \begin{pmatrix} f^2 \left(1 + \frac{H_d}{H} K_T\right) \\ \frac{H_d}{H} (1 - K_T f^2) \end{pmatrix} \end{pmatrix} \tag{A1}$$

Best energy efficiency: This work, Equation A2 proposes the following practical theoretical analysis to obtain the constraint of the search space and the values of the angles β_{max} and γ_{max} that maximise the energy obtained and minimise the cost.

$$\nabla \left(R_{DIR\beta,\gamma} + R_{DIF\beta,\gamma} + R_{ALB\beta,\gamma} \right) \Big|_{\beta_{max}, \gamma_{max}} = \overline{0} \quad \Rightarrow \quad \nabla \left(\cos(\theta) \right) \Big|_{\beta_{max}, \gamma_{max}} \approx \overline{0} \quad \forall \quad \nabla = \left(\frac{\partial}{\partial \beta}, \frac{\partial}{\partial \gamma} \right)$$
(A2)

Equation A3 has been obtained mathematically and graphically. In this sense, the angles θ_z [°] and A_z [°] are used as the most conservative choice. This means that if the tracker can be moved permanently, without considering the energy and economic costs, it is optimal to track the sun according to the angle of incidence of a horizontal plane facing north θ_z and the azimuth angle of the sun A_z . Although this solution is the costliest in energy and economic terms and the least efficient, it is the limit that can obtain the most energy and is used to calculate the fuzzy limits of the proposed optimisation model.

$$\begin{pmatrix} \gamma_{max} \\ \beta_{max} \end{pmatrix} \approx \begin{pmatrix} atan \left(-\frac{\cos(\delta)\sin(\omega)}{\sin(\delta)\cos(\varphi) - \cos(\delta)\sin(\varphi)\cos(\omega)} \right) \\ atan \left(\frac{tan(\gamma_{max}) \tan(\omega)}{\sin(\varphi)} - \frac{tan(\delta)}{\tan(\varphi)\cos(\omega)} + 1 \\ \frac{tan(\varphi) \tan(\delta)}{\cos(\omega)} + 1 \end{pmatrix} \right) \approx \begin{pmatrix} A_z \\ \theta_z \end{pmatrix}$$
(A3)

Search vector improve: Analysing Equation A3 gives the slope analyses in Equation A4 and Equation A5. This aspect is difficult to detect by the HFRCPSO-CF, resulting in the existence of peaks that are difficult to eliminate without a high computational cost. As a result, the optimisation would take too long.

$$\left|\gamma_{max}\right| = \begin{cases} decrease, & \forall \ (\varphi < 0) \cap \left(\left(0 < m < 183\right) \cup \left(H_{Sem} \le h \le H_{Stm}\right)\right) \\ increase, & \forall \ (\varphi < 0) \cap \left(\left(183 < m < 365\right) \cup \left(H_{Sem} \le h \le H_{Stm}\right)\right) \end{cases}$$
(A4)

$$\left|\beta_{max}\right| = \begin{cases} increase, \ \forall \ (\varphi < 0) \cap \left(\left(0 < m < 183\right) \cup \left(H_{Snm} \le h \le H_{Stm}\right)\right) \\ decrease, \ \forall \ (\varphi < 0) \cap \left(\left(183 < m < 365\right) \cup \left(H_{Sem} \le h \le H_{Snm}\right)\right) \end{cases}$$
(A5)

Therefore, a sorting function is performed, taking into account these specifications, to obtain a vector that meets the technical requirements, to facilitate the search, to further reduce the search space and the execution time, and to obtain better solutions. In addition, the search vector can be considerably reduced by considering only the hours in which there is sunlight, for which some algorithms are designed. As a disadvantage, this process can distort the solution obtained, so that good solutions are lost (with respect to a certain instantaneous index in a day and an hour), which can be analysed in future work.

Dynamic search space constraint: then, Equation A6 gives the upper and lower limits of $\beta[\circ]$ and $\gamma[\circ]$ (see Section 2.2.1.).

$$(45 \ge \theta_z + 15 \ge \beta \ge 15) \cap (90 \ge A_z + 90 \ge \gamma \ge A_z - 90 \ge -90) \tag{A6}$$

 β is constrained to the range $\begin{bmatrix} 15,45 \end{bmatrix}$ and γ to the range $\begin{bmatrix} -90,90 \end{bmatrix}$. Within this set, β is constrained to the range $\begin{bmatrix} 15,\theta_z+15 \end{bmatrix}$ and γ to the range $\begin{bmatrix} A_z-90,A_z+90 \end{bmatrix}$. These ranges are obtained by studying the efficiencies of the solar panels with different inclinations and orientations (see Section 2.2.1). Then, two fuzzy ramp functions for β and γ are used to satisfy this equation. For the tilt angle, the first constraint considers $\xi=0$ and restricts the movements between the range $\begin{bmatrix} \theta_z, \theta_z+15 \end{bmatrix}$, aiming to be as close to θ_z as possible. The second constraint considers $\xi=1$ and restricts the movements between the range $\begin{bmatrix} 15, \theta_z \end{bmatrix}$, also trying to be as close as possible to θ_z . The best and worst case scenarios are used to calculate the respective best and worst indices associated with the attributes to be optimised and the search space constraints (see Section 2.2.8 to Section 2.2.11). The maximum, minimum and average restrictions β and γ are obtained from an analysis of radiation maps produced by this model. These maps show that for β between 45° and 60°, a higher level of energetic irradiance is not achieved; rather, it decreases. The minimum restriction of 15° was determined by calculating the minimum viable inclination to prevent water accumulation on the panels, which could affect their performance. A safety factor was applied to this calculation. β and γ are intended to have a maximum difference of 90° with respect to the sun's orientation, and these limits are defined accordingly.

A.2. Radial Basis Neural Networks and Gaussian Fuzzy Inference System parameters

Radial Basis Function (RBF): Table A.1 summarises the key parameters used to train the Radial Basis Function (RBF) neural networks within the proposed methodology. The input variables are the hour of the day, the day of the year, air temperature (T), dew point temperature (T_d) , and cloudiness factor (F_{clim}) , while the output variables are the optimal tilt (β) and orientation (γ) angles of the solar panels. Each input and output variable was sampled hourly over a ten-year period (24 hours × 365 days × 10 years), resulting in 43800 data points (by city). These samples were used for each output variable during the training process, which was guided by hyperparameters such as the maximum number of hidden neurons, target error (mean squared error (MSE) of less than 3%) and maximum allowable deviations (d_{max}) . The d_{max} parameter sets a maximum distance threshold for clustering in the RBF training process, controlling the spread and granularity of the hidden neurons. The maximum number of hidden neurons varies depending on the variable; higher values are allocated to those with more complex dynamics (e.g. day of the year). These parameters were crucial for capturing local environmental variability and improving the model's predictive accuracy. This configuration allows the dynamic relationships between environmental variables and solar tracking angles to be modelled accurately in real-world climatic conditions.

Table A.1. Radial Basis Function (RBF) neural network summary by city.

Inputs	Samples Input	Outputs	Samples Output	Maximum hidden neuron	RBF Error Metric	Goal	d_{max}	Learning Method
Hour [h]	24 x 365 x 10 x (8 cases)	-	-	43800	MSE	3%	1	K - Means
Day[d]	365 x 10 x (8 cases)	-	-	43800	MSE	3%	10	K - Means
-	-	$\beta \left[^{\circ }\right]$	12 x 365 x 10 x (8 cases)	350400	MSE	3%	1	K - Means
-	-	γ[°]	12 x 365 x 10 x (8 cases)	350400	MSE	3%	1	K - Means
-	-	$T [^{\circ}C]$	12 x 365 x 10	43800	MSE	3%	1	K - Means
-	-	T_d [°C]	12 x 365 x 10	43800	MSE	3%	1	K - Means
-	-	$F_{clim}[u]$	24 x 365 x 10	43800	MSE	3%	0.1	K - Means

Source: The Authors.

Limitations: The RBF used in this study has certain limitations that must be recognised. Firstly, the model's scope is dependent on the availability and representativeness of historical meteorological data from the provinces under study. While the large training dataset enables high accuracy, it also restricts the model's capacity to adapt when applied to regions with limited or incomplete climatic records. Secondly, changes in environmental patterns not present in the training data affect the network's performance, such as extreme weather events or long-term climate shifts. This may necessitate retraining with updated datasets. Thirdly, processing and training such a large number of samples is computationally demanding, particularly when tuning hyperparameters such as the maximum number of hidden neurons, error thresholds, and Gaussian spread parameters. These requirements may limit the model's feasibility in real-time or resource-constrained environments. Further research should therefore focus on strategies to balance accuracy and computational efficiency, such as model simplification or hybridisation.

Gaussian Fuzzy Inference System (FIS):

Table A.2 shows a summary of the Gaussian FIS and its fuzzy subjective valuation rules. These data represent various scenarios that combine qualitative assessments across multiple criteria. These are fed into the FIS to simulate decision-making in uncertain situations. Each row corresponds to a specific combination of inputs, evaluated by the FIS using predefined membership functions and inference rules. The input dataset was constructed to reflect a range of representative operating conditions, enabling the FIS to generate robust and generalisable output recommendations (see Equation A4 to Equation A6).

Table A.2. A summary of the Gaussian fuzzy inference system and its fuzzy subjective valuation rules.

	Hour[h]	Day[d]	$etaig[^\circig]$	γ[°]
Rule 1	Very low	Min	Max	Min
Rule 2	Very low	Very low	Very High	Min
Rule 3	Very low	Low	High	Low
Rule 4	Very low	Medium	Medium	Very High
Rule 5	Very low	High	High	Max
Rule 6	Very low	Very High	Very High	Max
Rule 7	Very low	Max	Max	Min
Rule 8	Low	Min	Very High	Very low
Rule 9	Low	Very low	High	Very low
Rule 10	Low	Low	Medium	Low
Rule 11	Low	Medium	Low	Medium
Rule 12	Low	High	Medium	High
Rule 13	Low	Very High	High	Very High
Rule 14	Low	Max	Very High	Min
Rule 15	Medium	Min	Medium	Very low
Rule 16	Medium	Very low	Low	Very low
Rule 17	Medium	Low	Very low	Low
Rule 18	Medium	Medium	Min	Medium
Rule 19	Medium	High	Very low	High
Rule 20	Medium	Very High	Low	Very High
Rule 21	Medium	Max	Medium	Min
Rule 22	High	Min	Very High	Very low
Rule 23	High	Very low	High	Very low
Rule 24	High	Low	Medium	Low
Rule 25	High	Medium	Low	Medium
Rule 26	High	High	Medium	High
Rule 27	High	Very High	High	Very High
Rule 28	High	Max	Very High	Min
Rule 29	Very High	Min	Max	Min
Rule 30	Very High	Very low	Very High	Min
Rule 31	Very High	Low	High	Low
Rule 32	Very High	Medium	Medium	Very High
Rule 33	Very High	High	High	Max
Rule 34	Very High	Very High	Very High	Max
Rule 35	Very High	Max	Max	Min

Source: The Authors.

Table A.3 summarises the parameters of the Gaussian FIS. It defines the centres of the Gaussian membership functions for the following input variables: hour, day, panel tilt angle (β) and orientation angle (γ). The standard deviation (σ) associated with each variable controls the spread of the membership functions, enabling smooth transitions between fuzzy sets.

Table A.3. A summary of the parameters of the Gaussian Fuzzy Inference System.

Gaussian Fuzzy Inference System Parameters										
	Centre 1	Centre 2	Centre 3	Centre 4	Centre 5	Centre 6	Centre 7	σ		
Hour [h]	H_{Se}	$H_{Se} + \frac{H_{St} - H_{Se}}{4}$	$H_{Se} + \frac{H_{St} - H_S}{2}$	$H_{Se} + 3\frac{H_{St} - H_{Se}}{4}$	H_{St}	-	-	1.5		
Day[d]	0	90	180	270	360	-	-	30		
$\beta\bigl[^\circ\bigr]$	0	8	16	24	32	40	48	10		
$\gamma [\circ]$	0	30	60	90	120	150	180	4		

Source: The Authors.

Limitations: The FIS implemented in this study also has limitations that merit consideration. The accuracy and reliability of the model depend heavily on the granularity and completeness of the meteorological and operational datasets used to define the membership functions and tuning parameters. Therefore, in regions with scarce or low-resolution data, the model may require significant recalibration before it can deliver robust results. In terms of adaptability, the FIS is designed to handle the climatic and operational variability represented in the training data. However, it may underperform when faced with environmental conditions or operational scenarios that fall outside these bounds, such as extreme weather patterns or atypical seasonal behaviour. Finally, the FIS's computational demands primarily arise during the parameter tuning phase, particularly when optimising multiple Gaussian membership functions across several input variables. Although runtime during inference is relatively low, the initial calibration process, particularly when integrated into a hybrid optimisation framework, can be computationally intensive. This could limit the model's application in time-sensitive or resource-constrained environments.

A.2.1. Summary of meteorological data used for RBF training

Figure A.1. summarises the meteorological data used for RBF training in Section 2.2.4 and Section 3 for the regions of La Rioja (LR), San Juan (SJ) and Entre Ríos (ER). It illustrates the number of days in each month with a specific maximum temperature and level of cloud cover. LR experiences a peak in sunny days in winter, while partly cloudy and rainy days are more frequent in summer. SJ, however, experiences a significant increase in cloudy days during the winter months. ER shows a more balanced distribution of sunny, partly cloudy, and cloudy days throughout the year. Temperature trends indicate that LR and SJ experience high summer temperatures, with SJ reaching higher extremes. Meanwhile, ER displays more moderate seasonal variations. Overall, the figure highlights the differences in cloud cover and temperature patterns across Argentina's regions.

Due to space constraints, this article does not include more detailed statistical summaries of these climate datasets. However, future publications will focus specifically on the neural network's performance and its ability to generalise under different climatic scenarios.

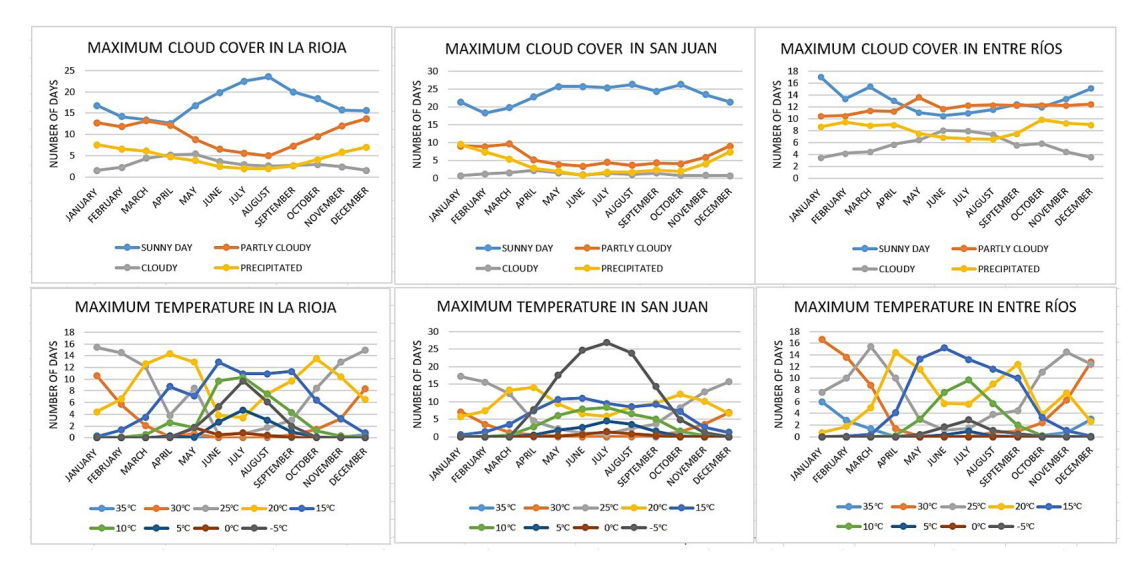


Figure A.1. Summary of meteorological data used for RBF training.

Source: The authors.